

# Integral Asymmetric Isoporous Membrane Formation From Novel Block Copolymers



## Dissertation

Dissertation submitted in partial fulfillment of the requirements for the

Degree of Doctor of Science (Dr. rer. nat.)

To

The University of Hamburg,

Institute of Physical Chemistry, Department of Chemistry, MIN Faculty

Submitted by

Sarah Saleem

Hamburg, 2020

Reviewer 1: Prof. Dr. Volker Abetz

Reviewer 2: Prof. Dr. Gerrit A. Luinstra

Date of Defense: 27.11.2020

Examiner 1: Prof. Dr. Volker Abetz

Examiner 2: Prof. Dr. Hans-Ulrich Moritz

Examiner 3: Priv. Doz. Dr. Christoph Wutz

The work presented in this dissertation was conducted from June, 2015-October, 2019 at the Institute of Polymer Research, Helmholtz-Zentrum Geesthacht (HZG) under the supervision of Prof. Dr. Volker Abetz.

## List of Publications

1. Block Copolymer Membranes from Polystyrene-*b*-poly(solketal methacrylate) (PS-*b*-PSMA) and Amphiphilic Polystyrene-*b*-poly(glyceryl methacrylate) (PS-*b*-PGMA). **Sarah Saleem**, Sofia Rangou, Clarissa Abetz, Brigitte Lademann, Volkan Filiz, Volker Abetz, *Polymers* 2017, 9(6), 216.
2. Isoporous Membranes from Novel Polystyrene-*b*-poly(4-vinylpyridine)-*b*-poly(solketal methacrylate) (PS-*b*-P4VP-*b*-PSMA) Triblock Terpolymers and Their Post-Modification. **Sarah Saleem**, Sofia Rangou, Clarissa Abetz, Volkan Filiz, Volker Abetz, *Polymers* 2020, 12(1), 41.

# Table of Contents

List of Figures	ix
List of Schemes	xiii
List of Tables	xiii
List of Symbols	xiv
List of Abbreviations	xv
<b>Chapter 1: Introduction</b>	<b>1</b>
1.1 Objective	6
1.2 Strategy of work and layout of the thesis	6
<b>Chapter 2: Theoretical background</b>	<b>8</b>
2.1 Anionic polymerization	8
2.1.1 Mechanism of anionic polymerization	9
2.1.2 Molar mass distribution in living polymerizations	14
2.2 Block copolymers	15
2.2.1 Self-assembly of block copolymers and phase separation behavior	16
2.2.2 Block copolymers in solution	20
2.3 Types of membranes	23
2.3.1 Phase separation membranes	24
2.3.2 Isoporous block copolymer membranes via SNIPS	25
<b>Chapter 3: Experimental work</b>	<b>31</b>
3.1. Materials	31
3.1.1 Cleaning of chemicals	31
3.1.2 Anionic polymerization of block copolymers	32
3.1.3 Synthesis of poly(solketal methacrylate) (PSMA) homopolymer	32
3.1.4 Synthesis of poly(glycidyl methacrylate) (PGM) homopolymer	33
3.1.5 Synthesis of polystyrene- <i>block</i> -poly(4-vinylpyridine) (PS- <i>b</i> -P4VP) diblock copolymer	34
3.1.6 Synthesis of polystyrene- <i>block</i> -poly(solketal methacrylate) (PS- <i>b</i> -PSMA) diblock copolymer	35
3.2 Modification of PS- <i>b</i> -PSMA diblock copolymers	37
3.2.1 Acidic hydrolysis of PS- <i>b</i> -PSMA	37

3.2.2 Synthesis of polystyrene- <i>block</i> -poly(glycidyl methacrylate) (PS- <i>b</i> -PGM) diblock copolymer .	37
3.3 Synthesis of triblock terpolymers by anionic polymerization .....	39
3.3.1 Synthesis of polystyrene- <i>block</i> -poly(4-vinylpyridine)- <i>block</i> -poly(solketal methacrylate) (PS- <i>b</i> -P4VP- <i>b</i> -PSMA) triblock terpolymer .....	39
3.3.2 Acidic hydrolysis of triblock terpolymers .....	40
3.3.3 Synthesis of polystyrene- <i>block</i> -poly(4-vinylpyridine)- <i>block</i> -poly(glycidyl methacrylate) (PS- <i>b</i> -P4VP- <i>b</i> -PGM) triblock terpolymer.....	41
3.4 Membrane formation.....	43
3.4.1 Hand casting.....	43
3.4.2 Machine casting .....	43
3.4.3 Spin coating of polymer film .....	44
3.4.4 Post modification of triblock terpolymer membranes.....	44
3.4.5 Preparation of GO/PGO-PS- <i>b</i> -PGMA membranes .....	44
3.5 Characterization techniques .....	45
3.5.1 Size exclusion chromatography (SEC) .....	45
3.5.2 Nuclear magnetic resonance spectroscopy (NMR) .....	46
3.5.3 Scanning electron microscopy (SEM) .....	47
3.5.4 Transmission electron microscopy (TEM) .....	49
3.5.5 Atomic force microscopy (AFM).....	50
3.5.6 Contact angle measurements .....	51
3.5.7 Water flux measurements.....	52
3.5.8 Static protein adsorption.....	53
3.5.9 Retention measurements.....	54
3.5.10 X-ray photoelectron spectroscopy (XPS).....	55
<b>Chapter 4: Results and discussion .....</b>	<b>56</b>
Synthesis of polystyrene- <i>b</i> -poly(solketal methacrylate) (PS- <i>b</i> -PSMA) and formation of membranes via SNIPS .....	56
4.1. Brief introduction .....	56
4.1.1 Synthesis and characterization of poly(solketal methacrylate) (PSMA) .....	56
4.1.2 Synthesis and characterization of polystyrene- <i>block</i> -poly(4-vinylpyridine) (PS- <i>b</i> -P4VP) diblock copolymer.....	58
4.1.3 Synthesis and characterization of polystyrene- <i>block</i> -poly(solketal methacrylate) (PS- <i>b</i> -PSMA) diblock copolymer .....	59
4.1.4 Bulk Morphology of the PS- <i>b</i> -PSMA diblock copolymers .....	63
4.1.5 Membrane fabrication via SNIPS.....	65
4.2. A comparative study of amphiphilic polystyrene- <i>b</i> -poly(glyceryl methacrylate) (PS- <i>b</i> -PGMA) and hydrophobic polystyrene- <i>b</i> -poly(solketal methacrylate) (PS- <i>b</i> -PSMA) membranes .....	70

4.2.1 Brief Introduction .....	70
4.2.2 Acidic hydrolysis of PS- <i>b</i> -PSMA and formation of PS- <i>b</i> -PGMA diblock copolymer .....	70
4.2.3 Protection of hydroxyl groups (-OH) of PGMA.....	72
4.2.4 Benzoylation of polystyrene- <i>block</i> -poly(glyceryl methacrylate) (PS- <i>b</i> -PGMA).....	72
4.2.5 Silylation of polystyrene- <i>block</i> -poly(glyceryl methacrylate) (PS- <i>b</i> -PGMA).....	73
4.2.6 Analysis of bulk morphology of the PS- <i>b</i> -PGMA by TEM .....	75
4.2.7 Fabrication of PS- <i>b</i> -PGMA membranes via SNIPS.....	77
4.2.8 Addition of nano-fillers.....	81
4.2.9 Addition of PDEA-GO to the PS- <i>b</i> -PGMA polymer solution .....	85
4.2.10 Membrane morphology and functional group characterization .....	86
4.2.11 Comparison of static adsorption of proteins/antifouling behavior .....	91
4.2.12 Comparison of dynamic contact angle measurements.....	93
4.2.13 Water flux measurements.....	94
<b>Chapter 5 .....</b>	<b>97</b>
Isoporous membranes from novel polystyrene- <i>b</i> -poly(4-vinylpyridine)- <i>b</i> -poly(solketal methacrylate) (PS- <i>b</i> -P4VP- <i>b</i> -PSMA) triblock terpolymers and their post-modification.....	97
5.1. Brief Introduction .....	97
5.1.1 Synthesis and characterization of polystyrene- <i>block</i> -poly(4-vinylpyridine)- <i>block</i> -poly(solketal methacrylate) (PS- <i>b</i> -P4VP- <i>b</i> -PSMA) triblock terpolymer.....	98
5.1.2 Bulk morphology of the triblock terpolymers .....	101
5.1.3 Preparation of the membrane by SNIPS .....	103
5.1.4 Post-modification of PS <sub>71</sub> - <i>b</i> -P4VP <sub>17</sub> - <i>b</i> -PSMA <sub>12</sub> <sup>91</sup> triblock terpolymer.....	107
5.1.5 Membrane fabrication after post-modification of triblock terpolymer .....	109
5.1.6 Post-modification of PS <sub>71</sub> - <i>b</i> -P4VP <sub>26</sub> - <i>b</i> -PSMA <sub>3</sub> <sup>145</sup> membranes.....	110
5.2 Comparison of the performance of membranes .....	110
5.2.1 Comparison of contact angle measurements .....	111
5.2.2 Water permeation and pH responsive behavior .....	112
5.2.3 BSA retention measurements .....	114
5.2.4 Static adsorption of hemoglobin.....	115
<b>Chapter 6: Summary and outlook.....</b>	<b>118</b>
6.1. Summary and outlook .....	118
6.2. Zusammenfassung und Ausblick .....	120
<b>Chapter 7: References .....</b>	<b>122</b>
<b>Chapter 8: Appendix .....</b>	<b>137</b>
8.1.Toxicity of chemicals .....	137
8.2. Calculation of the solubility parameters according to HOY method.....	139

8.3. Synthesis and characterization of poly(glycidyl methacrylate) (PGM) homopolymer.....	141
8.3.1 Synthesis and characterization of polystyrene- <i>block</i> -poly(glycidyl methacrylate) (PS- <i>b</i> -PGM) diblock copolymer .....	142
8.3.2 Synthesis and characterization of polystyrene- <i>block</i> -poly(4-vinylpyridine)- <i>block</i> -poly(glycidyl methacrylate) (PS- <i>b</i> -P4VP- <i>b</i> -PGM) triblock terpolymer .....	144
<b>Acknowledgements</b>	<b>147</b>
<b>Curriculum Vitae</b>	<b>148</b>
<b>Declaration of Oath</b>	<b>149</b>

## List of Figures

<b>Figure 1. 1.</b> Membrane separation processes for water purification and desalination based on the size of solute. Reprinted with permission from ref [7].....	2
<b>Figure 1. 2.</b> Schematic illustration of a wide range of target applications where block copolymer membranes with well-controlled functional pore wall chemistries could be utilized. Reprinted with permission from ref [19].....	3
<b>Figure 2. 1.</b> Molecular weight conversion curves for various kinds of polymerization methods (A) living polymerization (B) free radical polymerization and (C) condensation polymerization. Reprinted with permission from ref [55] .....	9
<b>Figure 2. 2.</b> Typical structures of block copolymers containing A, B and C block .....	15
<b>Figure 2. 3.</b> Theoretical phase diagram of a linear diblock copolymer by self-consistent mean field theory. Body-centered cubic (BCC), hexagonally packed cylinder (HEX), minimal surfaces (gyroid (GYR) and alternating simple lamellar phase (LAM). Reprinted with permission from ref [84]. .....	18
<b>Figure 2. 4.</b> Ternary phase diagram of polystyrene- <i>block</i> -polybutadiene- <i>block</i> -poly(methyl methacrylate) (SBM) triblock terpolymers. Reprinted with permission from ref [102].....	20
<b>Figure 2. 5.</b> Basic morphologies of (AB) block copolymer aggregates in solution. Reprinted with permission from ref [106, 107] .....	21
<b>Figure 2. 6.</b> Schematic representation of different types of micelles formed by ABC triblock terpolymers. Core-shell-corona micelles with a compartmentalized core (a), micelles with a mixed corona (no chain segregation) (b), core-shell-corona micelles with a compartmentalized corona (radial chain segregation) (c), Janus micelles with an asymmetric corona (lateral chain segregation) (d), and vesicles (e). Reprinted with permission from ref [99]. .....	22
<b>Figure 2. 7.</b> Schematic illustration of symmetric and asymmetric membrane structure. Reprinted with permission from ref [112].....	24
<b>Figure 2. 8.</b> Scanning electron microscopy (SEM) images of the surface and cross-section of the integral asymmetric isoporous PS- <i>b</i> -P4VP diblock copolymer film following SNIPS. The scale bar correspond to 500 nm. The evaporation time before immersion into non-solvent bath is 10 s. Reprinted with permission from ref [121] .....	27
<b>Figure 2. 9.</b> Schematic illustration of the structure formation of isoporous membrane from the solution: i) Disordered or weakly segregated diblock copolymer in mixed selective solvents (  polystyrene rich domains,  poly(4-vinylpyridine) rich domains ii) microphase separation with polystyrene rich matrix after film casting; iii) solidification of the matrix due to solvent evaporation; iv) open pores in the poly(4-vinylpyridine) rich domains after non-solvent induced phase separation; v) Porous structure of dried membrane. This figure is reprinted from reference.[122] .....	27
<b>Figure 2. 10.</b> Representation of possible hydrogen bonding between PS- <i>b</i> -P4VP as hydrogen bond acceptor and carbohydrate molecule. Reprinted with permission from ref [139].....	29

<b>Figure 3. 1.</b> Schematic representation (a) and (b) of the in-house built casting machine used for fabrication of membrane via SNIPS. Reprinted with permission from ref [123].....	44
<b>Figure 3. 2.</b> Illustration of separation principle of size exclusion chromatography.[145] .....	46
<b>Figure 3. 3.</b> Representative image of key components of Scanning Electron Microscope (SEM).[148] .....	48
<b>Figure 3. 4.</b> Schematic illustration of the primary electron interaction with sample and generation of secondary electrons, back scattered electrons and X-ray radiation.[149].....	48
<b>Figure 3. 5.</b> Main components of Transmission Electron Microscopy.[150].....	49
<b>Figure 3. 6.</b> Schematic illustration of contact angle .....	51
<b>Figure 3. 7.</b> Classification of surfaces based on contact angle with water.....	52
<b>Figure 3. 8.</b> Test cell EMD Millipore™ XFUF04701 .....	54
<b>Figure 4.1.1.</b> <sup>1</sup> H-NMR spectra of PSMA homopolymer in CDCl <sub>3</sub> .....	57
<b>Figure 4.1.2.</b> <sup>1</sup> H-NMR spectra of PS <sub>85</sub> - <i>b</i> -P4VP <sub>15</sub> <sup>166</sup> in CDCl <sub>3</sub> .....	58
<b>Figure 4.1.3.</b> <sup>1</sup> H-NMR spectrum of PS <sub>81</sub> - <i>b</i> -PSMA <sub>19</sub> <sup>170</sup> in CDCl <sub>3</sub> .....	60
<b>Figure 4.1.4.</b> SEC traces of PS homopolymer and PS <sub>81</sub> - <i>b</i> -PSMA <sub>19</sub> <sup>170</sup> diblock copolymer (measurement in THF at 30 °C using PS standards).....	61
<b>Figure 4.1.5.</b> TEM image of an ultrathin section of PS <sub>81</sub> - <i>b</i> -PSMA <sub>19</sub> <sup>170</sup> , film cast from 5 wt% polymer solution in THF, the diameter of the brighter spheres is approximately 25-30 nm ...	64
<b>Figure 4.1.6.</b> SEM images of the top surface of cast membranes from 24 wt% PS <sub>76</sub> - <i>b</i> -PSMA <sub>24</sub> <sup>200</sup> from (left) THF/DMF 50/50 wt%, (right) THF/DMF 40/60 wt%. The time of evaporation before the immersion into the precipitant was 10 s.....	66
<b>Figure 4.1.7.</b> SEM topography images of the surface of the generated membrane from 25 wt% PS <sub>76</sub> - <i>b</i> -PSMA <sub>24</sub> <sup>200</sup> in THF/DMF 30/70 wt% with evaporation time 10 s (left) and 20 s (right).....	67
<b>Figure 4.1.8.</b> SEM images of surfaces of the membranes made from 24 wt% PS <sub>81</sub> - <i>b</i> -PSMA <sub>19</sub> <sup>170</sup> in THF/DMF 50/50 wt%. Evaporation time before immersion: (a) 5 s, (b) 10 s, (c) 20 s, (d) 25 s. ....	68
<b>Figure 4.1. 9.</b> SEM images of the cross-section of the membrane prepared from 24 wt% PS <sub>81</sub> - <i>b</i> -PSMA <sub>19</sub> <sup>170</sup> in THF/DMF 50/50 wt% at (a) 5 s, (b) 25 s time of evaporation.....	69
<b>Figure 4.2.1.</b> <sup>1</sup> H-NMR spectrum of PS- <i>b</i> -PGMA after the removal of 1, 3-dioxolane ring of PSMA block.....	71
<b>Figure 4.2.2.</b> Structure of benzoylated PS- <i>b</i> -PGMA diblock copolymer .....	73
<b>Figure 4.2.3.</b> Silylation of PS- <i>b</i> -PGMA diblock copolymer.....	74
<b>Figure 4.2.4.</b> TEM image of an ultrathin section of PS <sub>81</sub> - <i>b</i> -PSMA <sub>19</sub> <sup>170</sup> , film cast from 5 wt% diblock copolymer solution in DMF, the diameter of the brighter spheres is approximately 30-35 nm.....	76
<b>Figure 4.2.5.</b> TEM image of an ultrathin section of PS <sub>82</sub> - <i>b</i> -PSMA <sub>18</sub> <sup>126</sup> , film cast from diblock copolymer in THF and DMF solution, stained with RuO <sub>4</sub> (20min).....	77

<b>Figure 4.2.6.</b> SEM topography images of membranes prepared from (a) 23 wt% PS <sub>76</sub> - <i>b</i> -PSMA <sub>24</sub> <sup>135</sup> and (b) 23 wt% PS <sub>81</sub> - <i>b</i> -PGMA <sub>19</sub> <sup>128</sup> in THF/DMF 50/50 wt%. The corresponding cross-section views for each case are shown in (c) and (d) images, respectively. The time of evaporation was 10s. ....	78
<b>Figure 4.2.7.</b> SEM images of surface of the membranes prepared from 22 wt % PS <sub>81</sub> - <i>b</i> -PGMA <sub>19</sub> <sup>128</sup> in THF/DMF/DOX (1:1:1); time of evaporation (a) 10 s (b) 20 s. ....	80
<b>Figure 4.2.8.</b> SEM images of surface of the membranes prepared from 23 wt% (left) PS <sub>82</sub> - <i>b</i> -PGMA <sub>18</sub> <sup>126</sup> (right) PS <sub>79</sub> - <i>b</i> -PGMA <sub>21</sub> <sup>120</sup> in THF/DMF/DOX (2:1:1); time of evaporation 20 s. 81	
<b>Figure 4.2.9.</b> Structure of graphene oxide layer.[171] .....	82
<b>Figure 4.2.10.</b> SEM images of surface of the membranes prepared from 23 wt% PS <sub>82</sub> - <i>b</i> -PGMA <sub>18</sub> <sup>126</sup> (a) pristine membrane, time of evaporation 20 s. (b) 0.5 (c) 1 wt% GO nanosheets in THF/DMF/DOX (2:1:1); time of evaporation 10 s.....	83
<b>Figure 4.2.11.</b> Surface SEM images of the membranes prepared from 23 wt% PS <sub>82</sub> - <i>b</i> -PGMA <sub>18</sub> <sup>126</sup> 1 wt% GO nanosheets in THF/DMF/DOX (2:1:1); time of evaporation 10 s.....	84
<b>Figure 4.2.12.</b> The cross-sectional SEM images of pristine (a) 23 wt% PS <sub>82</sub> - <i>b</i> -PGMA <sub>18</sub> <sup>126</sup> (b) 1 wt% GO in PS <sub>82</sub> - <i>b</i> -PGMA <sub>18</sub> <sup>126</sup> in THF/DMF/DOX (2:1:1). The evaporation time after addition of GO was shifted to 10 s. ....	85
<b>Figure 4.2.13.</b> SEM images of surface and cross-section of the membranes prepared from 23 wt% PS <sub>82</sub> - <i>b</i> -PGMA <sub>18</sub> <sup>126</sup> in THF/DMF/DOX (2:1:1); time of evaporation 20 s. ....	87
<b>Figure 4.2.14.</b> Scanning electron micrograph images of cross section and surface (from left to right) with 1.5 % (w/w) PDEA-GO in THF/DMF/DOX (2:1:1). The evaporation time after addition of PDEA-GO nanosheets was shifted to 10 s.....	88
<b>Figure 4.2.15.</b> XPS analysis of PS- <i>b</i> -PGMA diblock copolymer membrane and hybrid membranes of PS- <i>b</i> -PGMA/PDEA-GO nanosheets .....	89
<b>Figure 4.2.16.</b> Atomic force micrograph of the surface and three dimensional images of membranes (a) PS- <i>b</i> -PGMA (b) 1.5 wt% PS- <i>b</i> -PGMA/PDEA-GO nanosheets .....	89
<b>Figure 4.2.17.</b> SEM topography and cross-section images of membranes prepared from (left) 23 wt% PS <sub>82</sub> - <i>b</i> -PGMA <sub>18</sub> <sup>126</sup> in THF/DMF/DOX (2:1:1) and (right) 28 wt% PS <sub>81</sub> -P4VP <sub>19</sub> <sup>123</sup> in THF/DMF 50/50 wt%. The corresponding cross-section views for each case are shown under the surface images (left) and (right), respectively. The time of evaporation was 10 s (left) and 5 s (right) .....	92
<b>Figure 4.2.18.</b> Adsorbed amount of foulants bovine serum albumin (BSA), gamma globulin (γ-Glob), hemoglobin (Hem) at pH 7.4 for PS <sub>82</sub> - <i>b</i> -PGMA <sub>18</sub> <sup>126</sup> and PS <sub>81</sub> - <i>b</i> -P4VP <sub>19</sub> <sup>123</sup> membranes .....	93
<b>Figure 4.2.19.</b> Graphical representation of the dynamic contact angle measurement of water droplets (5 μL) onto membrane surfaces developed from block copolymers PS <sub>76</sub> - <i>b</i> -PSMA <sub>24</sub> <sup>135</sup> and PS <sub>81</sub> - <i>b</i> -PGMA <sub>19</sub> <sup>128</sup> (previously shown in Figure 4.2.6 a, b).....	94
<b>Figure 4.2.20.</b> Time dependent water flux measurements of PS <sub>81</sub> - <i>b</i> -PGMA <sub>19</sub> <sup>128</sup> membrane .	95
<b>Figure 5.1.1.</b> <sup>1</sup> H-NMR spectra of PS <sub>71</sub> - <i>b</i> -P4VP <sub>26</sub> - <i>b</i> -PSMA <sub>3</sub> <sup>145</sup> in CDCl <sub>3</sub> .....	98
<b>Figure 5.1.2.</b> SEC chromatogram of PS homopolymer, PS- <i>b</i> -P4VP and PS <sub>72</sub> - <i>b</i> -P4VP <sub>17</sub> - <i>b</i> -PSMA <sub>11</sub> <sup>91</sup> triblock terpolymer (measurement in THF at 30 °C using PS standards).....	99

<b>Figure 5.1.3.</b> TEM micrographs of PS- <i>b</i> -P4VP- <i>b</i> -PSMA triblock terpolymer cast from chloroform (a) PS <sub>71</sub> - <i>b</i> -P4VP <sub>17</sub> - <i>b</i> -PSMA <sub>12</sub> <sup>91</sup> stained with RuO <sub>4</sub> (b), with RuO <sub>4</sub> and I <sub>2</sub> .....	102
<b>Figure 5.1. 4.</b> (a) TEM image of PS <sub>71</sub> - <i>b</i> -P4VP <sub>26</sub> - <i>b</i> -PSMA <sub>3</sub> <sup>145</sup> stained with I <sub>2</sub> (b) AFM height image (in tapping mode) of the film surface of the asymmetric PS <sub>71</sub> - <i>b</i> -P4VP <sub>26</sub> - <i>b</i> -PSMA <sub>3</sub> <sup>145</sup> triblock terpolymer.....	102
<b>Figure 5.1.5.</b> SEM images of PS <sub>71</sub> - <i>b</i> -P4VP <sub>26</sub> - <i>b</i> -PSMA <sub>3</sub> <sup>145</sup> membrane surfaces prepared from different solutions: 22 wt% copolymer at 10 sec evaporation time in (a) 60/40 THF/DMF; (b) 50/50 THF/DMF; (c) 70/30 THF/DMF .....	103
<b>Figure 5.1.6.</b> SEM images of the PS <sub>71</sub> - <i>b</i> -P4VP <sub>26</sub> - <i>b</i> -PSMA <sub>3</sub> <sup>145</sup> membranes cast from a 22 wt% copolymer solution in (a) THF/DMF/DOX 1/1/1 (b) THF/DMF/DOX 40/30/30. The evaporation time before immersion into the precipitant was 10 seconds. ....	104
<b>Figure 5.1.7.</b> SEM images of (a) top view and (b) cross-section of PS <sub>71</sub> - <i>b</i> -P4VP <sub>26</sub> - <i>b</i> -PSMA <sub>3</sub> <sup>145</sup> membranes cast from 22 wt% solution in a THF/DMF/acetone: 50/30/20 wt%. Evaporation time was 10 seconds before immersion in water .....	105
<b>Figure 5.1.8.</b> Surface SEM images of PS <sub>71</sub> - <i>b</i> -P4VP <sub>26</sub> - <i>b</i> -PSMA <sub>3</sub> <sup>145</sup> membranes cast from solutions THF/DMF/Acetone: 50/30/20 wt%. (a) 20 seconds (b) 30 seconds evaporation time before immersion into non-solvent bath.....	106
<b>Figure 5.1.9.</b> Surface SEM images of PS <sub>71</sub> - <i>b</i> -P4VP <sub>26</sub> - <i>b</i> -PSMA <sub>3</sub> <sup>145</sup> membranes cast from 21 wt%, 23 wt%, and 24 wt% terpolymer solutions in THF/DMF/Acetone: 50/30/20 wt%. The evaporation time before immersion into the precipitant was 10 s.....	107
<b>Figure 5.1.10.</b> <sup>1</sup> H-NMR spectrum of the linear triblock terpolymer PS <sub>71</sub> - <i>b</i> -P4VP <sub>17</sub> - <i>b</i> -PGMA <sub>12</sub> <sup>91</sup> in DMF- <i>d</i> <sub>7</sub> .....	108
<b>Figure 5.1.11.</b> SEM images of (a) PS <sub>71</sub> - <i>b</i> -P4VP <sub>17</sub> - <i>b</i> -PSMA <sub>12</sub> <sup>91</sup> membrane (b) PS <sub>71</sub> - <i>b</i> -P4VP <sub>17</sub> - <i>b</i> -PGMA <sub>12</sub> <sup>91</sup> membrane obtained after acidic hydrolysis. The evaporation time before immersion into water bath was 10 s. ....	110
<b>Figure 5.2.1.</b> Dynamic contact angle measurements of water droplets (2μL each) onto the PS <sub>71</sub> - <i>b</i> -P4VP <sub>26</sub> - <i>b</i> -PSMA <sub>3</sub> <sup>145</sup> (black squares) and PS <sub>71</sub> - <i>b</i> -P4VP <sub>26</sub> - <i>b</i> -PGMA <sub>3</sub> <sup>145</sup> (red circles) membranes .....	111
<b>Figure 5.2.2.</b> SEM images of pristine PS <sub>71</sub> - <i>b</i> -P4VP <sub>26</sub> - <i>b</i> -PSMA <sub>3</sub> <sup>145</sup> membrane before acidic hydrolysis and (b) PS <sub>71</sub> - <i>b</i> -P4VP <sub>26</sub> - <i>b</i> -PGMA <sub>3</sub> <sup>145</sup> membrane.....	112
<b>Figure 5.2.3.</b> Water permeability of PS <sub>71</sub> - <i>b</i> -P4VP <sub>26</sub> - <i>b</i> -PGMA <sub>3</sub> <sup>145</sup> membrane measured at various pH, at pH > 4 high water permeability was observed, due to deswelling of the deprotonated P4VP blocks at larger pH, leading to their collapse on the pore walls .....	113
<b>Figure 5.2.4.</b> Protein adsorption of hemoglobin of PS <sub>74</sub> - <i>b</i> -P4VP <sub>26</sub> <sup>162</sup> , PS <sub>71</sub> - <i>b</i> -P4VP <sub>26</sub> - <i>b</i> -PSMA <sub>3</sub> <sup>145</sup> and PS <sub>71</sub> - <i>b</i> -P4VP <sub>26</sub> - <i>b</i> -PGMA <sub>3</sub> <sup>145</sup> membranes at pH 7.4 .....	116
<b>Figure 8. 1.</b> <sup>1</sup> H-NMR spectra of PGMA homopolymer in CDCl <sub>3</sub> .....	142
<b>Figure 8. 2.</b> <sup>1</sup> H-NMR spectrum of PS <sub>79.5</sub> - <i>b</i> -PGM <sub>20.5</sub> <sup>112</sup> in CDCl <sub>3</sub> .....	143
<b>Figure 8. 3.</b> SEC chromatogram of PS homopolymer and PS <sub>79.5</sub> - <i>b</i> -PGM <sub>20.5</sub> <sup>112</sup> diblock copolymer.....	144
<b>Figure 8. 4.</b> <sup>1</sup> H-NMR spectra of PS- <i>b</i> -P4VP- <i>b</i> -PGM in CDCl <sub>3</sub> .....	145

## List of Schemes

<b>Scheme 2. 1.</b> Attachment of anion to monomer and delocalization of charge .....	8
<b>Scheme 2. 2.</b> General way to initiate styrene with (a) mono and (b) di-functional initiators..	11
<b>Scheme 2. 3.</b> Side reactions in the polymerization of methyl methacrylate, (a) initiator attack on the monomer ester group (b) backbiting reaction of enolate anion.....	12
<b>Scheme 2. 4.</b> Ion pairs in a polar solvent for different concentrations.[61-63] .....	13
<b>Scheme 3. 1.</b> Synthesis of PSMA homopolymer .....	33
<b>Scheme 3. 2.</b> Synthesis of PGM homopolymer .....	34
<b>Scheme 3. 3.</b> Synthesis of PS- <i>b</i> -P4VP.....	35
<b>Scheme 3. 4.</b> Synthetic route leading to PS- <i>b</i> -PSMA by sequential anionic polymerization of styrene and solketal methacrylate .....	36
<b>Scheme 3. 5.</b> Acidic hydrolysis of PS- <i>b</i> -PSMA .....	37
<b>Scheme 3. 6.</b> Synthetic route leading to PS- <i>b</i> -PGM by sequential anionic polymerization of styrene and glycidyl methacrylate (GM).....	38
<b>Scheme 3. 7.</b> General reactions for the synthesis of PS- <i>b</i> -P4VP- <i>b</i> -PSMA triblock terpolymer <i>via</i> sequential anionic polymerization.....	40
<b>Scheme 3. 8.</b> Deprotection reaction of the ketal-PSMA moiety.....	41
<b>Scheme 3. 9.</b> General reactions for the synthesis of linear triblock terpolymer PS- <i>b</i> -P4VP- <i>b</i> -PGM by following anionic polymerization technique. ....	42

## List of Tables

<b>Table 4. 1.</b> Molecular weight and dispersity index of the PSMA homopolymer .....	57
<b>Table 4. 2.</b> Molecular weight, weight percentage of P4VP and dispersity index of PS- <i>b</i> -P4VP .....	59
<b>Table 4. 3.</b> Characterization data of PS- <i>b</i> -PSMA diblock copolymers .....	61
<b>Table 4. 4.</b> Hansen solubility parameters ( $\delta$ ) of homopolymers, solvents and non-solvents [157] .....	63
<b>Table 4. 5.</b> Characterization data of PS- <i>b</i> -PGMA diblock copolymers .....	75
<b>Table 4. 6.</b> Roughness parameters for membranes PS- <i>b</i> -PGMA and PS- <i>b</i> -PGMA/PDEA-GO nanosheets .....	91
<b>Table 5. 1.</b> Composition and molecular weights of PS- <i>b</i> -P4VP- <i>b</i> -PSMA triblock terpolymer .....	100
<b>Table 5. 2.</b> Retention results from experiments in a 1 mg/1 mL BSA solution in (PBS buffer pH = 7.4). ....	114

<b>Table 8. 1.</b> Molecular weight and dispersity index of the PGM homopolymer .....	142
<b>Table 8. 2.</b> Characterization data of PS- <i>b</i> -PGM block copolymers .....	143
<b>Table 8. 3.</b> Characterization data of PS- <i>b</i> -P4VP- <i>b</i> -PGM triblock terpolymer .....	146

### List of Symbols

$\alpha$	Molecular aggregation number
$b$	Grafting distance
$\delta_D$	Dispersion solubility parameter
$\delta_P$	Polar solubility parameter,
$\delta_H$	Hydrogen Bonding solubility parameter
$m_0$	Mass of the protein before the adsorption
$m_1$	Mass of the protein after the adsorption
$\Delta t$	Time between two mass measurements
$\Delta p$	Trans-membrane pressure
$\lambda$	Wavelength
$A$	Active surface area of the membrane
$AB$	Diblock copolymer with A and B block
$ABC$	Triblock terpolymer with A, B and C block
$\mathcal{D}$	Dispersity index
$F_t$	Molar attraction function
$F_p$	Polar component
$N$	Degree of polymerization
$R_a$	Mean surface roughness
$R_q$	Root mean square
$V$	Molar volume

## List of Abbreviations

AFM	Atomic Force Microscopy
BCP	Block copolymer
BSA	Bovine Serum Albumin
C or C'	Cylinder
CaH <sub>2</sub>	Calcium Hydride
CDCl <sub>3</sub>	Deuterated chloroform
DMAc	Dimethylacetamide
DMF	<i>N,N</i> -dimethylformamide
DOX	Dioxane
DPE	1,1-Diphenylethylene
EtAlCl <sub>2</sub>	Ethylaluminium dichloride
G or G'	Gyroid
GO	Graphene oxide
γ-Glob	Gamma-Globulin
<sup>1</sup> H-NMR	Proton nuclear magnetic resonance spectroscopy
HCl	Hydrochloric acid
Hem	Hemoglobin
IPGMA	<i>Iso</i> -propylglyceryl methacrylate
IEP	Isoelectric point
L	Lamellar
LiCl	Lithium chloride
MeOH	Methanol
MgBu <sub>2</sub>	Dibutylmagnesium
M <sub>n</sub>	Number average molecular weight

$M_w$	Weight average molecular weight
MWCO	Molecular weight cut-off
MWD	Molecular weight distribution
NaOH	Sodium hydroxide
NH	Amine
NIPS	Non-solvent induced phase separation
PDEAEMA	Poly(2-(diethylamino)ethyl methacrylate)
PGM	Poly(glycidyl methacrylate)
PGMA	Poly(glyceryl methacrylate)
PS	Polystyrene
PSF	Polysulfone
PSMA	Poly(solketal methacrylate)
PS- <i>b</i> -P4VP	Polystyrene- <i>block</i> -poly(4-vinylpyridine)
PS- <i>b</i> -PGM	Polystyrene- <i>block</i> -poly(glycidyl methacrylate)
PS- <i>b</i> -PGMA	Polystyrene- <i>block</i> -poly(glyceryl methacrylate)
PS- <i>b</i> -PSMA	Polystyrene- <i>block</i> -poly(solketal methacrylate)
PS- <i>b</i> -P4VP- <i>b</i> -PSMA	Polystyrene- <i>block</i> -poly(4-vinylpyridine)- <i>block</i> -poly(solketal methacrylate)
PS- <i>b</i> -P4VP- <i>b</i> -PGMA	Polystyrene- <i>block</i> -poly(4-vinylpyridine)- <i>block</i> -poly(glyceryl methacrylate)
PS- <i>b</i> -PQ4VP- <i>b</i> -PGMA	Polystyrene- <i>block</i> -quarternized poly(4-vinylpyridine)- <i>block</i> -poly(glyceryl methacrylate)
PS- <i>b</i> -P4VP- <i>b</i> -PGM	Polystyrene- <i>block</i> -poly(4-vinylpyridine)- <i>block</i> -poly(glycidyl methacrylate)
PVDF	Poly(vinylidene fluoride)
RuO <sub>4</sub>	Rutheniumtetraoxide

S or S'	Spherical
<i>sec</i> -BuLi	<i>sec</i> -butyl lithium
SEC	Size-exclusion Chromatography
SEM	Scanning Electron Microscopy
SH	Thiol
SNIPS	Self-assembly and non-solvent induced phase separation
SSL	Strong segregation limit
TEM	Transmission Electron Microscopy
THF	Tetrahydrofuran
TMS	Tetramethylsilane
4VP	4-vinyl pyridine
WSL	Weak segregation limit
XPS	X-ray Photoelectron Spectroscopy

## **Chapter 1: Introduction**

Water is one of the most precious resources for life. Although there are many sources of water on the planet but most of them are dispensable or have inadequate quality for human consumption or chemical and pharmaceutical industry/agricultural purposes. Increasing demands of industrialization, urbanization and climate change are major factors on the way to access clean water. It becomes one of the biggest challenges of our time to access fresh water. The world population is rapidly increasing overall and over one third of world's population lives in the developing countries, where the economic impact of poor water and sanitation ability is devastating. The contamination of drinking water resources by flowing streams of wastewater (e.g., industrial, municipal and agricultural wastewater) is a worldwide problem. To address this challenge, there is an important need for the development of energetically efficient, low cost and sustainable methods for decontamination of water [1-3].

Membrane-based technologies are currently used in various processes for gas separation, bioprocessing, biomedical applications, chemical productions, and considered inherently more energy efficient than thermal separation approaches [4]. In the field of water, reverse osmosis (RO) membranes of satisfactory flux and salt rejection are well-established for seawater desalination [5]. With the development of modern science and technologies, various materials have been applied for the fabrication of polymeric hemodialysis membranes [6].

Size based separation of particles through membrane technology can be divided according to the size of solutes in four types: microfiltration (MF) (0.1-10  $\mu\text{m}$ ), ultrafiltration (UF) (2-100 nm), nanofiltration (NF) (1-10 nm) and reverse osmosis (RO) (less than 1 nm), a process as shown in Figure 1.1.

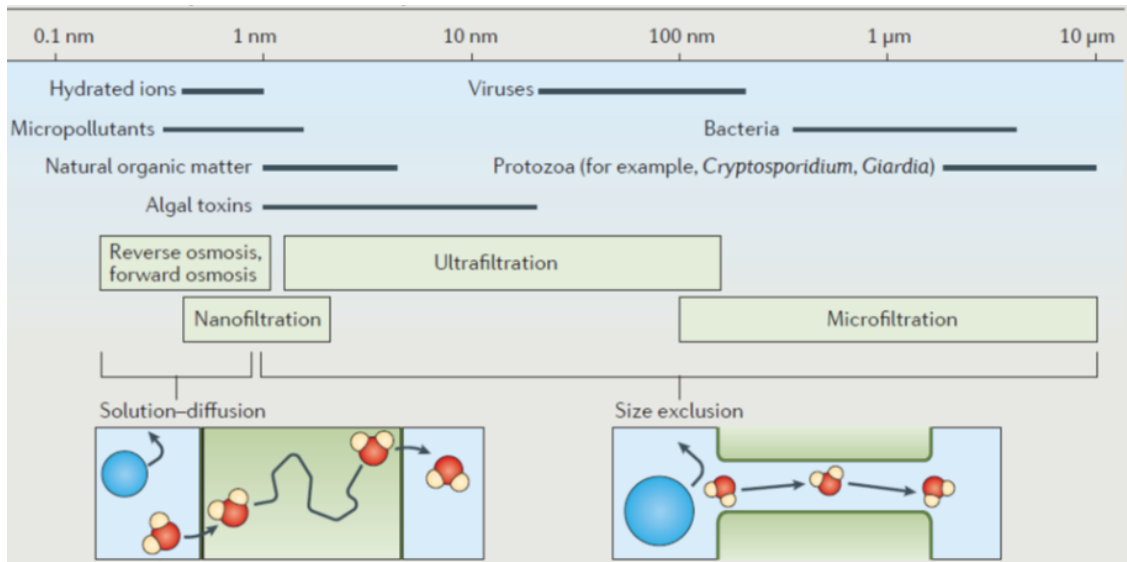


**Figure 1.** Membrane separation processes for water purification and desalination based on the size of solute. Reprinted with permission from ref [7].

MF and UF membranes separation are based on the size of the solute, In specie solutes larger than the membrane pore size are rejected/retained on the membrane surface [8] [9]. RO membranes are dense (non-porous) membranes that can remove salts from water through solution-diffusion mechanism [10]. NF membranes are using a combination of diffusive, convective and electrostatic models for separation of multivalent ions [11, 12]. MF and UF membranes are useful for removing large colloids, microbes and viruses from the feed. In the field of biomedicines, membrane technology plays a vital role in the hemodialysis (purifying blood) to treat chronic kidney failure which saves the lives of more than 2.5 million patients worldwide [13]. For the targeted separations, well-defined nanostructure and surface properties of block copolymer membranes can be modified chemically to the specific demands, considered an emerging area of study [14, 15]. Self-assembled membranes with specific functional moieties have been achieved in several ways, including the incorporation of the desired chemistry into the precursor block copolymer material during synthesis with the purpose of the fabrication of porous membranes where the pore wall constitutes from the respective functional groups. Polystyrene-*block*-poly(4-vinylpyridine) (PS-*b*-P4VP) block copolymers represent this type of

system due to the presence of the functional P4VP block which can, for example, form complexes with metal salts. Apart from size-selective membranes decorated with specific functionalities, advanced technologies also focus on charge-selective membranes that exhibit preferential permeability for electrolytes and retain small nonionic molecules [16-18].

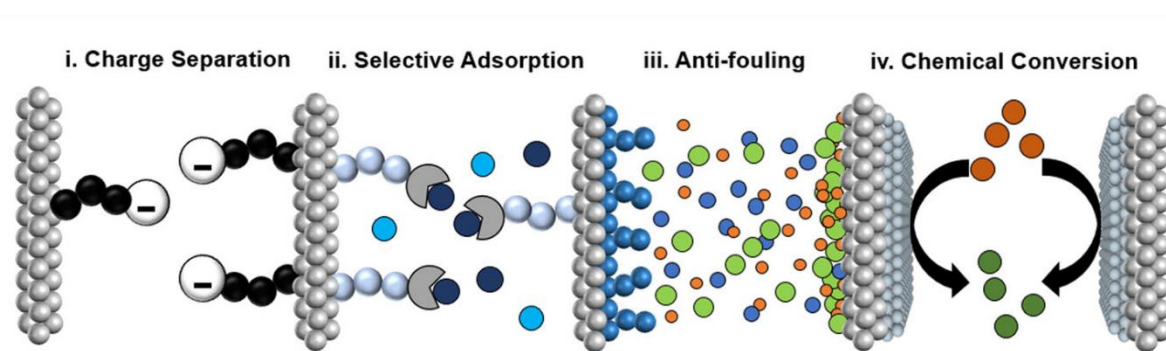


**Figure 1. 2.** Schematic illustration of a wide range of target applications where block copolymer membranes with well-controlled functional pore wall chemistries could be utilized. Reprinted with permission from ref [19].

In the field of water purification and protein separation, block copolymer filtration membranes attracted immense attention [20-23]. To date, majority of the membranes have been modified using chemistries aimed at reducing the deleterious effects of fouling. Foulants like proteins, emulsified oils, microorganisms, and a fraction of natural organic matters can be separated by many polymeric membranes, as a higher affinity for adhesion is observed for hydrophobic than hydrophilic membranes. Poor antifouling properties are mainly caused by the hydrophobic behavior of membranes surfaces. Therefore, many surface modifications focus on hydrophilizing a hydrophobic membrane surface, as it is hypothesized that surfaces with these chemical properties are prone to tightly bind a thin layer of water, providing a steric or energetic barrier to adhesion [24-26]. Hydrophilic surfaces which do not contain hydrogen bond donor but only acceptor functions or are neutral, tend to be best at resisting protein adhesion [4, 27-31].

Block copolymer membranes fabrication with a focus on reducing the fouling propensity involves different approaches from simple coating, to radiation and photochemical grafting of hydrophilic polymers [32, 33], or using directly synthesized appropriate block copolymers for the membrane formation. Block copolymer membranes may be directly coated with another material that is simply adsorbed to the membrane surface through (e.g., van der Waals or electrostatic interactions) [34, 35] or covalently coupled to the membrane polymer to afford enhanced stability [36]. One of the earliest published works to improve the biocompatibility of block copolymer membranes was performed by Matsuda and Ito. They coated a hydrophobic polyacrylonitrile hemodialyser membrane with block copolymers of poly(methyl methacrylate) and a hydrophilic segment of either poly(methoxy polyethylene glycol methacrylate) or poly(dimethyl acrylamide) [37].

Another approach was to tailor the surface chemistry of membranes by the addition of surface modifying macromolecules/additives in the membrane casting solution. In related studies, hydrophilic surface modifying macromolecules of polyurethanes end-capped with poly(ethylene glycol) (PEG) were incorporated in the poly(ether sulfone) (PES) casting solution. The resulting membranes showed high water flux and lower contact angle measurements than the PES membranes [38]. Blending of block copolymers was shown to be a facile way to tune the pore size of isoporous membranes [39] and to alter in parallel the transport properties of the membranes. Ma and co-workers reported high protein adsorption resistant ultrafiltration membranes by blending an amphiphilic copolymer PS-*b*-PEG with PES membranes [40, 41]. More specifically it was reported that during the process of the pore formation, the hydrophilic block was prone to come to the surface of the membrane, decreasing the contact angle.

Rather than incorporating a material into the casting solution or coating the membrane surface to impart desirable properties, our aim was to design new functional block copolymers with

improved hydrophilic and thus also antifouling properties, and furthermore to find ways to design the chemical properties of the pores in the new membrane. The most-studied hydrophilic segments in the field of amphiphilic block copolymers are poly(ethylene oxide) [42], poly(methacrylic acid) [43], and poly(2-hydroxy ethyl methacrylate) [44]. In our group for the first time, a series of triblock terpolymers of PS-*b*-P2VP-*b*-PEO was synthesized and integral asymmetric membranes with pH responsive pores were developed via SNIPS. The presence of a water-soluble short poly(ethylene oxide) (PEO) end block offers possibilities for post-modification [45].

Poly(isopropylidene glycerol methacrylate)—commonly known as poly(solketal methacrylate) acts as a precursor polymer of poly(glyceryl methacrylate) (PGMA) which was reported for the first time in 1990. Mori et al. reported the sequential anionic polymerization of styrene and solketal methacrylate (polystyrene-*b*-poly(solketal methacrylate)), (PS-*b*-PSMA) followed by the deprotection of acetonide groups to obtain PS-*b*-PGMA [46]. Poly(glyceryl methacrylate) (PGMA) is a potential alternative for the less hydrophilic 2-hydroxyethyl methacrylate (HEMA) due to the presence of one extra hydroxyl group (–OH) per repeating unit of the polymer in products such as contact lenses, drug delivery, and hydrogels. Zhang et al. used a combination of living anionic polymerization of allyl methacrylate (PAMA) and afterwards functionalization of the allyl side groups with osmium tetroxide to achieve PGMA [47]. It has also been reported as a material for ultrafiltration barriers mimicking the natural membranes in kidneys [48]. The first attempt to prepare a membrane from this diblock copolymer was reported by Hahn et al. who used PS-*b*-PSMA for air brush spraying on a PVDF support membrane [49]. Poly(isopropylidene glycerol methacrylate) is one of those polymers not yet studied widely in the context of block copolymer membranes produced via the SNIPS process.

## 1.1 Objective

Based on this background the main objective of the present work is to prepare integral asymmetric isoporous membrane via self-assembly and non-solvent induced phase separation process. In this regard, synthesis of a series of novel diblock and triblock terpolymers performs via sequential anionic polymerization of AB and ACB architecture. In the second step of this investigation, different parameters concentration of the polymer, (mixed) solvent interactions to different blocks, evaporation time, composition of the solvents are optimized to obtain integral asymmetric isoporous membranes from diblock and triblock terpolymers by following self-assembly and non-solvent induced phase separation (SNIPS) process. In the third step, post-modification of membranes is performed in a non-solvent while the isoporous structure of the membrane is preserved. Finally, a comparative analysis is conducted to compare the performance of membranes before and after modification.

## 1.2 Strategy of work and layout of the thesis

The present doctoral work is organized as follows:

-In **Chapter 2**, theoretical background briefly presenting the mechanism of anionic polymerization, the principles of non-solvent induced phase separation (NIPS), the role of self-assembly, the phase separation of block copolymers and the formation of isoporous membrane via SNIPS.

-In **Chapter 3**, the materials used in this work are presented and the experimental procedures employed for the synthesis and post-modification of polymers are explained. Later, it deals with the characterization techniques used in this study.

-**Chapter 4** is subdivided in two topics as follows: (i) **Chapter 4.1** portrays the results of (PS-*b*-PSMA) diblock copolymers synthesized by anionic polymerization and description of optimization of different parameters to obtain isoporous membranes. (ii) **Chapter 4.2** deals

with the modification of (PS-*b*-PSMA) diblock copolymers whereas a comparative analysis of (PS-*b*-PGMA) with (PS-*b*-PSMA) and (PS-*b*-P4VP) diblock copolymer membranes is demonstrated in the second part of this chapter.

-**Chapter 5** is divided in two sub chapters as follows (i) **Chapter 5.1** describes the results obtained from synthesis of linear triblock terpolymers by anionic polymerization and the optimization of the triblock terpolymers solutions to obtain integral asymmetric membranes with an isoporous surface by SNIPS. (ii) **Chapter 5.2** deals with the performance of isoporous membranes obtained from triblock terpolymers and additionally a comparative study before and after the modification of membranes was performed.

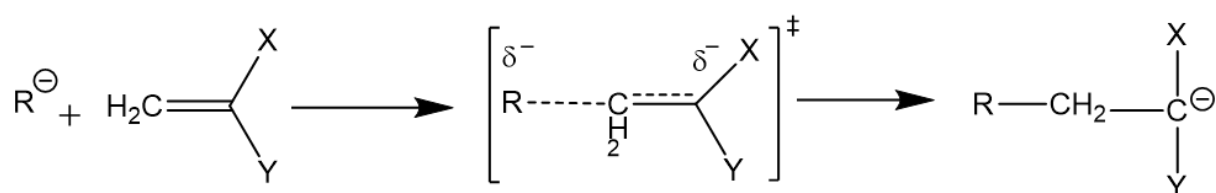
-**Chapter 6** depicts the summary and outlook of this work

-**Chapter 7 and 8** are dedicated to references and appendix

## Chapter 2: Theoretical background

### 2.1 Anionic polymerization

Anionic living polymerization is an established versatile approach for the synthesis of block copolymers that proceeds in the absence of termination and chain transfer [50, 51]. In 1956, Szwarc and coworkers demonstrated for the first time living anionic polymerization of polydienyl-lithium and polystyryl sodium chains in hydrocarbon media [52]. The term ‘living’ defines systems where no irreversible chain transfers and terminations occur during the course of polymerization [53]. This implies that polymerization proceeds until all the monomer is consumed and further addition of monomer would continue the growth of chain, thus increasing the degree of polymerization. Polymers with predetermined molar mass and very narrow molecular weight distribution could be obtained if the rate of initiation ( $R_i$ ) is much faster than that of propagation ( $R_p$ ). Only in the living anionic polymerization, molecular weight is directly proportional to monomer conversion (see Figure 2.1). In anionic polymerization, monomers that are capable of making stable carbanion, can be polymerized anionically, Scheme (2.1) [54].



**Scheme 2. 1.** Attachment of anion to monomer and delocalization of charge

The kinetics of rate of initiation in polar and non-polar solvents are highly dependent on the reaction conditions.  $k_i$  is the rate constant of the initiation step and  $k_p$  is the rate constant for the propagation step.

The chains will stay active unless there is a deliberate termination. Inert atmosphere or high vacuum conditions are maintained throughout the polymerization to avoid rapid termination of

active living chains due to reaction with oxygen, moisture and carbon dioxide (CO<sub>2</sub>). Different reaction products are made by such termination. The stability of propagating centers, termination, transfer and other chain breaking reactions can be suppressed by reducing the temperature during polymerization.

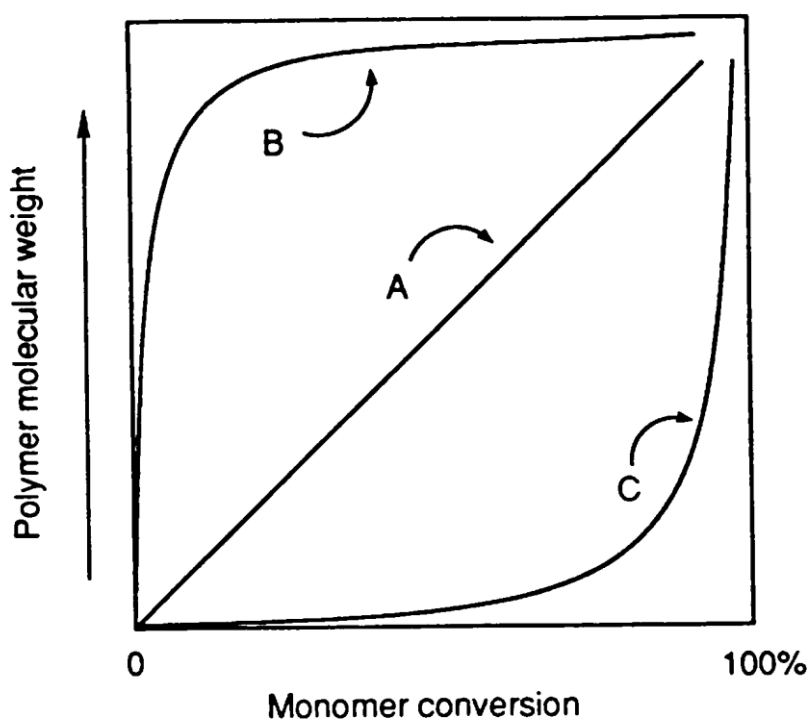


**Figure 2. 1.** Molecular weight conversion curves for various kinds of polymerization methods (A) living polymerization (B) free radical polymerization and (C) condensation polymerization. Reprinted with permission from ref [55].

Anionic polymerization is widely exploited in industry to create BCPs on a massive scale as compared to radical polymerization, due to its remarkable control over the molecular weight, composition and functionality [56].

### 2.1.1 Mechanism of anionic polymerization

According to M. Szwarc ‘polymeric molecules are born in an initiation process, they grow by a propagation process, and finally they ‘die’ in a termination process’

The mechanism of anionic polymerization divided into three principal steps

(a) Initiation

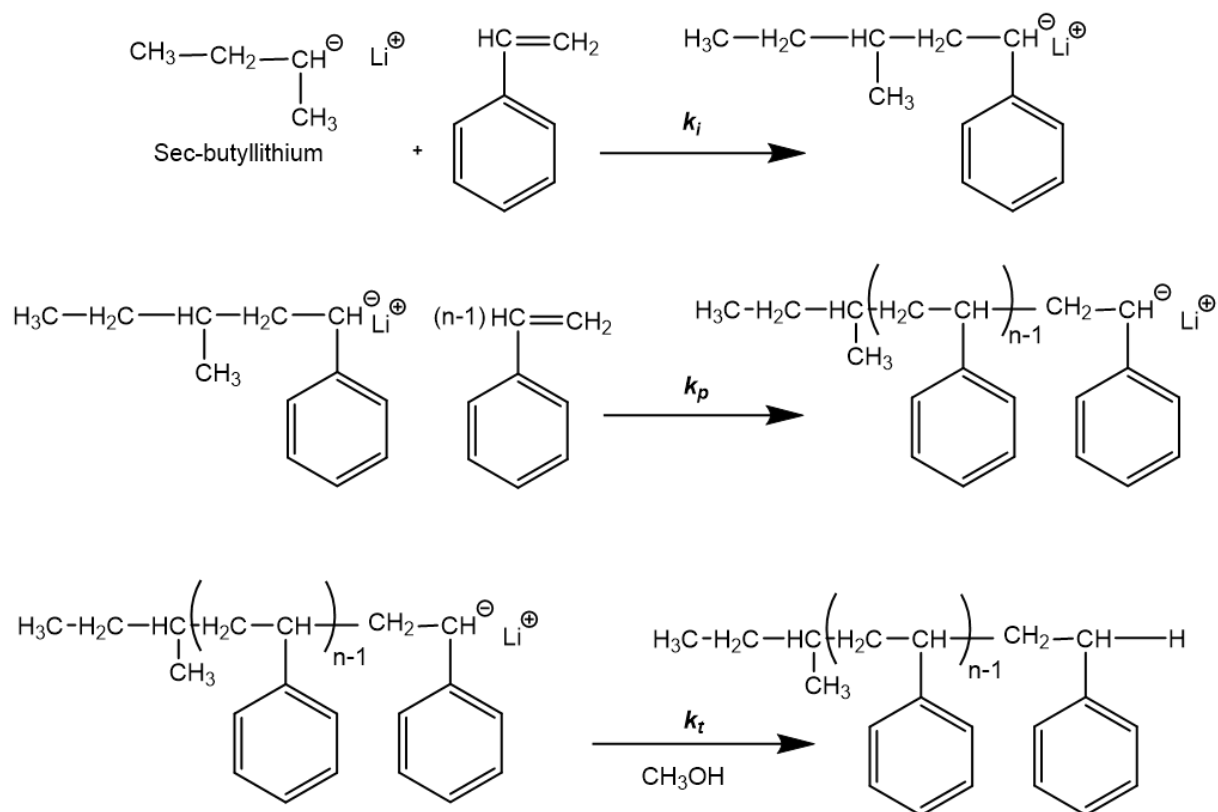
(b) Propagation

(c) Termination

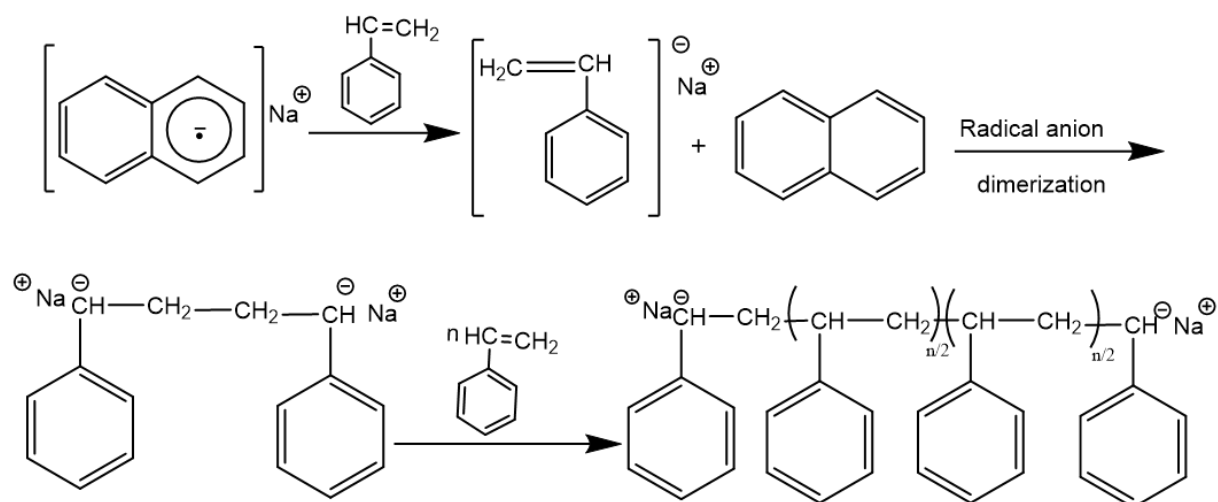
**(a) Initiation**

In anionic polymerization, the rate of initiation has to be faster than the rate of propagation if a narrow molecular weight distribution is aimed for. Thus for a successful initiation, the reactivity of monomer has to be matched with the appropriate initiating species. The rate of initiation (where alkyl lithium compounds act as initiator) is strongly influenced by the aggregation state of the anion and intermolecular interactions of ion pair formed after the opening of monomer bonds. Different type of initiators are used to accomplish initiation of polymerization. In the past alkali metals were used as initiators for the anionic polymerization of dienes through which radical anions are generated in a heterogeneous state. The radical anions rapidly undergo dimerization to form new dianions. The electron transfer initiators work more efficiently in polar solvents as compared to non-polar solvents. Another important class of initiators are organolithium compounds, obtained directly from the reaction of alkyl halides and lithium. Butyl lithium and alkali metal naphthalenide are examples of some initiators used for anionic polymerization where butyl lithium is a mono-functional initiator which forms one polymer chain per initiator molecule, while sodium naphthalenide is a di-functional initiator which gives a polymer with two reactive ends. A general way to initiate styrene is given in Scheme (2.2)

(a)



(b)

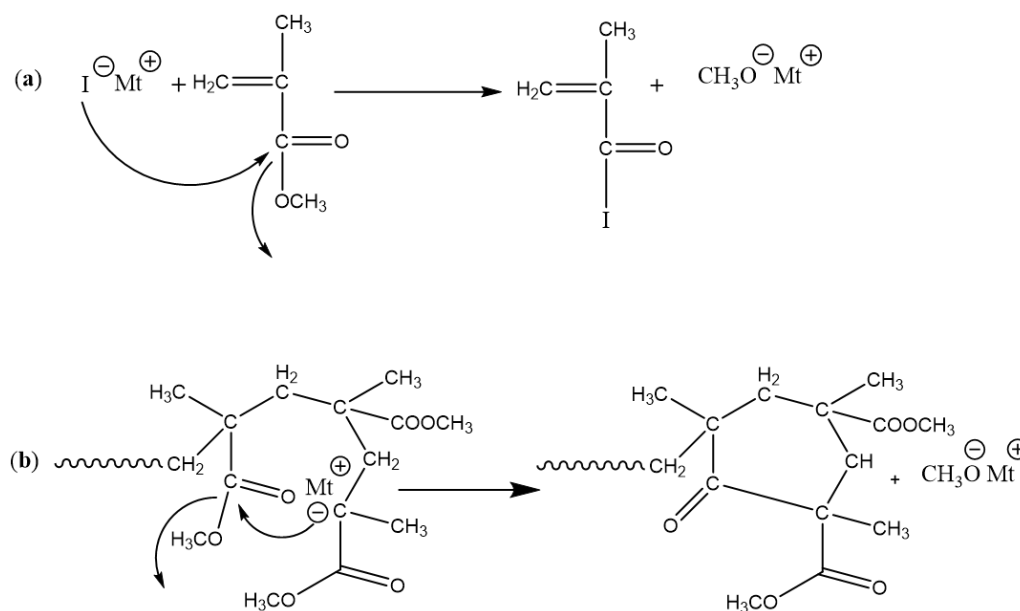


**Scheme 2. 2.** General way to initiate styrene with (a) mono and (b) di-functional initiators

In the case of alkyl (meth) acrylate polymerization classical anionic initiators such as metal alkyls generally yield polymers with broad molecular weight distribution (MWD) with low conversion. It is due to the probable attack of initiator on the polar ester group, which undergoes many side reactions during initiation and propagation. Aggregation of the active chain ends, having an ester enolate structure could be another reason (Scheme 2.3).

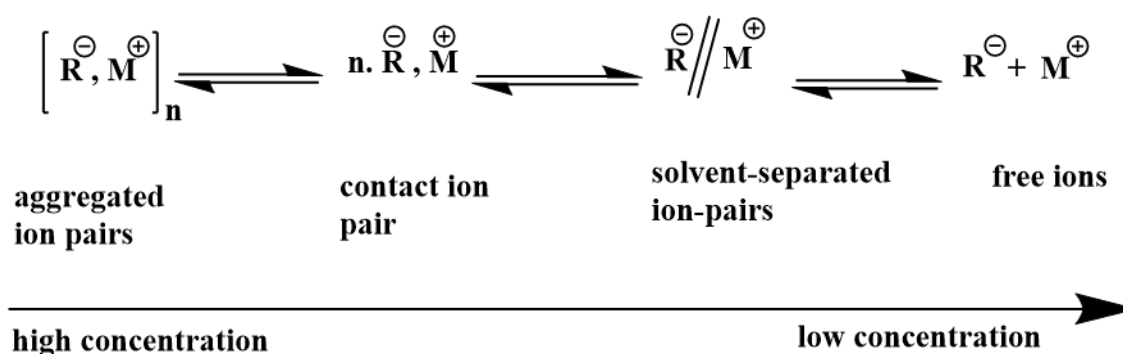
To avoid the attack of more reactive initiators on carbonyl groups of alkyl(meth)acrylate, nucleophilicity of carbanions was reduced by end capping the macro-initiator [57]. 1,1-diphenylhexyl [58] or triphenylmethyl anions or larger aromatic systems (e.g., fluorenyl anions) are some of the examples where the charge distribution over two or three phenyl rings adjusts the nucleophilicity enough [58, 59]. Although it is not the only operating factor, steric hindrance appears to have a determining effect in maintaining the controlled living polymerization [60].

In short, the selection of an initiator for a particular monomer is very important in order to obtain the control of the propagation.



**Scheme 2.3.** Side reactions in the polymerization of methyl methacrylate, (a) initiator attack on the monomer ester group (b) backbiting reaction of enolate anion

The behavior of carbanions in polar and nonpolar solvents is different due to different states of solvation and aggregation. In case of a polar solvent, this is mostly dependent on the intermolecular ionic interactions of the solvent, monomer, initiator and the size of the metallic counter ion. The intermolecular interaction of anion/carbanion in polar solvents forms different associated states called aggregates. The association of carbanion with the counter cation further classified as contact ion pair and solvent separated ion-pairs due to the tight and loose association of carbanion [61] (Scheme 2.4) At low concentration, solvent separated ion pairs dissociate into free ions. This degree of association of different ion pairs exist at equilibrium and is influenced by temperature. For example, the anionic polymerization of styrene and dienes initiated by *n*-butyl lithium in hydrocarbon medium is incomplete due to the high aggregation. In nonpolar solvents, electron transfer is inefficient due to the lack of solvation and significantly more aggregation observed.



**Scheme 2. 4.** Ion pairs in a polar solvent for different concentrations.[61-63]

### (b) Propagation

Reactive intermediates are continuously regenerated through a repeating cycle of elementary steps during propagation as shown in Figure 2.1. The rate of propagation is always first order with respect to monomer concentration and fractional orders with respect to chain end

concentrations in non-polar solvent. The fractional order supports the presence of inactive aggregated species.

### (c) Termination

Termination is the final step of anionic living polymerization where living anionic chains are deactivated by addition of a terminating agent. Alcohols are usually used to deactivate the polymerization reaction. The terminating agent should be degassed several times on the vacuum line to remove impurities. The quality of a polymer is determined by molar mass distribution.

#### 2.1.2 Molar mass distribution in living polymerizations

The number average molar mass ( $M_n$ ) is a linear function of the conversion for a living polymerization and anionic polymerization of styrene is precisely controlled by the stoichiometry of the reaction in a wide range from  $10^3$  to even  $10^6$  g/mol.

$$M_n = \text{grams of monomer/moles of initiator}$$

Polymers with extremely narrow molecular weight distribution are attained where molecular weight distribution is operationally defined as  $M_w/M_n \leq 1.1$  [64], for these systems  $M_w/M_n$  values being 1.05 or even smaller. The expression [65], which correlates dispersity index ( $\mathcal{D}$ ) and degree of polymerization for living anionic polymerization is given as

$$\mathcal{D} = X_w / X_n = 1 + [ X_n / ( X_n + 1 )^2 ] \approx 1 + [ 1 / X_n ]$$

In anionic polymerization, various functional groups like protic functionalities (-OH, -NH<sub>2</sub>) are required to be protected during polymerization [66-68]. Well-defined block copolymers with complex architectures such as star, comb, graft, dendritic, etc. were produced by anionic polymerization in combination with linking chemistry [69-72]. In this study, anionic polymerization was used for the formation of linear block copolymers.

## 2.2 Block copolymers

Anionic polymerization provides a way to the creation of well-defined block copolymers by sequential addition of monomers. It is a notable class of soft matter constructed by linking together discrete linear chains comprising dozens to hundreds of chemically identical repeating units. Sequential addition of distinct monomers to an active polymer chain can generate diblocks, A-B, triblocks, A-B-C or A-B-A, and more complex alternate multiblock structures.

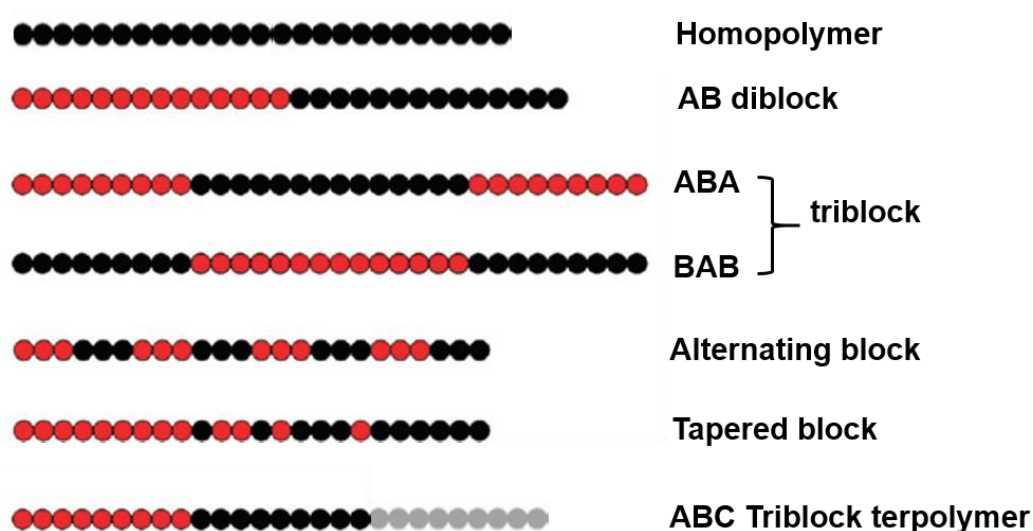


**Figure 2. 2.** Typical structures of block copolymers containing A, B and C block

Each of the blocks can be prepared with controlled molecular weight and narrow molecular weight distribution. A variety of  $\omega$ -functionalized block copolymers have been synthesized by controlled termination of living anionic chain ends using various electrophilic reagents.[73-75] Where AB and ABA copolymers typically adopt four familiar microphase structures (lamellae, double gyroid, cylinders and spheres), however introduction of a third block C, dramatically expands the spectrum of nanostructured morphologies.

Monomers with similar reactivity can follow any addition order without any limitation. It is difficult to synthesize a block copolymer from monomers of different reactivity by sequential

living polymerization, if the nucleophilicity of the living polymer anion does not match the electrophilicity of the following monomer. Nevertheless, a large number of triblock terpolymers and multiblock copolymers with more than four blocks were synthesized by sequential living polymerization using monomers with different reactivities. PS-*b*-P2VP-*b*-PtBMA was the first ABC triblock terpolymer reported by Stadler and Giebelier [76]. In recent years, synthesis of ABC triblock terpolymers has received much attention due to novel characteristics and complicated morphological behavior. The addition of chemically distinct blocks expands the number of unique sequences each capable of producing different nanostructures. Polymers from monomers with “active” protons (i.e., OH, SH, or NH groups) cannot be directly synthesized through anionic polymerization, as these react immediately with the initiator anions or the growing chain end [77]. To overcome this difficulty, either controlled radical polymerization can be employed, or protective groups are introduced into the monomeric unit blocking the reactive site during the course of anionic polymerization and these protected groups can be easily and readily cleaved afterwards to get the required functional groups [46]. Functional block copolymers have received extensive scientific and technological attention due to their potential applications in electronics [78], fabrication of nanoporous membranes [79], drug delivery, [80] nano-reactors, [81] and smart materials [82, 83].

### **2.2.1 Self-assembly of block copolymers and phase separation behavior**

Block copolymers composed of incompatible blocks phase separated at macromolecular level to a variety of three-dimensional nanostructures in bulk and also often in solution. However, the final microphase separated morphologies depend on the architecture of the block copolymer(s) involved, molecular weight, composition and thermodynamic properties. Diblock copolymers with immiscible blocks can microphase separate into four different morphologies

including spheres (S), cylinders (C), bicontinuous gyroids (G), and lamellae (L), as shown in Figure 2.3

Unfavorable mixing enthalpy coupled with entropy drives the process of self-assembly along with the blocks connected by covalent bond for microscopic phase separation. The microphase separation of (AB) block copolymers is determined by three experimentally controllable key parameters: the degree of polymerization,  $N$ , the volume fractions of the blocks,  $f$ , and the Flory-Huggins segmental interaction parameter,  $\chi$ . The first two factors influence the translational and conformational entropy of the block copolymers and are regulated by the polymerization stoichiometry, while  $\chi$  is a measure of the enthalpic interactions between two blocks, it specifies the degree of incompatibility associated with linking the two dissimilar polymer chains, which drives the phase separation. Phase behavior will further be influenced by the rigidity and topology of the chains. Figure 2.3 shows the phase diagram of the equilibrium morphology of diblock copolymers where  $\chi N$  is shown as a function of  $f$ . At the minimum value of  $\chi N \sim 10.495$ , a transition between ordered and disordered state occurs when  $f = 0.5$ .

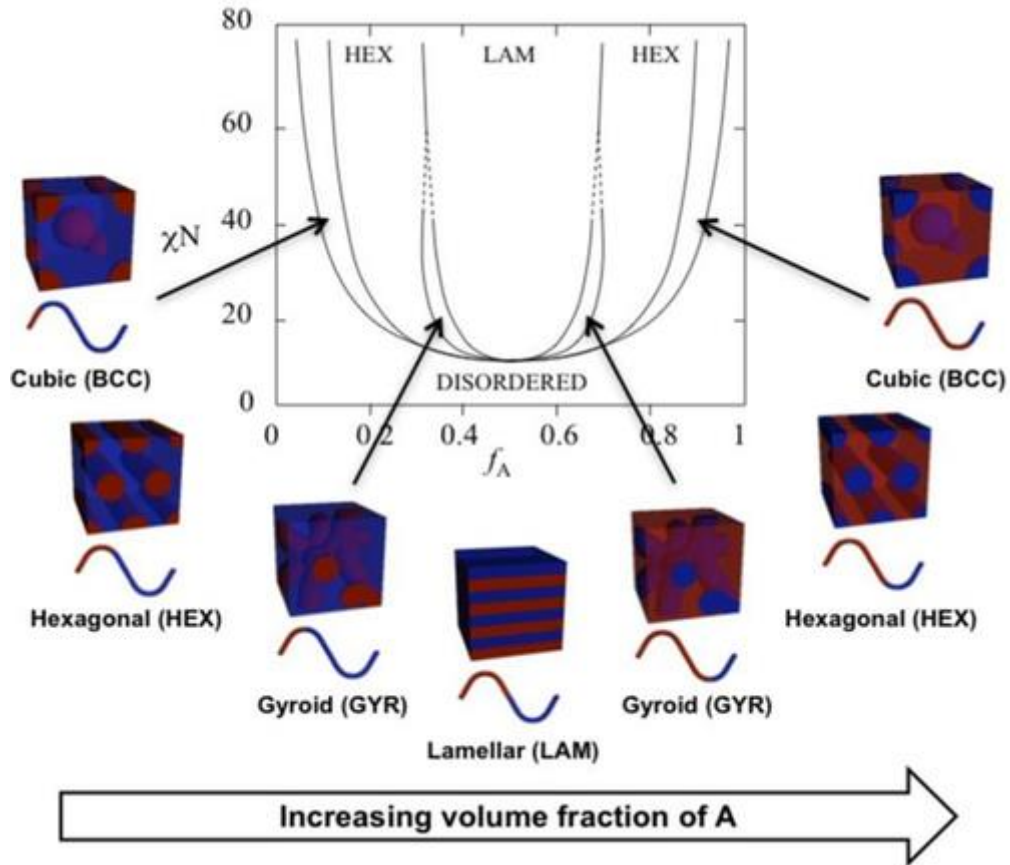


**Figure 2. 3.** Theoretical phase diagram of a linear diblock copolymer by self-consistent mean field theory. Body-centered cubic (BCC), hexagonally packed cylinder (HEX), minimal surfaces (gyroid (GYR) and alternating simple lamellar phase (LAM). Reprinted with permission from ref [84].

The Flory-Huggins interaction parameter  $\chi_{AB}$ , describes the driving force for microphase-separation. The relationship between  $\chi$  and temperature ( $T$ ) is given in the following equation [85, 86].

$$\chi_{AB} = (z/k_B T)$$

Where  $z$  is the number of nearest neighbors per repeat unit in the polymer and  $k_B$  is the Boltzman constant. The segregation product,  $\chi_{AB}N$ , represents the interaction per chain and determines the degree of microphase separation of diblocks. Temperature and  $\chi N$  are two important parameters, which influence the incompatibility between the constituents' blocks. The incompatibility

between the blocks decreases with increasing temperature or decreasing  $\chi N$ , the copolymers show order-to-disorder transition (ODT). The strength of segregation of block is determined by  $\chi N$  and classified into two limiting regimes whereas volume fraction ( $f$ ) defines micro-domain geometry. When the values of  $10 \leq \chi N \leq 15$  [87, 88], it represents the weak segregation limit (WSL) and  $\chi N \geq 100$  shows the strong segregation limit (SSL) [89, 90].

The number of possible morphologies of triblock terpolymers are higher as compared to diblock copolymers due to the larger number of experimental parameters. Linear triblock terpolymers have three different Flory-Huggins interaction parameters  $\chi_{AB}$ ,  $\chi_{BC}$ ,  $\chi_{AC}$  and two independent volume fractions of blocks  $f_A, f_B$ . Together with the total degree of polymerization,  $N$ , these are in total six independent parameters that determine the equilibrium structure of the given triblock terpolymer. However, unlike diblock copolymers (AB) the sequence of a block in the triblock terpolymers (ABC) affect the final phase diagram i.e., whether it is sequenced A-B-C, B-C-A or C-A-B [91, 92].

A combination of very extensive theoretical and experimental studies illustrate the bulk morphologies of triblock terpolymers and in this regard, Stadler et al. made significant contributions. They studied polystyrene-*block*-polybutadiene-*block*-poly(methyl methacrylate) (SBM) triblock terpolymers in detail to explore the morphological behavior [93-101]. The ternary phase diagram of SBM is shown in Figure 2.4 with morphologies discovered so far at room temperature.

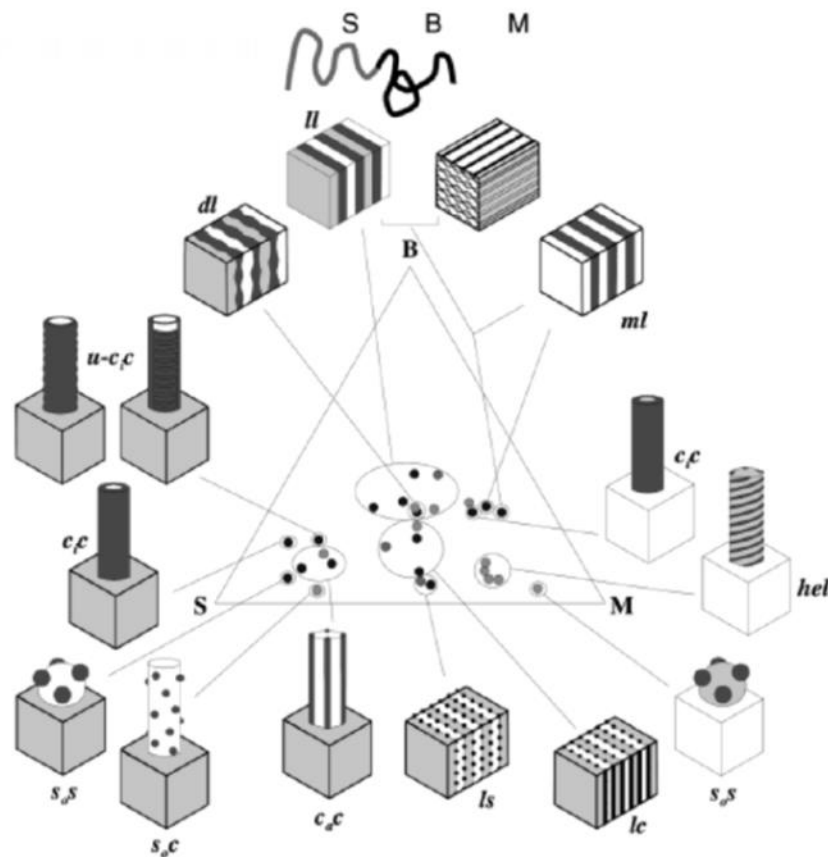


**Figure 2. 4.** Ternary phase diagram of polystyrene-*block*-polybutadiene-*block*-poly(methyl methacrylate) (SBM) triblock terpolymers. Reprinted with permission from ref [102].

### 2.2.2 Block copolymers in solution

Amphiphilic block copolymers can be dissolved in polar or non-polar solvents due to the presence of hydrophilic and hydrophobic segments. However, the presence of solvents increase the complexity of the system as compared to the bulk systems. The dissolution of block copolymer in the selective solvent i.e. a solvent which is good solvent for one block but a precipitant for another block, induces self-assembly into micelles of different shapes. Micelle formation requires two opposing forces, attractive forces between the insoluble moieties that leads to aggregation and the repulsion between soluble parts, which prevents unlimited growth of the micelles.

The polymer chains spontaneously organize into domains of defined geometry like spheres, cylinders or lamellar vesicles [103, 104] shown in Figure 2.5. The geometry of a system depends on many factors and somehow can be predicted by following the approach of Israelachvili [105] and coworkers who introduced the packing parameter ( $p$ ) which is related to three parameters. Nevertheless, changes in the morphological aggregates are also observed by other factors such as solvent composition and temperature that affect the force balance.

$$p = \frac{v}{al}$$

Where  $v$  is the volume occupied by the solvophobic segment,  $l$  its length and  $a$  represents the contact area between the solvophobic and solvophilic segments.

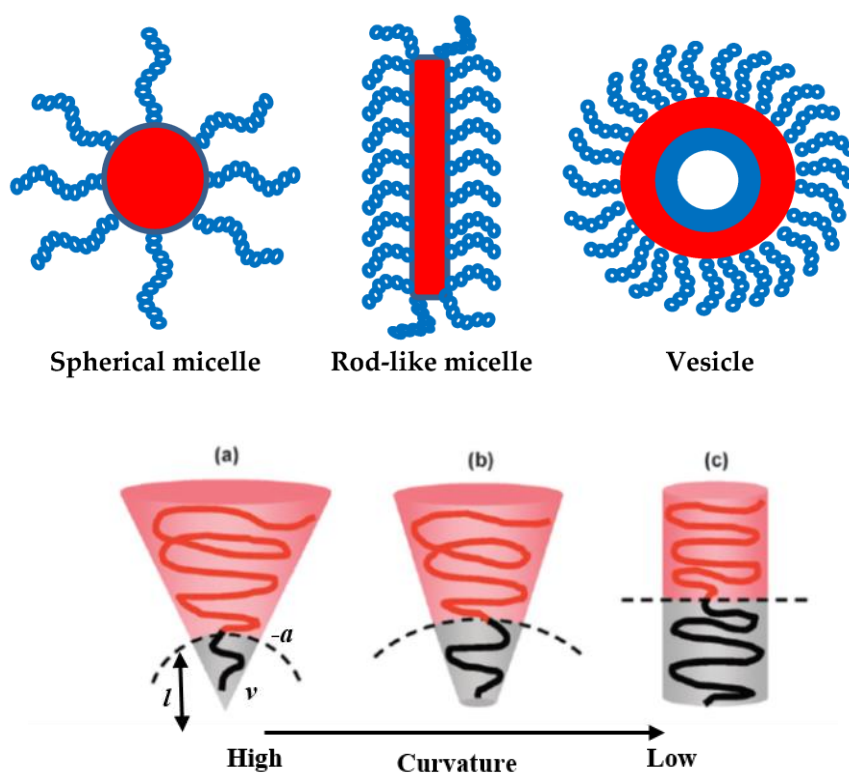


**Figure 2. 5.** Basic morphologies of (AB) block copolymer aggregates in solution. Reprinted with permission from ref [106, 107].

If  $p < 1/3$ , spherical micelles are expected, cylinders for  $1/3 < p < 1/2$ , vesicles if  $1/2 < p < 1$ , lamellae if  $p = 1$ , and inverted structures if  $p > 1$ . However, a variety of other morphologies of block copolymers in solution have been added and revised by scientists [108-111].

Also in solution, the number of possible self-assembled structures of triblock terpolymers are higher as compared to diblock copolymers. Triblock terpolymers in which two incompatible blocks are insoluble in the respective solvent form micelles with compartmentalized core and a homogenous corona; however, a homogenous core is formed when only one block is insoluble whereas the other two build the corona. Within the latter, no chain segregation (mixed corona) or lateral chain segregation (Janus micelle) can take place, if the middle block is insoluble. Radially segregated corona with AB diblock copolymer arms results, if one of the outer blocks is the insoluble one. Triblock terpolymers can also form vesicles in solution [99]. Figure 2.6 shows all mentioned morphologies of micelles.



**Figure 2. 6.** Schematic representation of different types of micelles formed by ABC triblock terpolymers. Core-shell-corona micelles with a compartmentalized core (a), micelles with a mixed corona (no chain segregation) (b), core-shell-corona micelles with a compartmentalized corona (radial chain segregation) (c), Janus micelles with an asymmetric corona (lateral chain segregation) (d), and vesicles (e). Reprinted with permission from ref [99].

### 2.3 Types of membranes

Membrane, a discrete barrier with thin interface between two phases and can be completely uniform in composition and structure, or may be chemically or physically heterogeneous [56, 112-114]. Membranes can be categorized on the basis of a number of parameters (geometry, bulk structure, production method and separation regime *etc.*), however here we discuss about the classification of membranes according to their physical structure. Two principal types of membranes are isotropic (symmetric) and anisotropic (asymmetric) as shown in Figure 2.7.

Asymmetric porous membrane has a rigid, highly voided structure with randomly distributed interconnected pores that is very similar in structure and function to a conventional filter. However, pores diameter of these membranes are extremely small as compared to the conventional filter (pore size larger than  $10\mu\text{m}$ ). In case of nonporous dense membranes, a driving force in the form of pressure, concentration or electrical potential gradient is required to transport permeants by diffusion. The relative transport rate is determined by diffusivity and solubility of the component in the membrane material.

In contrast, asymmetric membranes contain an extremely thin surface layer with gradient in pore sizes i.e. pore size get bigger from the surface to the bottom of the membrane. Loeb and Sourirajan invented such integral asymmetric membranes in the early 1960s. The separation performance of the asymmetric membrane is dependent exclusively on the surface layer and the substructure provides mechanical support. Composite membranes, on the other hand, consist of layers of different materials each performing a specific function and are usually used in processes where permeation is controlled by solution-diffusion mechanism. The porous support layer can be symmetric or asymmetric and provides support to the top thin layer.

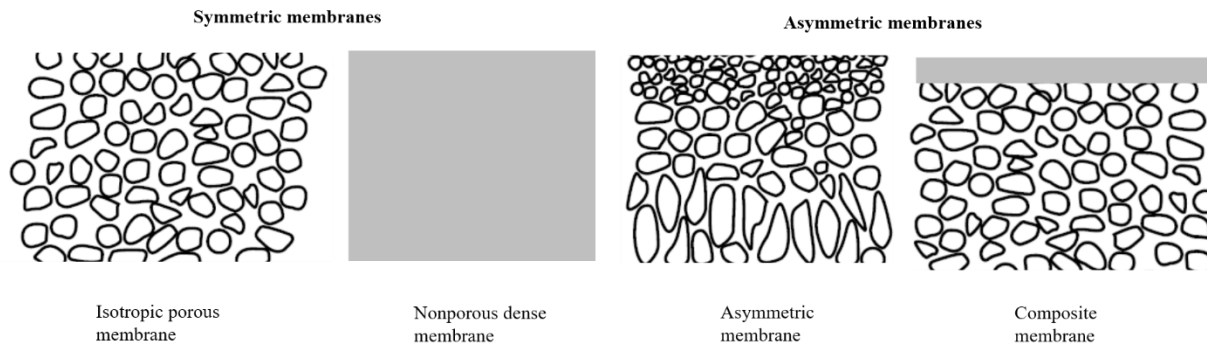


**Figure 2. 7.** Schematic illustration of symmetric and asymmetric membrane structure. Reprinted with permission from ref [112].

The morphology (pore size and distribution) of the membrane is the key factor to control the performance and determines its field of application. Micro- and ultrafiltration membranes allow size based separations of different components such as dissolved macromolecules of proteins from solutions. Ultrafiltration membranes are usually anisotropic where the porous surface is supported by the more open porous support. There are different types of anisotropic membranes such as phase separation membranes, interfacial composite membranes and solution coated composite membranes named after the fabrication method. In this work, the phase inversion method was followed to fabricate the membranes and is explained in the following section.

### 2.3.1 Phase separation membranes

The technique introduced by Loeb-Sourirajan for the formation of reverse osmosis membranes is now recognized as a phase separation process, also known as phase inversion process or polymer precipitation process. This can be explained in simple words as changing of a one phase casting solution into two separate phases where the matrix of the membrane forms by the polymer rich phase and polymer poor phase forms the pores of the membrane. The precipitation of cast polymer solution can be induced by several ways. The precipitation of the cast film can be induced by immersing in non-solvent bath usually water (the Loeb-Sourirajan process)

where the exchange of solvent from the polymer solution with non-solvent (from the bath) results into an asymmetric membrane. This process is also known as non-solvent induced phase separation or NIPS.

The cast polymer film is placed in humid (vapor) atmosphere to induce precipitation to form microporous structure. This is known as vapor induced phase separation (VIPS). A change in temperature (usually cooling) can also cause precipitation of the polymeric solution and is named as temperature induced phase separation (TIPS) or thermal gelation. In a solvent evaporation process, evaporation of one of the good volatile solvents from the mixture of less volatile solvents of the casting solution changes the solution composition and causes precipitation, so called evaporation induced phase separation (EIPS) [115].

In this study ultrafiltration membranes from block copolymers were studied which fall in the category of anisotropic membranes. These membranes have smaller surface pores (micro/nanoporous structure) supported by the more open porous substructure. As typical for anisotropic membranes, they should act as surface selective membranes. This means that particles which needs to be excluded are rejected on the surface of these membranes [116].

### **2.3.2 Isoporous block copolymer membranes via SNIPS**

Block copolymers can self-assemble into uniformly sized micro domains due to microphase separation. Non-solvent induced phase separation (NIPS) is immensely popular technique for the formation of permeable materials used in pervaporation, reverse osmosis and ultrafiltration [117-119]. However, membranes prepared from the commercially available polymers (*e.g.* polysulfone (PSF), poly(vinylidene fluoride) (PVDF), *etc.*) *via* NIPS, often suffer from a poor control on membrane structure [1, 4]. In the earlier days solution casting was performed on a dense solid substrate and required a transfer step of the block copolymer membrane on porous

support [120]. Later, block copolymer solution was attempted to be cast directly on a porous support, with membrane of finite length of straight cylinders typically achieved in this way.

In 2007, the group of Abetz reported a straight forward method for the preparation of block copolymer (BCP) integral asymmetric membranes with isoporous surface on a large scale through the combination of the self-assembly and non-solvent induced phase separation (SNIPS) [121, 122]. Polystyrene-*b*-poly(4-vinylpyridine) PS-*b*-P4VP was the first block copolymer used to develop isoporous membranes by SNIPS, where the matrix comprises the hydrophobic PS block and the pore walls are lined with the more hydrophilic P4VP block [123-129]. PS-*b*-P4VP is a non-ionic amphiphilic block copolymer and strongly segregated in bulk state due to the large segmental interaction parameter of its constituent blocks. A binary solvent system (THF/DMF) was chosen to dissolve PS-*b*-P4VP.

During the phase inversion process, a concentrated solution of block copolymer is cast on a support or a glass plate using a doctor blade and the film is exposed to air for a specified evaporation time. Afterwards, the film is immersed into a non-solvent, usually water. The exchange of solvent by non-solvent below the surface layer is slowed-down and a concentration gradient develops from the top to bottom part of the solution cast polymer film, which results in a rather coarse, sponge-like structure under the dense top layer. The cross-section of the resulting integral asymmetric membrane displays a rather dense surface layer interconnected to partially disordered sponge or finger like sublayer of increasing porosity towards the bottom in Figure 2.8. The highly porous surface is influenced by many parameters such as the casting solution viscosity, concentration, molecular weight and composition of the polymer, presence of additives in the casting solution, solvent evaporation rate, time of evaporation prior to precipitation, quality of the precipitant, temperature of the casting solution and precipitant, and the humidity of the surrounding environment [122, 130-132].

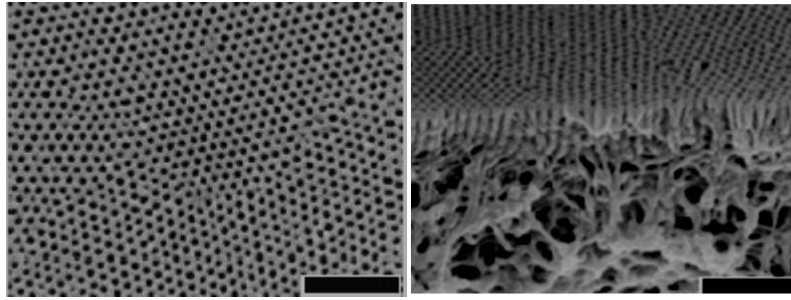


**Figure 2. 8.** Scanning electron microscopy (SEM) images of the surface and cross-section of the integral asymmetric isoporous PS-*b*-P4VP diblock copolymer film following SNIPS. The scale bar correspond to 500 nm. The evaporation time before immersion into non-solvent bath is 10 s. Reprinted with permission from ref [121].

Several studies have been carried out on the SNIPS ultrafiltration membranes structure formation and block copolymer solution. Phillip et al. have described very well the mechanism of SNIPS. According to that the micro/nanoporous surface structure of the cast film is formed by the development of concentration gradient between the block copolymer and solvent composition created by the the evaporation of solvents from the surface of the membrane. This variation accompanies a change in the viscosity of the block copolymer solution cast film and causes a change in incompatibility among different polymer segments. As a result of the concentration gradient from top to bottom of the film, the length of the ordered microdomains is limited to a few hundred nanometer with a random microphase separated structure underneath [133].

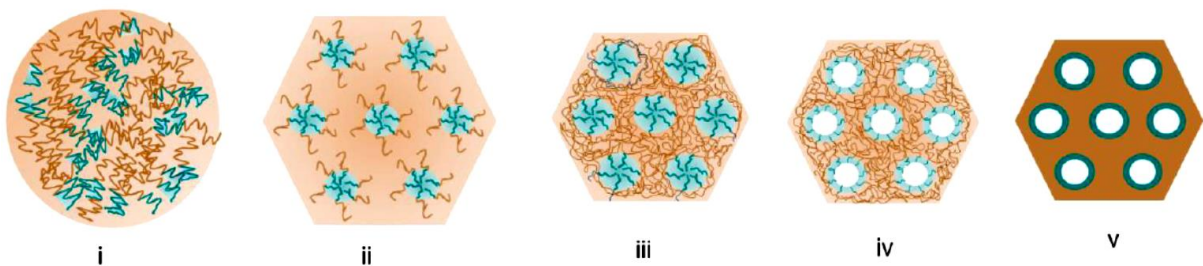


**Figure 2. 9.** Schematic illustration of the structure formation of isoporous membrane from the

solution: i) Disordered or weakly segregated diblock copolymer in mixed selective solvents (  polystyrene rich domains,  poly(4-vinylpyridine) rich domains ii) microphase separation with polystyrene rich matrix after film casting; iii) solidification of the matrix due to solvent evaporation; iv) open pores in the poly(4-vinylpyridine) rich domains after non-solvent induced phase separation; v) Porous structure of dried membrane. This figure is reprinted from reference [122].

There are some studies that claims the formation of self-assembled ordered structure in the solution whereas some other have proven no structure formation prior to casting [39]. Figure 2.9 illustrates the mechanism of SNIPS membrane structure formation proposed by Abetz in the following steps [122].

Hahn and coworkers reported isoporous *PtBS-b-P4VP* and *PTMSS-b-P4VP* diblock copolymer membranes of higher thermal stability as compared to *PS-b-P4VP* membranes by replacing the matrix forming block of higher glass transition temperature  $T_g$  [134]. On the other hand, William et al. improved the mechanical properties of the membrane by introducing a third soft matrix forming PI block. The isoporous membranes of *PI-b-PS-b-P4VP* where *PI-b-PS* block contributes in the formation of the matrix of the membrane, shows higher toughness than *PS-b-P4VP* membranes [130, 135-137]. Jung and coworkers conducted a comparative study of *PS-b-P2VP* diblock copolymer and *PS-b-P2VP-b-PEO* isoporous membranes where the addition of a short water-soluble PEO block enhanced the hydrophilicity and antifouling properties of the membrane. The presence of a stimuli responsive block can open the way to introduce switchable functionalities in the isoporous block copolymer membranes by undergoing swelling/de-swelling transition in response to a controlled environment (e.g., pH value, ionic strength, light, temperature).

Integration of different additives into a block copolymer system (with functional groups e.g., nitrogen atoms of P2VP/P4VP chains of the pore forming block) may alter the dimensions of microphase separated domains by forming supramolecular interactions.

A detailed study of the addition of metal ions/salts to the PS-*b*-P4VP block copolymer solution demonstrated an increase in conformational changes and segmental interaction ( $\chi$ ) via metal-ligand coordination [125, 128, 138]. Later, Clodt et al. used biocompatible  $\alpha$ -cyclodextrin,  $\alpha$ -(D)-glucose and saccharose as an additive for the pore formation in the PS-*b*-P4VP system achieving membranes with higher porosity and narrow pore size distribution [139]. Additionally, less amount of the block copolymer was required for the fabrication of membranes due to the viscosity increment (Figure 2.10).

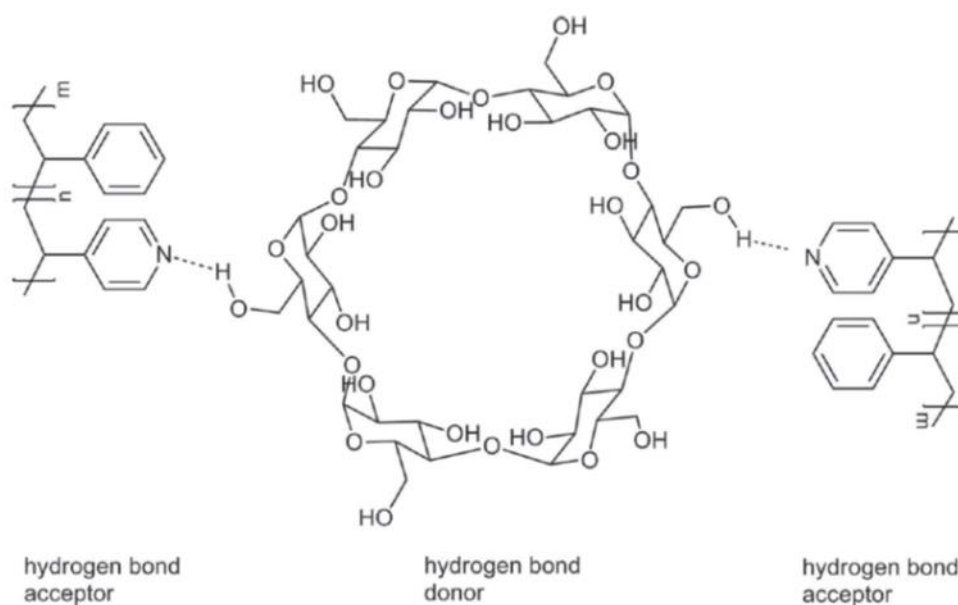


**Figure 2. 10.** Representation of possible hydrogen bonding between PS-*b*-P4VP as hydrogen bond acceptor and carbohydrate molecule. Reprinted with permission from ref [139].

In another approach, hybrid isoporous membranes were fabricated by incorporating highly functional polymer-grafted graphene oxide (pGO) nanosheets into the block copolymer

solution. The new hybrid membranes showed improved antifouling and anti-bactericidal capabilities [140].

Post-modification of the block copolymer membranes, while preserving the self-assembled nanostructure offers a convenient way to introduce desired functionalities into the membranes to overcome performance limitation such as fouling. Lee et al. reported the multifunctional surface coating of a thin adherent reactive poly(dopamine) (PDA) onto a wide range of organic and inorganic materials [141]. This coating in turn serve as a versatile platform for secondary surface mediated reactions. Later, a novel double stimuli responsive membrane was fabricated by integrating thermos-responsive moiety (e.g., amine terminated PNIPAM) into pH responsive PS-*b*-P4VP isoporous membrane via a Michael addition reaction.

## Chapter 3: Experimental work

### 3.1. Materials

Tetrahydrofuran (THF) and *N,N*-dimethylformamide (DMF) were ordered from Sigma Aldrich. Styrene (Sigma-Aldrich, Schnelldorf, Germany, 99%), *sec*-butyllithium (*sec*-BuLi) (Sigma-Aldrich, Schnelldorf, Germany, 1.4 M solution in cyclohexane) and triisobutylaluminium (1M in hexane, Sigma-Aldrich, Darmstadt, Germany), 4-vinyl pyridine (4VP) (Sigma-Aldrich, Munich, Germany), ethylaluminium dichloride (EtAlCl<sub>2</sub>, 1M in hexane) (Sigma-Aldrich, Schnelldorf, Germany), Di-*n*-butylmagnesium (MgBu<sub>2</sub>) (Sigma-Aldrich, Schnelldorf, Germany, 1.0 M solution in heptane), calcium hydride (CaH<sub>2</sub>) (Sigma-Aldrich, Munich, Germany), 1,1-diphenylethylene (Sigma-Aldrich, Schnelldorf, Germany), bovine serum albumin (BSA), hemoglobin (from bovine blood) were purchased from Sigma-Aldrich. *iso*-propylglycidyl methacrylate (SMA) was received from BASF SE (Ludwigshafen, Germany).

#### 3.1.1 Cleaning of chemicals

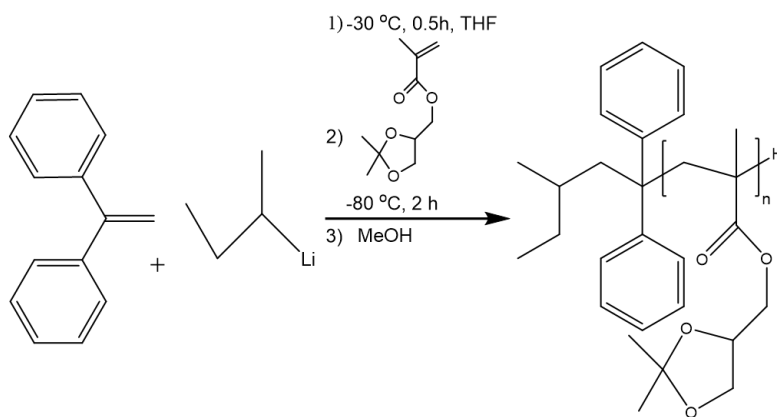
THF was purified by distillation and titration with *sec*-butyl lithium under argon (Argon 7.0, linde AG, Pullach, Germany) atmosphere. To obtain highly pure THF, first distillation was carried out and the residual protic impurities were neutralized by the addition of *sec*-BuLi at -30°C, yellow color solution disappear after 15 minutes. THF was further left under the Schlenk line for 15 h. Styrene (Sigma Aldrich, 99%) was purified via aluminum oxide column and subsequently distilled from di-*n*-butylmagnesium under inert environment. 4-vinyl pyridine was purified via distillation from calcium hydride and distilled twice again after treating with ethyl aluminium dichloride. Solketal methacrylate (SMA) was cleaned by using calcium hydride and triisobutylaluminum. Glycidyl methacrylate was purified by distillation over calcium hydride twice. 1,1-diphenylethylene was distilled over *sec*-BuLi. All the chemicals were distilled under an inert atmosphere of high vacuum (10<sup>-7</sup>-10<sup>-8</sup> mbar) and argon supply.

### 3.1.2 Anionic polymerization of block copolymers

The synthesis of block copolymers was carried out in a flask by using a Schleck line apparatus. The synthesis was performed under inert environment of high vacuum supply and without moisture. The temperature of the flask was maintained by the addition of liquid nitrogen / ethanol bath. The reaction temperature was monitored by using a thermometer. Pressure inside the reaction flask can also be controlled by a pressure gauge. The reactants were injected with a dried syringe into the flask opening covered with rubber septum.

### 3.1.3 Synthesis of poly(solketal methacrylate) (PSMA) homopolymer

To understand the nature of solketal methacrylate (SMA), the experimental conditions were optimized to obtain a homopolymer of PSMA by means of anionic polymerization. THF (Sigma Aldrich) was used as polymerization solvent. To ensure the complete monomer conversion by living anionic polymerization, sterically hindered initiators of moderate nucleophilicity were used. The calculated volume of DPE (0.1 mL, 0.6 mmol) was introduced at once into the reactor and was co-stirred with the initiator *sec*-BuLi (0.2 mL, 0.3 mmol). The solution became immediately red. After 30 minutes stirring at -30 °C, 5 mL of purified SMA was transferred to the reactor. The solution became colorless. The temperature was maintained around -80 °C and the polymerization of SMA being completed within 2 h. The polymerization was terminated with degassed methanol and the solution was concentrated under reduced pressure and precipitated with *n*-hexane. The white solid was dried in vacuum at 40 °C for 48 h. The chemical path for the synthesis of (PSMA) is shown in Scheme (3.1).



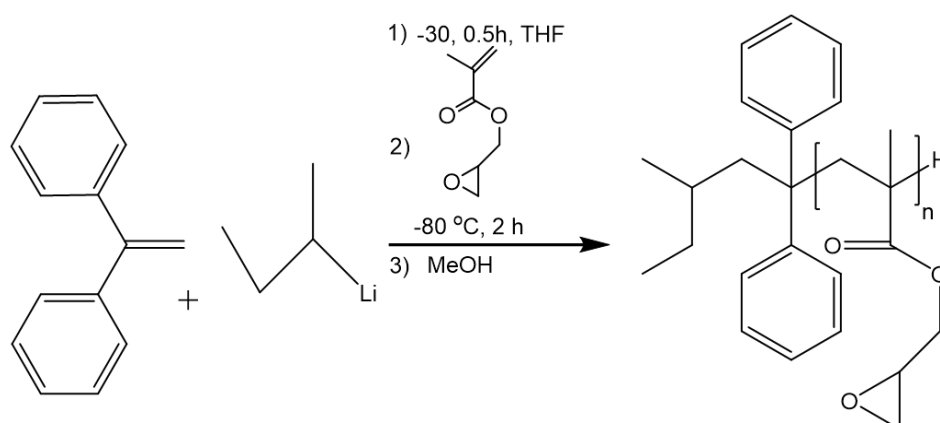
**Scheme 3. 1.** Synthesis of PSMA homopolymer

### 3.1.4 Synthesis of poly(glycidyl methacrylate) (PGM) homopolymer

Glycidyl methacrylate is an interesting monomer with three reactive functional groups, carbon-carbon double bond, ester carbonyl group, and epoxy group. In this study, carbon-carbon double bonds were utilized to synthesize poly(glycidyl methacrylate) via anionic polymerization whereas the epoxy and carbonyl groups remained unaffected. The epoxy groups of poly(glycidyl methacrylate) could be ring opened after polymerization to get hydroxyl groups containing polymer like poly(glyceryl methacrylate) (PGMA).

A chosen amount of lithium chloride (LiCl) added to the reactor first and was submitted to several argon/vacuum cycles. THF (Sigma Aldrich) was used as polymerization solvent. Purification of THF was performed by following the same procedure mentioned in the Section 3.1.1. The calculated amount of linking agent DPE (0.25 mL, 1.4 mmol) and initiator (*sec*-BuLi) (0.5 mL, 0.7 mmol) was introduced into the reactor at -30 °C. After 30 minutes, temperature of the reactor was maintained at around -80 °C and purified glycidyl methacrylate was added. The red color of the initiator solution vanishes at once and the polymerization was quenched with degassed methanol after 2 h. The polymer was precipitated in a methanol/water

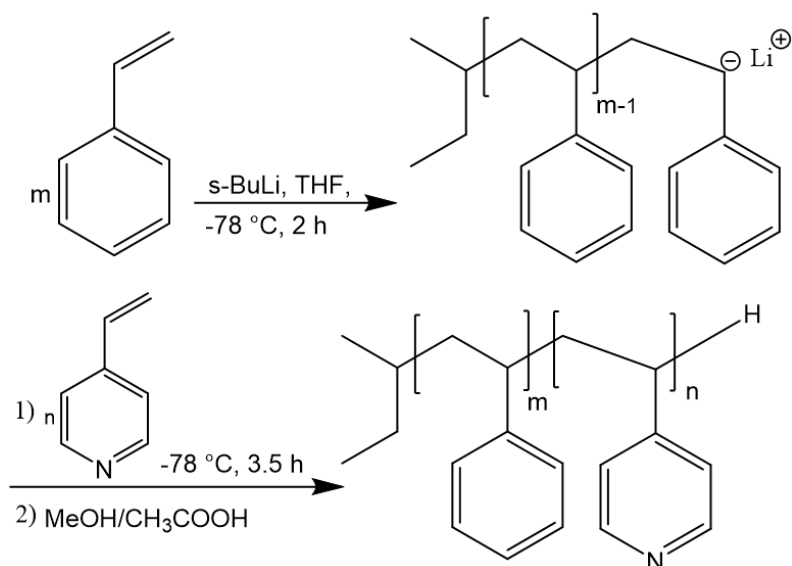
mixture (85/15 v/v) and dried at 50 °C. The synthetic route of poly(glycidyl methacrylate) (PGM) polymerization is depicted in Scheme (3.2).



**Scheme 3. 2.** Synthesis of PGM homopolymer

### 3.1.5 Synthesis of polystyrene-*block*-poly(4-vinylpyridine) (PS-*b*-P4VP) diblock copolymer

THF (Sigma Aldrich) was used as polymerization solvent and all the polymers were synthesized under inert atmosphere of high vacuum ( $10^{-7}$ – $10^{-8}$  mbar) and argon supply (Argon 7.0, linde AG, Pullach, Germany). . (19 mL) of styrene was transferred to the flask and initiated with (0.07 mL, 0.1 mmol) *sec*-BuLi at  $-78^{\circ}\text{C}$ . The solution turned yellow. An aliquot of polystyrene was sampled out from the reactor after 2 h for molecular characterization of the first block followed by the addition of (3 mL) 4VP. The solution was stirred overnight for ensure the complete polymerization of 4VP. The polymerization was quenched with degassed methanol/acetic acid (10:1 v/v) mixture. The polymer solution was concentrated under reduced pressure and precipitated in water. The polymer was dried at  $40^{\circ}\text{C}$  under vacuum. The synthetic route of PS-*b*-P4VP polymerization is depicted in Scheme (3.3).

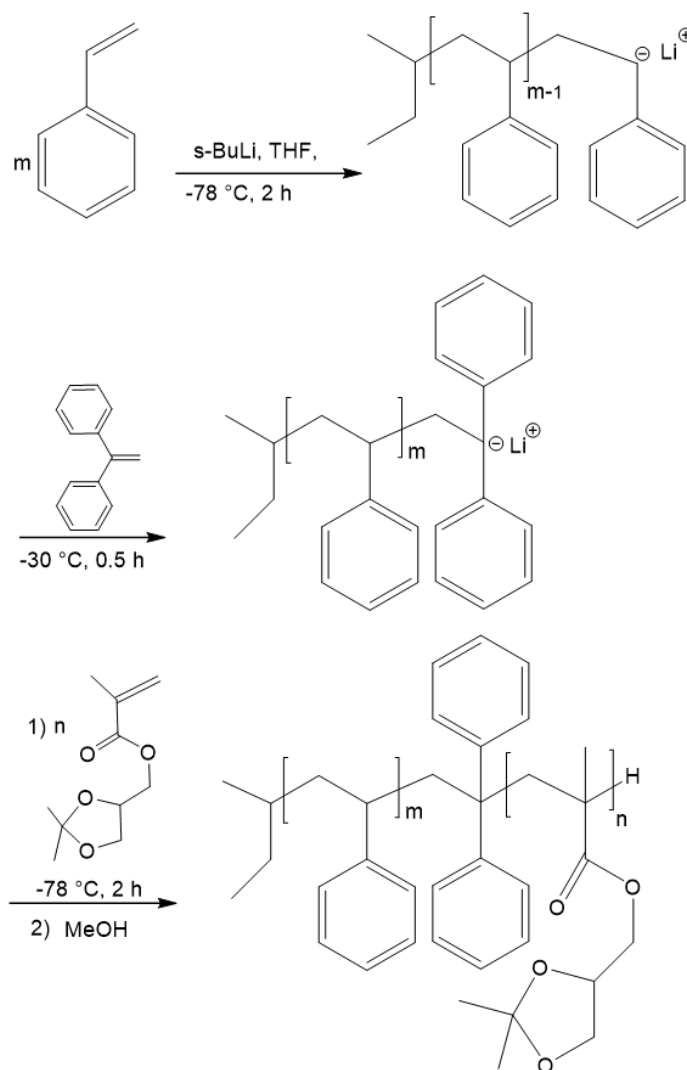


**Scheme 3. 3.** Synthesis of PS-*b*-P4VP

### 3.1.6 Synthesis of polystyrene-*block*-poly(solketal methacrylate) (PS-*b*-PSMA) diblock copolymer

All diblock copolymers were synthesized via sequential anionic polymerization under an inert atmosphere of high vacuum ( $10^{-7}$ – $10^{-8}$  mbar) and argon supply (Argon 7.0, linde AG, Pullach, Germany). In the first step of polymerization, (28 mL) styrene was initiated with (0.1 mL, 0.15 mmol) *sec*-BuLi (1.4 M solution in hexane) at  $-78^{\circ}\text{C}$  having THF as reactor solvent, and was left for 2 h to make sure that its polymerization was complete. An aliquot of polystyrene was sampled out from the reactor, terminated with degassed methanol for molecular characterization of the first block. Methacrylic ester containing monomer exhibits high electron affinity as compared to styrene, and was added last in the polymerization procedure. Prior to the second monomer addition, (0.13 mL, 0.75 mmol) 1,1-diphenylethylene (DPE) was added to end-cap the polystyrene macro-initiator and the temperature was maintained at  $-30^{\circ}\text{C}$  for half an hour. The flask was cooled down to  $-78^{\circ}\text{C}$  before the addition of the purified SMA. The polymerization of the second block was left to complete for 2 h. Degassed methanol was used

to terminate the polymerization. All diblock copolymers were precipitated from their THF solution by a water/methanol mixture (80/20 v/v). The polymer was dried at 40 °C under vacuum. The synthetic route of PS-*b*-PMA polymerization is depicted in Scheme (3.4).

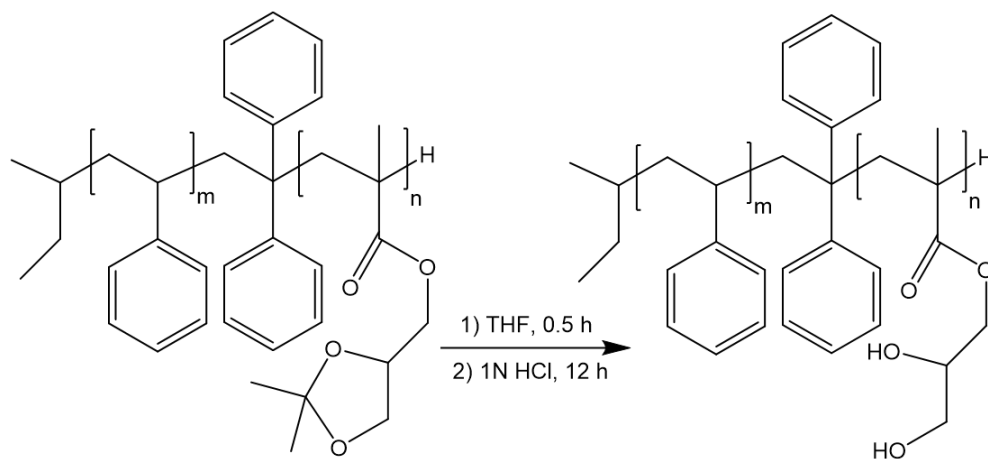


**Scheme 3. 4.** Synthetic route leading to PS-*b*-PSMA by sequential anionic polymerization of styrene and solketal methacrylate

### 3.2 Modification of PS-*b*-PSMA diblock copolymers

#### 3.2.1 Acidic hydrolysis of PS-*b*-PSMA

To deprotect the isopropylidene acetal group of PSMA, 1g block copolymer was dissolved in 40 mL THF and 1 N HCl (20 mL) was added drop-wise to the polymer solution under continuous stirring. After the complete addition of HCl, the mixture was stirred for 12 h and then the polymer was precipitated in methanol. The hydrolyzed polymer was dried at 40°C under vacuum and characterized by <sup>1</sup>H-NMR. The complete chemical reaction is shown in Scheme (3.5).

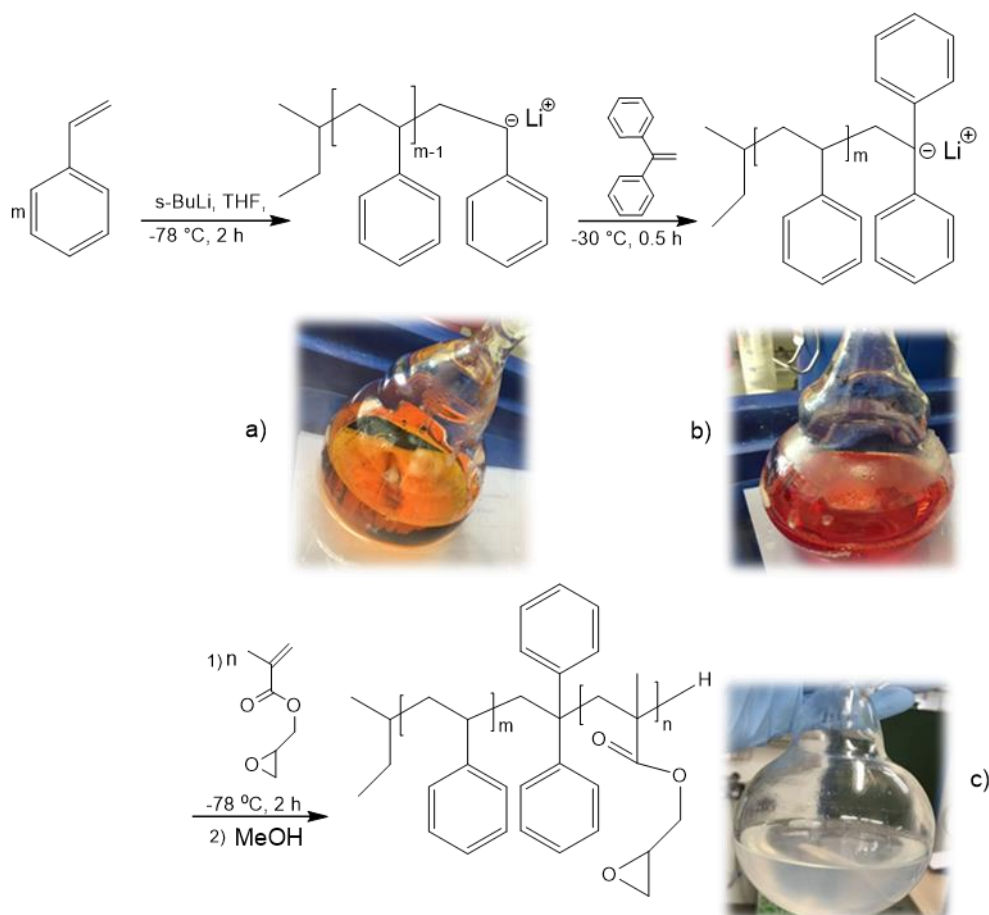


**Scheme 3. 5.** Acidic hydrolysis of PS-*b*-PSMA

#### 3.2.2 Synthesis of polystyrene-*block*-poly(glycidyl methacrylate) (PS-*b*-PGM) diblock copolymer

PS-*b*-PGM diblock copolymers were synthesized by sequential anionic polymerization as given in Scheme (3.6). All the polymers were synthesized under inert atmosphere of high vacuum ( $10^{-7}$ – $10^{-8}$  mbar) and argon supply (Argon 7.0, linde AG, Pullach, Germany). The required amount of dried lithium chloride (LiCl) introduced into the reactor first and dried under vacuum line for 4 h. THF was used as polymerization solvent. The temperature of reaction medium was

maintained around  $-80\text{ }^{\circ}\text{C}$ . Purified styrene (8.8 mL) was then added into the reactor under efficient stirring and was initiated with *sec*-BuLi (0.07 mL, 0.1 mmol). The solution turned yellow and after three hours of stirring an aliquot was taken for SEC analysis. The high nucleophilicity of polystyrene carbanion (as shown in Scheme (a) with orange color) was reduced by adding 1,1-diphenylethylene (DPE) and the solution turned red shown in Scheme (3.6). The temperature was maintained at  $-30\text{ }^{\circ}\text{C}$  for half an hour. The solution becomes immediately red after addition of DPE. Subsequently, the flask was cooled down to  $-78\text{ }^{\circ}\text{C}$ , before (1.85 mL) of purified glycidyl methacrylate (GM) were added. After 2 h the polymerization was terminated with degassed methanol and precipitated from their THF solution by a methanol/water mixture (85/15 v/v).

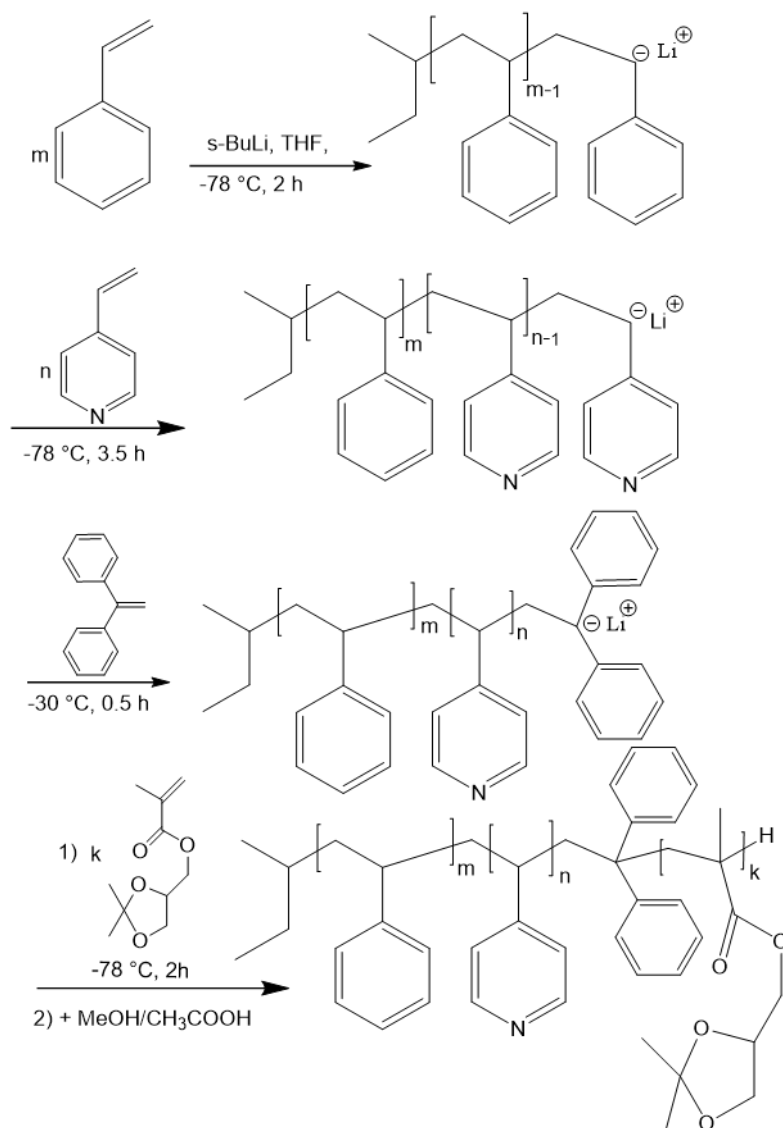


**Scheme 3. 6.** Synthetic route leading to PS-*b*-PGM by sequential anionic polymerization of styrene and glycidyl methacrylate (GM)

### 3.3 Synthesis of triblock terpolymers by anionic polymerization

#### 3.3.1 Synthesis of polystyrene-*block*-poly(4-vinylpyridine)-*block*-poly(solketal methacrylate) (PS-*b*-P4VP-*b*-PSMA) triblock terpolymer

The linear triblock terpolymer PS-*b*-P4VP-*b*-PSMA was synthesized by sequential living anionic polymerization in a Schlenk line apparatus using high vacuum ( $10^{-7}$ - $10^{-8}$  mbar) and Argon supply (Argon 7.0, linde AG, Pullach, Germany). All the chemicals were purified corresponding to the description before in Section 3.1.1. The synthetic procedure involves first the anionic polymerization of (17.1 mL) styrene in THF with (0.060 mL, 0.085 mmol) *sec*-BuLi at  $-78$  °C. After two hours an aliquot was taken for (SEC) analysis, followed by the addition of (3.5 ml) 4-vinylpyridine and the solution was stirred overnight. Another aliquot was taken from the polymerization reactor and was terminated with degassed methanol for molecular characterization. PS-*b*-P4VP macro-initiator was end capped with 0.03 mL (0.17 mmol) 1,1-diphenylethylene by maintaining the temperature at  $-30$  °C for half an hour. Afterwards, purified 1 mL solketal methacrylate was added to the mixture and temperature was decreased again to  $-78$  °C. Finally, the polymerization was quenched with degassed methanol/acetic acid (10:1) after two hours. After removal of THF under reduced pressure, the polymer was precipitated in water/methanol mixture (80/20 v/v). The final product was dried in a vacuum oven for 48 h at  $50$  °C to give a colorless powder. The polymerization route is depicted in Scheme (3.7).

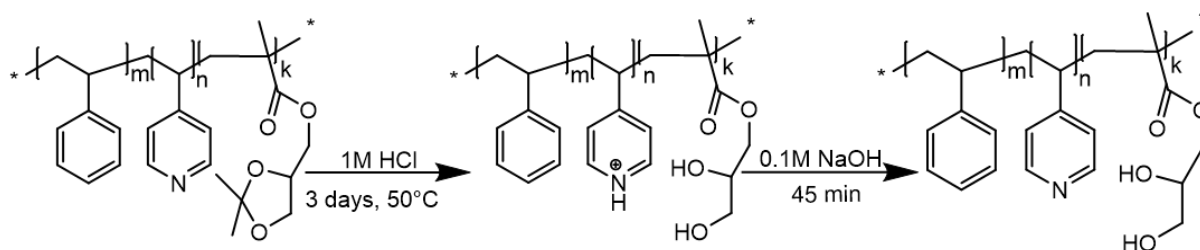


**Scheme 3. 7.** General reactions for the synthesis of PS-*b*-P4VP-*b*-PSMA triblock terpolymer *via* sequential anionic polymerization.

### 3.3.2 Acidic hydrolysis of triblock terpolymers

The acidic hydrolysis of PS-*b*-P4VP-*b*-PSMA triblock terpolymer (crude polymer) was performed following the same chemical route explained for triblock terpolymer membranes post modification. The procedure was monitored by  $^1\text{H-NMR}$  to ensure the removal of the

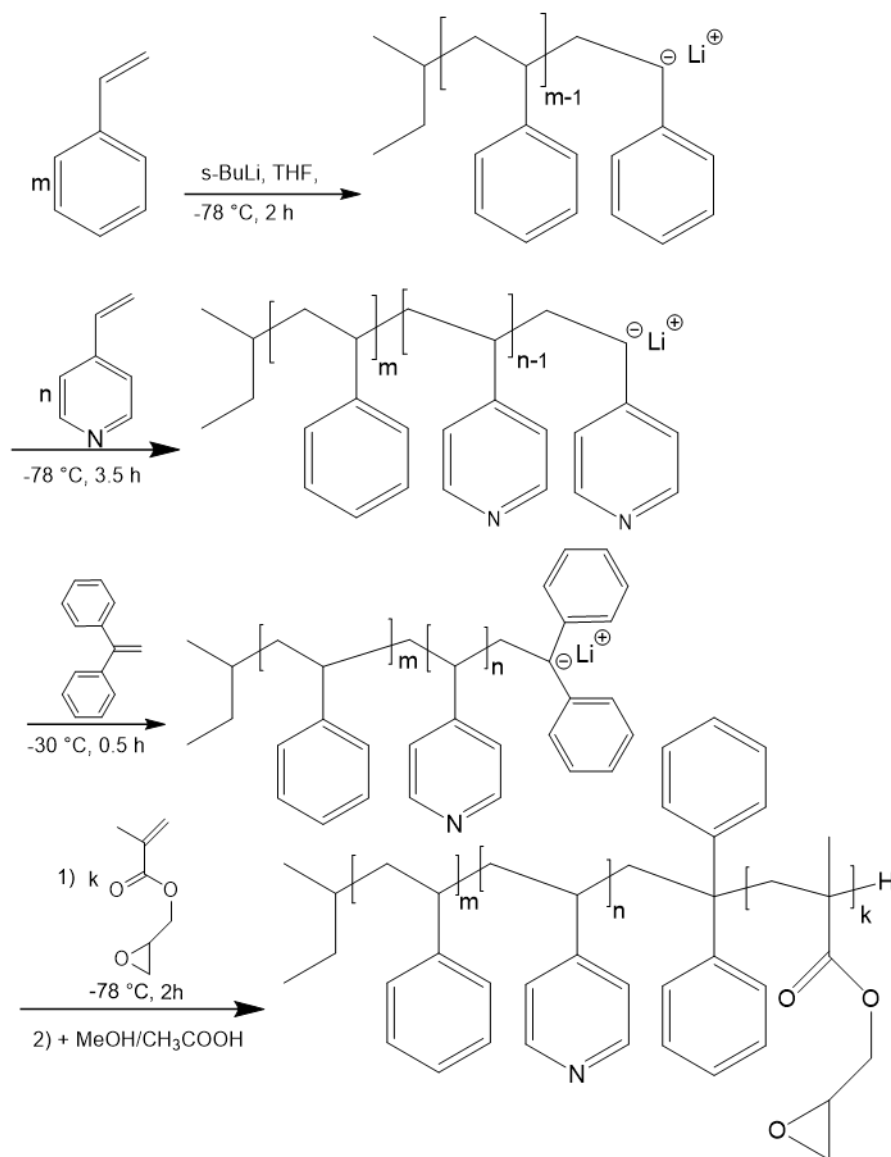
isopropylidene acetal group. After each step, the crude polymer was re-dissolved in deuterated solvents and spectra were recorded. The complete chemical process is shown in Scheme (3.8)



**Scheme 3. 8.** Deprotection reaction of the ketal-PSMA moiety

### 3.3.3 Synthesis of polystyrene-*block*-poly(4-vinylpyridine)-*block*-poly(glycidyl methacrylate) (PS-*b*-P4VP-*b*-PGM) triblock terpolymer

500 ml of dry THF was treated as described in section and transfer to the reactor containing dried lithium chloride (LiCl). Synthesis of PS-*b*-P4VP was carried out analogously as described in Section 3.1.5. (8.26 mL, 71.3 mmol) of styrene and (2.05 mL, 19.2 mmol) of P4VP were used for this purpose. After complete polymerization of the diblock copolymer, an aliquot was taken out for (SEC) and <sup>1</sup>H-NMR studies. Afterwards, (0.17 mL, 1 mmol) DPE is added to the reactor under efficient stirring at 30°C for half an hour. The temperature of the reaction mixture was maintained again to -80°C and (0.5 mL, 3.5 mmol) of glycidyl methacrylate added via a syringe into the reactor. The polymerization was quenched with degassed methanol/acetic acid (10:1 vol. %) after 2 h. After the removal of excess THF under reduced pressure, the polymer was precipitated in methanol/water mixture (85/15 v/v). The polymer was dried at 40 °C under vacuum. The polymerization route is depicted in Scheme (3.9).



**Scheme 3. 9.** General reactions for the synthesis of linear triblock terpolymer PS-*b*-P4VP-*b*-PGM by following anionic polymerization technique.

### **3.4 Membrane formation**

#### **3.4.1 Hand casting**

Different block copolymers were dissolved in a mixture of solvents to prepare solutions of different concentrations and compositions. Block copolymer membranes were cast on a non-woven support by using a doctor blade with a gap height of 200  $\mu\text{m}$ . The gap height of the doctor blade was adjustable and as a result the thickness of the film can be varied. The cast film was exposed to air for a definite period for evaporation of the solvent and then immersed into a non-solvent bath (water). For a complete transfer of non-solvent (water) and solvents, the membranes were immersed in the precipitation bath for 6 h. The membrane obtained was initially dried at room temperature for 24 h and then for 48 h at 50  $^{\circ}\text{C}$  in a vacuum oven.

#### **3.4.2 Machine casting**

For machine casting an automated casting machine was used which was equipped with nonwoven support (polyester), doctor blade and coagulation bath (mostly water). The speed of non-woven was adjusted according to the evaporation time required. The thickness of the cast film can be changed by adjusting the height of doctor blade. The casting machine used in this study is shown in Figure (3.1) [123].

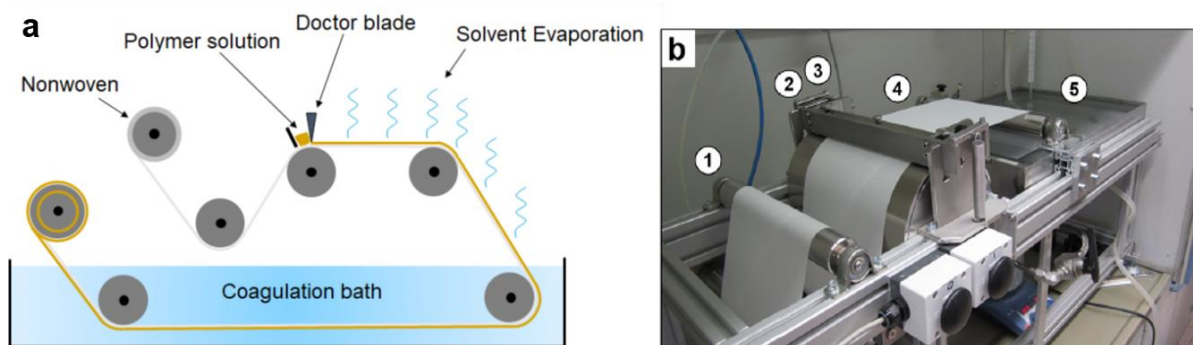


**Figure 3. 1.** Schematic representation (a) and (b) of the in-house built casting machine used for fabrication of membrane via SNIPS. Reprinted with permission from ref [123].

### 3.4.3 Spin coating of polymer film

PS<sub>71</sub>-*b*-P4VP<sub>26</sub>-*b*-PSMA<sub>3</sub><sup>142</sup> films were prepared by spin coating a solution of 2 wt% polymer in chloroform on a silicon wafer for at 2000 rpm. The samples were dried under reduced pressure at 60°C. The dried film was analyzed by AFM.

### 3.4.4 Post modification of triblock terpolymer membranes

Isoporous membranes of triblock terpolymers were treated with 1M HCl solution at 50°C for 3 days to remove the acetonide moiety of PSMA blocks. The acid treated membranes were further dipped in 0.1M NaOH solution for 45 minutes to completely deprotonate the quaternized P4VP blocks. Finally, the membranes were rinsed with deionized water and dried in the vacuum oven at 50 °C.

### 3.4.5 Preparation of GO/PGO-PS-*b*-PGMA membranes

The GO/PGO nanosheets (0.5, 1.0 and 1.5 wt% based on the weight of polymer) were added to the ternary mixture of solvents THF-DMF-DOX (2:1:1 wt%) and sonicated for 20 min in an

ultrasound bath. After that PS-*b*-PGMA diblock copolymer was dissolved in GO/PGO suspension by continuous stirring for 24h at room temperature. The resulting mixture was cast onto a glass plate using a doctor blade with gap height of 200  $\mu\text{m}$ . After doctor blading, the volatile solvents were partially evaporated and the cast film immersed in water bath. The prepared membranes were dried at room temperature for 12h and then in the vacuum oven at 50°C for 48h.

### **3.5 Characterization techniques**

#### **3.5.1 Size exclusion chromatography (SEC)**

Size exclusion chromatography is a technique used to sort molecules by size and provides information about the molecular weight of materials. Mostly synthetic polymers are composed of hundreds to thousands of chains of different molecular weights (MW) that result in characteristic molecular weight distributions. The molecular weight or molecular weight distribution (MWD) plays a critical role for the determination of mechanical, bulk and solution properties of polymeric materials. SEC has two basic versions. One is gel permeation chromatography (GPC) which involves a non-aqueous mobile phase and hydrophobic column packing material to separate, fractionate, or measure the molecular weight distribution of synthetic polymers. On the other hand, in gel filtration chromatography hydrophilic packing material and an aqueous mobile phase is used to separate the molecules. SEC is usually performed within a column that consists of hollow tubes tightly packed with micron scale polymer beads containing pores of different sizes. The polymer under analysis is dissolved in an appropriate solvent which also acts as mobile phase and injected into a packed porous column. High molecular weight material elutes first from an SEC column, followed by lower molecular weight component with smaller hydrodynamic volume which effectively sorts the molecules by size. After the separation of the polymers, retention time is recorded by different

detectors, most common is a differential refractometer which can detect the changes in refraction index of the eluted solution [142-144].

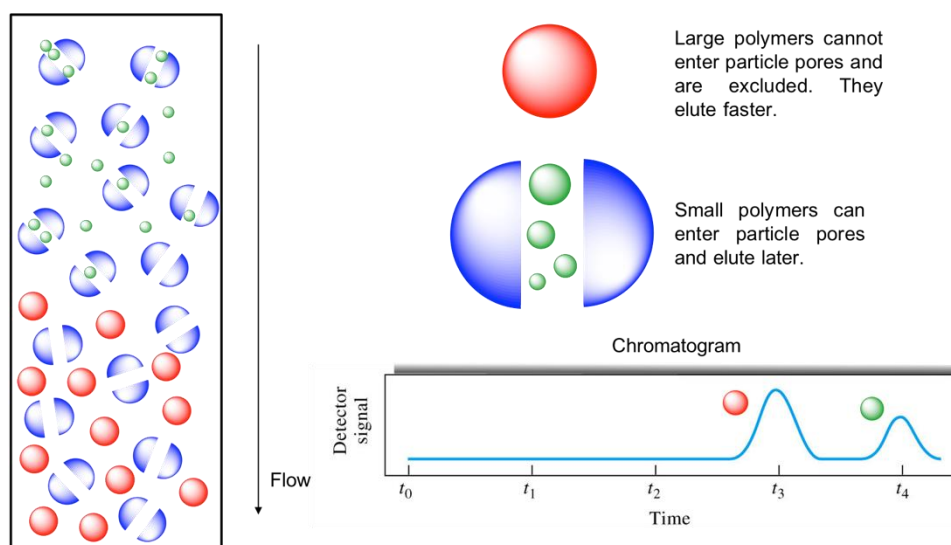


**Figure 3. 2.** Illustration of separation principle of size exclusion chromatography.[145]

The molecular weights of the polystyrene-precursor and molecular weight distribution of the block copolymer used in this study were determined by gel permeation chromatography calibrated with PS standards. The measurements were performed at 50 °C in *N,N*-dimethylacetamide with addition of lithium chloride using PSS GRAM columns [GRAM pre column (dimension 8·50 mm), GRAM column (porosity 3000 Å, dimension 8·300 mm, particle size 10 µm) and GRAM column (porosity 1000 Å, dimension 8·300 mm, particle size 10 µm)], at a flow rate of 1.0 mL min<sup>-1</sup> (VWR-Hitachi 2130 pump). A Shodex RI-101 refractive index detector with a polystyrene calibration was used.

### 3.5.2 Nuclear magnetic resonance spectroscopy (NMR)

The synthesized polymers and membranes were analyzed by proton nuclear magnetic resonance spectroscopy (<sup>1</sup>H-NMR). <sup>1</sup>H-NMR measurements were performed on a Bruker Ascend 300

NMR spectrometer (300 MHz) or Bruker Ascend 500 NMR spectrometer (500 MHz, Bruker) using deuterated chloroform ( $\text{CDCl}_3$ ) and deuterated dimethyl formamide ( $\text{DMF-}d_7$ ) as solvent, at room temperature. Tetramethylsilane (TMS) was used as an internal standard.

### **3.5.3 Scanning electron microscopy (SEM)**

A scanning electron microscope (SEM) scans a focused electron beam over a surface in a raster scan pattern to obtain information about surface topography and composition. It is one of the versatile instruments that is available for the examination and analysis of the microstructure morphology with a user friendly protocol. The main components of SEM are illustrated in Figure 3.3. As the accelerated primary electrons interact with the surface of the sample, secondary electrons, back scattered electrons and characteristic X-rays are produced as a result of elastic or inelastic scattering. The penetration depth of the electron beam that hits the surface of the sample depends on accelerating voltage and density of the sample. Low energy secondary electrons are collected by a positively charged electron detector, which in turn gives a three-dimensional image of the sample. The number of secondary electrons produced depends not only on the atomic number of the specimen but also on the angle between the primary beam and the surface of specimen. A sample analyzed by SEM has to be vacuum compatible and it helps to be a conducting material. Non conducting specimens must be coated with a thin conducting film of carbon, gold or some other metal [146, 147].

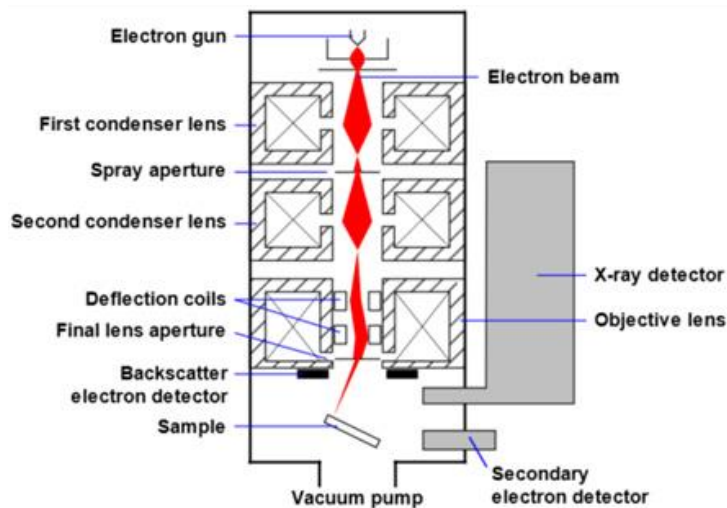


**Figure 3. 3.** Representative image of key components of Scanning Electron Microscope (SEM).[148]

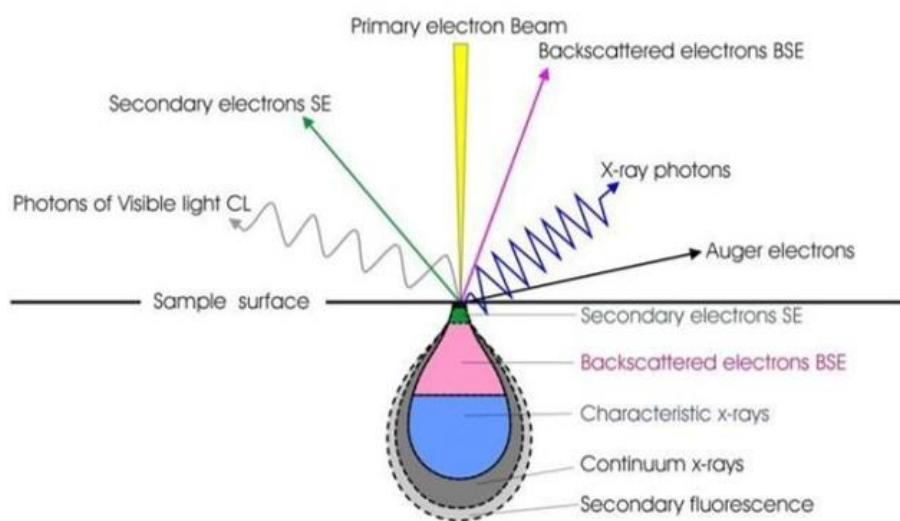


**Figure 3. 4.** Schematic illustration of the primary electron interaction with sample and generation of secondary electrons, back scattered electrons and X-ray radiation.[149]

To analyze the structure of the membranes under study, samples were examined on a LEO Gemini 1550 VP (Zeiss, Oberkochen, Germany) at a voltage of 3 or 5 kV. The samples were coated with 2.0 nm platinum. Cross-sections of the membranes were prepared while dipping

the membranes in isopropanol, freezing in liquid nitrogen, and breaking. Average pore size values were determined using the software Analysis (Olympus Soft Imaging Solutions GmbH, Münster, Germany) based on the SEM results.

### 3.5.4 Transmission electron microscopy (TEM)

Transmission electron microscopy (TEM) is widely applied in the field of membrane science to characterize the micro and nanoscale features of the membrane. It offers to examine some fine features whose characteristic dimensions are less than 100nm in size. Based on high resolution, it is suitable to characterize microphase separation of block copolymers in bulk. The schematic illustration of TEM is shown in Figure 3.5.

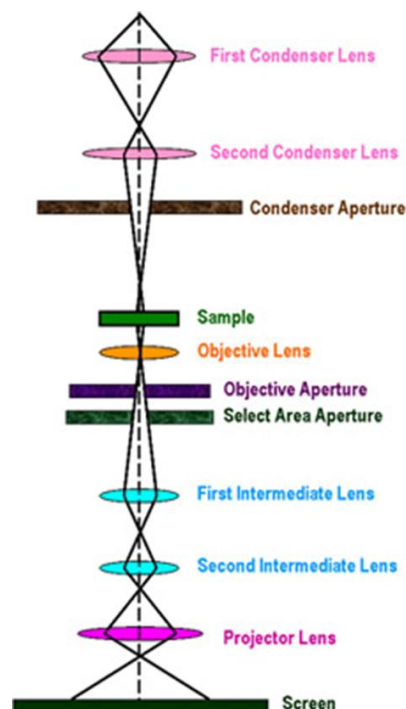


**Figure 3. 5.** Main components of Transmission Electron Microscopy.[150]

TEM operates on the same basic principle as the light microscope but uses electron instead of light. The optimal resolution of TEM images is many orders of magnitude better than that from light microscope and can reveal finest details of internal structures. Electron beams are emitted from the electron gun and transferred to the specimen with the help of magnetic lenses giving either a broad beam or focused beam. The thickness of a TEM specimen usually should be within 100 nm for electrons to pass through. The electrons are focused into a small thin coherent beam by the use of condenser lenses that strike the specimen. Some parts of electron beam are transmitted and focused by the objective lens into an image on phosphor screen or charged couple camera. The darker areas of the image represent those areas of the sample where fewer electrons are transmitted through (because of heavy atoms) whereas the lighter areas represent those areas where more electrons are transmitted through. This is the so-called bright field mode, which is used in this work exclusively. In the dark-field mode the strongly scattered electrons are used for imaging, leading to an inverse contrast. [151].

The bulk microphase morphology of the block copolymers was investigated with a Tecnai G2 F20 (FEI, Eindhoven, The Netherlands) transmission electron microscope (TEM). It was operated at acceleration voltage of 120 kV in bright-field mode. Thin sections (thin section thickness: 50 nm) were cut using a Leica Ultra microtome EM UCT (Leica Microsystems, Wetzlar, Germany) equipped with a diamond knife (Diatome AG, Biel, Switzerland).

### **3.5.5 Atomic force microscopy (AFM)**

The surfaces of the membranes were imaged with a Bruker MultiMode 8 (Bruker, Karlsruhe, Germany) in Peak Force QNM (Quantitative Nanomechanical Mapping) mode at room temperature. For measurements in dry state ScanAsyst-Air probes and for measurements in liquid ScanAsyst-Fluid+ probes in a liquid cell were used. For the analysis, the software NanoScope Analysis 1.5 (Bruker, Karlsruhe, Germany) was used.

### 3.5.6 Contact angle measurements

The wettability of the membrane can be determined by water contact angle measurement which is traditionally defined as the angle ( $\theta$ ) between the surface of the liquid and outline of the contact surface. This is geometrically determined by drawing a tangent from the contact point along the gas liquid interface as shown in Figure 3.6.

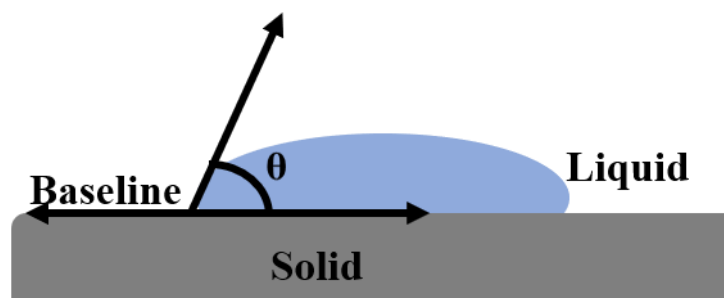


**Figure 3. 6.** Schematic illustration of contact angle

Contact angle can be large or small depending on the nature of the liquid as well as surface properties of the solid being investigated. Based on the contact angle of water on a solid interface is divided into three classes. If the contact angle between a liquid and solid surface is  $< 90^\circ$ , the solid surface is considered wettable (hydrophilic). When the contact angle is  $\geq 90^\circ$ , the liquid will not spread over the surface and is considered not wettable (hydrophobic). However, in case of superhydrophobic materials the value of contact angle approaches the limit of  $180^\circ$  [152]. This is illustrated in the following Figure 3.7

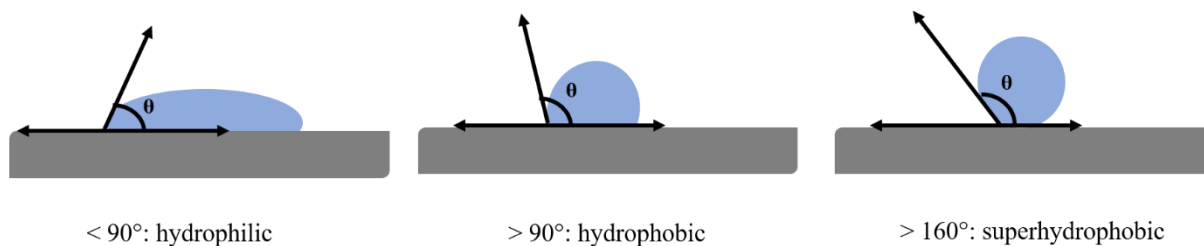


**Figure 3. 7.** Classification of surfaces based on contact angle with water

In this study, Drop Shape Analyzer DSA 100 (KRUSS, Hamburg, Germany) was used for the measurement of the dynamic contact angle of the membranes. For this piece of membrane was cut out and fixed on a slide or directly fixed on the stage of the instrument. Subsequently, the sessile droplet of 2  $\mu\text{L}$  of ultrapure water at room temperature applied on the membrane surface and immediately the process of the seeping droplet recorded until it disappears (in case of hydrophilic surfaces). This is recorded according to the method shown in Figure 3.7.

### 3.5.7 Water flux measurements

Water flux was performed in dead-end mode at a trans-membrane pressure (TMP) of 2 bar at room temperature using a homemade automatic test device. The instrument had three measuring cells and a feed container with a volume of 4L. The membrane area was 1.8  $\text{cm}^2$ . The determination of the permeate volume ( $\Delta V$ ) which penetrated the membrane per unit time  $\Delta t$  was done separately for each cell and using a digital scale (Kern EG 4200-2NM, Kern & Sohn, Balingen, Germany). The transmembrane pressure ( $\Delta p$ ) was calculated from the values of two digital pressure sensors of the type LEO3 ((Keller, Jestetten, Germany) which also recorded the ambient temperature. All the parameters were recorded in LABVIEW program (National Instruments, Austin, USA) at defined time intervals. These studies were conducted employing demineralized water with an electrical conductivity of  $\approx 0.055 \mu\text{Scm}^{-1}$ . The water flux ( $P$ ) is calculated as follows,

$$P = \Delta V / A \cdot \Delta t \cdot \Delta p$$

Where  $\Delta V$  is the volume of collected water between two mass measurements,  $A$  is the active surface area of membrane,  $\Delta t$  is the time between two mass measurements, and  $\Delta p$  is the transmembrane pressure.

### 3.5.8 Static protein adsorption

The protein adsorption capacity of the membranes was evaluated through static protein adsorption experiments using hemoglobin solutions with a concentration of 1.0 g/L in a PBS-buffer solution (10 mM PBS, 0.9 wt. % NaCl). To ensure a complete wetting of the membrane structure with the protein solution, all membrane samples were immersed in PBS-Buffer and washed twice. Subsequently, 2 mL of the protein solution was placed on each sample in a closed vial. To reach equilibrium, the samples were shaken for 24 h at 90 rpm and at 25°C. After that, each membrane sample was rinsed two times with 2 mL PBS-buffer for 10 min. The protein adsorption values were calculated as follows

$$\text{Protein adsorption} = m_0 - (m_1 + m_{w1} + m_{w2}) / A_{\text{membrane}}$$

Where

$m_0$  is mass of the protein before the adsorption experiment

$m_1$  is the protein mass after the adsorption experiment

$m_{w1}$  and  $m_{w2}$  are the protein masses in the washing solutions.

The adsorption value is related to the membrane surface area ( $A_{\text{membrane}}$ ). The concentrations of the protein were determined by UV/VIS spectroscopy at a wavelength of  $\lambda = 280$  nm.

### 3.5.9 Retention measurements

PEG and proteins retention was measured by using a stirred test cell (EMD Millipore™ XFUF04701, effective membrane diameter 2.0 cm) proteins The molecular weight cutoff (MWCO) (minimum molecular weight of the solute with 90% rejection), was checked using PEG (PSS polymer standards Service GmbH, Germany). The retention experiments were done in dead end mode using aqueous solutions of 0.02 wt. % of PEG.



**Figure 3. 8.** Test cell EMD Millipore™ XFUF04701

First, pure water flux was measured for 1 h at 2 bar transmembrane pressure and then the feed solution was supplied. A minimum of 3 membrane samples were utilized to finalize one measurement. The solution of proteins in PBS buffer at a concentration of 1 g/L was employed for the retention measurements. The concentrations of protein solutions were measured at the

wavelength of 280 nm with a UV–Vis spectrophotometer (GENESYS 10S, Thermo Fisher Scientific, Bremen, Germany). The protein retention was calculated by the following equation:

$$R = (1 - c(p) / c(f)) \times 100$$

where  $c(p)$  and  $c(f)$  represent the BSA concentrations (g/L) in the permeation and feed.

### **3.5.10 X-ray photoelectron spectroscopy (XPS)**

The XPS analysis of the graphene oxide loaded membranes was carried out by using a Kratos AXIS Ultra DLD spectrometer (Kratos, Manchester, United Kingdom) with an Al-K $\alpha$  X-ray source (monochromator) operated at 225 W and at vacuum of  $< 2.5 \times 10^{-9}$  Torr. After degassing in the ultra-high vacuum (UHV) pre-load chamber, membranes were positioned in the UHV analytics chamber. The analyzed area was 700  $\mu\text{m}$  x 300  $\mu\text{m}$ . The acceleration depth was approximately 5 nm. For the scanned region, the pass-energy was set to 20 eV while for survey spectra a pass-energy of 160 eV was used. All of the spectra were calibrated to 284.5 eV binding energy of the C1s signal. For all the samples charge neutralization was necessary. The evaluation and validation of the data were carried out with the software CASA-XPS version 2.3.18. For deconvolution of the region files, background subtraction (linear or Shirley) was performed before calculation.

## **Chapter 4: Results and discussion**

### **Synthesis of polystyrene-*b*-poly(solketal methacrylate) (PS-*b*-PSMA) and formation of membranes via SNIPS**

#### **4.1. Brief introduction**

In this study our main goal was to synthesize protective groups containing diblock copolymers via living anionic polymerization. Polymers resulting from monomers with “active” protons (i.e., OH, SH, or NH<sub>2</sub> groups) could not be directly synthesized through this technique, due to their spontaneous reaction with the initiator anions or the growing chain end [77]. To overcome this difficulty, either controlled radical polymerization can be employed, or protective groups are introduced into the monomeric unit reactive site, blocking the “active” protons during the course of anionic polymerization, which can be easily cleaved afterwards to get the required functional groups [46].

##### **4.1.1 Synthesis and characterization of poly(solketal methacrylate) (PSMA)**

Poly(isopropylidene glycerol methacrylate), commonly known as poly(solketal methacrylate) (PSMA), acts as a precursor polymer of poly(glyceryl methacrylate) (PGMA) which was reported for the first time by Mori et al. [46]. In this work, solketal methacrylate monomer was introduced to prepare diblock and triblock terpolymers by sequential living anionic polymerization. First, to optimize the synthetic conditions of (SMA) monomer, homopolymer was synthesized by living anionic polymerization. The composition of the diblock copolymer was calculated from the <sup>1</sup>H-NMR spectrum. The molecular weight and dispersity index (*D*) were determined by (SEC) at 50°C using THF as solvent and polystyrene as standard. Figure 4.1.1 shows the characteristic peaks of poly(solketal methacrylate). The synthesized polymer molecular characteristics are summarized in Table (4.1)

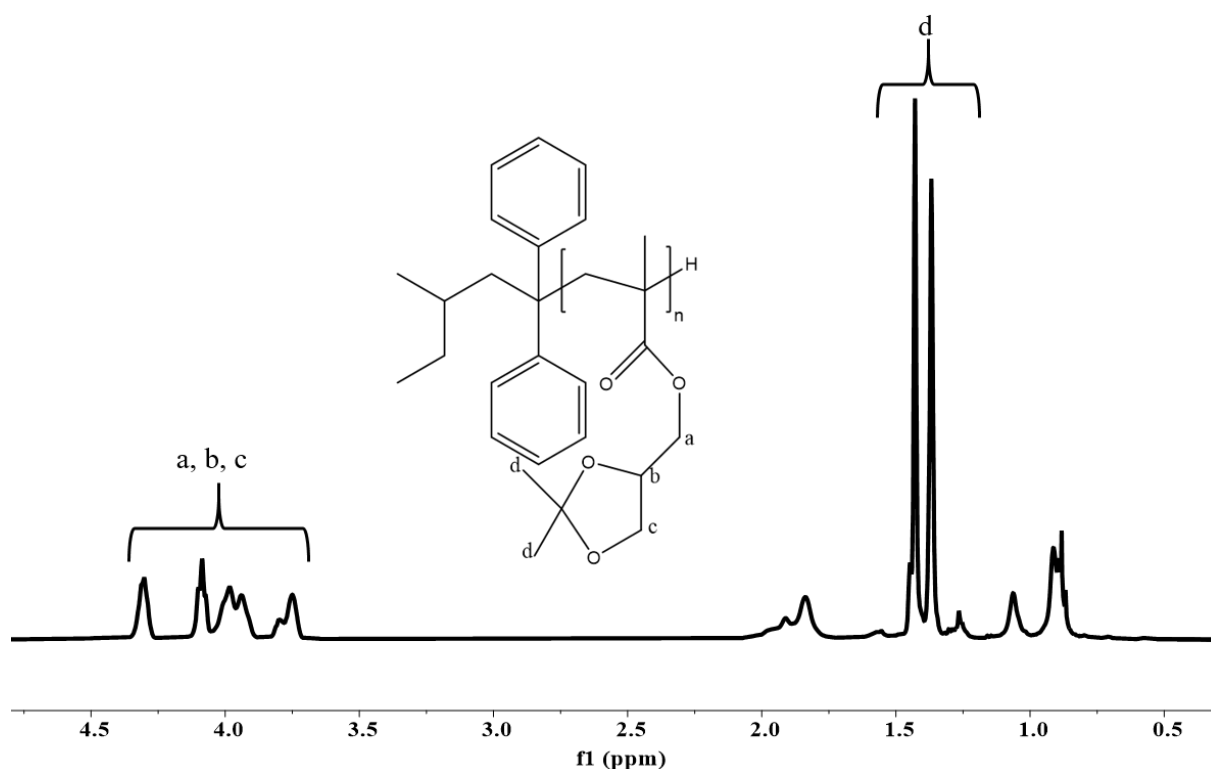


**Figure 4.1.1.** <sup>1</sup>H-NMR spectra of PSMA homopolymer in CDCl<sub>3</sub>

**<sup>1</sup>H-NMR** (CDCl<sub>3</sub>, 20 °C, 300 MHz, TMS):

$\delta$  [ppm] = 7.3(m', 10H, arom. H (DPE)), 4.31(m', 1H, H-7), 4.07(t', 1H, H-8a), 3.98(m', 2H, H-6), 3.75(m', 1H, H-8b), 1.83(m', 8H, H-1, H-2, H-3, H-4, H-5), 1.42(s', 9H, 2 × CH<sub>3</sub> (*s*-BuLi), CH<sub>3</sub>-a (PSMA)), 1.36(s', 3H, CH<sub>3</sub>-a2 (PSMA)), 1.06(s', 3H, CH<sub>3</sub>-a2 (PSMA)), 0.90(s', 3H, CH<sub>3</sub>-b2 (PSMA)).

**Table 4. 1.** Molecular weight and dispersity index of the PSMA homopolymer

Polymer	$M_n$ (kg/mol) <sup>a</sup>	$D^a$
PSMA	11	1.2

a. Molecular weight and dispersity index were determined with SEC.

#### 4.1.2 Synthesis and characterization of polystyrene-*block*-poly(4-vinylpyridine) (PS-*b*-P4VP) diblock copolymer

PS-*b*-P4VP block copolymers were synthesized by sequential living anionic polymerization described in the literature before [123, 153, 154]. The synthetic route of PS-*b*-P4VP polymerization is depicted in Section 3.1.5.

Figure 4.1.2 shows  $^1\text{H-NMR}$  spectrum of PS-*b*-P4VP where the peak labelled as 'a' was ascribed to the two protons of (4-vinylpyridine). The synthesized polymers are summarized in Table (4.2).

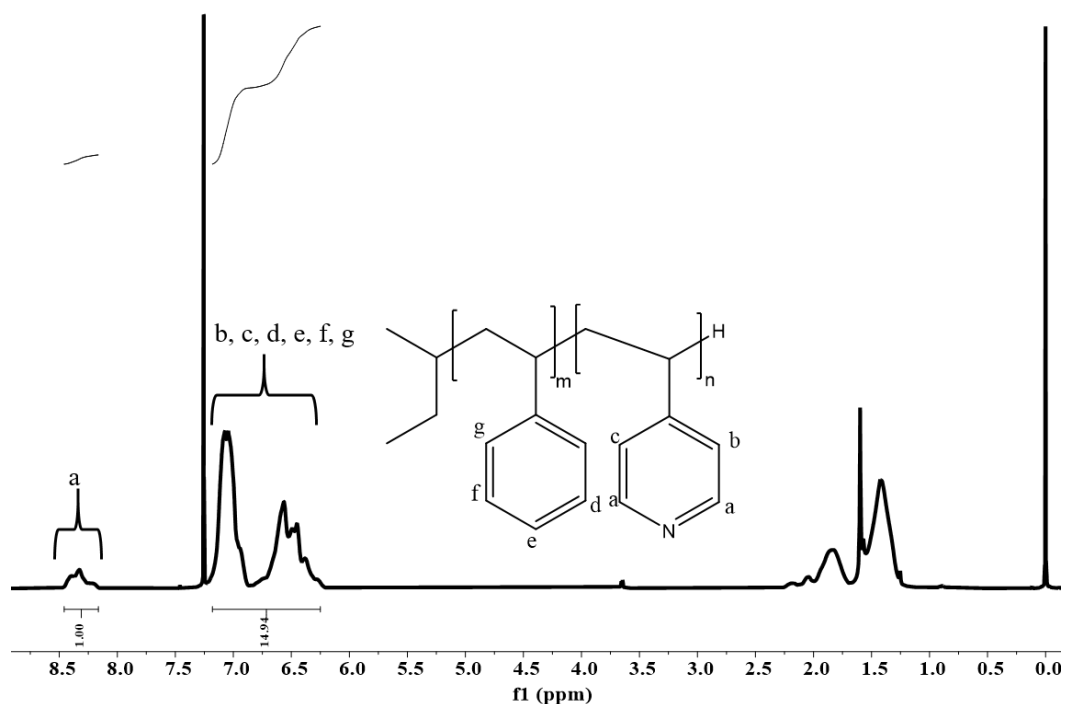


**Figure 4.1.2.**  $^1\text{H-NMR}$  spectra of PS<sub>85</sub>-*b*-P4VP<sub>15</sub><sup>166</sup> in CDCl<sub>3</sub>

$^1\text{H-NMR}$  (CDCl<sub>3</sub>, 20 °C, 300 MHz, TMS):

$\delta$  [ppm] = 8.32 (m', 2H, H-8), 7.07-6.45 (m', 7H, H-7, H-9, H-10, H-11), 1.84-0.90 (m', 16H, H-1, H-2, H-3, H-4, H-5, H-6, 2x CH<sub>3</sub>).

**Table 4. 2.** Molecular weight, weight percentage of P4VP and dispersity index of PS-*b*-P4VP

Polymer	M <sub>n</sub> (kg/mol) <sup>a</sup>	P4VP (wt%)	D <sup>a</sup>
PS <sub>85</sub> - <i>b</i> -P4VP <sub>15</sub>	166	15	1.08
PS <sub>85</sub> - <i>b</i> -P4VP <sub>15.3</sub>	166	15.3	1.1
PS <sub>80.5</sub> - <i>b</i> -P4VP <sub>19.5</sub>	123	19.5	1.03

a. Molecular weight and dispersity index were determined with SEC.

#### 4.1.3 Synthesis and characterization of polystyrene-*block*-poly(solketal methacrylate)

##### (PS-*b*-PSMA) diblock copolymer

PS-*b*-PSMA diblock copolymers were synthesized through sequential living anionic polymerization as given in the scheme below. The complete process of polymerization was optimized regarding monomer purification, monomer addition, block composition and molecular weight. PS-*b*-PSMA diblock copolymers were characterized by <sup>1</sup>H-NMR spectroscopy by recording the spectra where tetramethylsilane (TMS) was used as internal standard and deuterated chloroform (CDCl<sub>3</sub>) as a solvent. Figure 4.1.3 shows <sup>1</sup>H-NMR spectra of PS<sub>81</sub>-*b*-PSMA<sub>19</sub><sup>170</sup> where the peaks at 3.68-4.24 ppm (a, b, c) correspond to the five protons of solketal methacrylate. Block copolymers featuring molecular weights of up to 319 kgmol<sup>-1</sup> having a PSMA content between 17.2 and 26 wt% have been successfully polymerized. The results of synthesized polymers are compiled in Table (4.3). As shown in Figure 4.1.4 SEC and Table (4.3), all the diblock copolymers synthesized were free of their precursors and their molecular weight distributions (M<sub>w</sub>/M<sub>n</sub>) were narrow (1.01-1.04) which proved the control over the anionic polymerization.

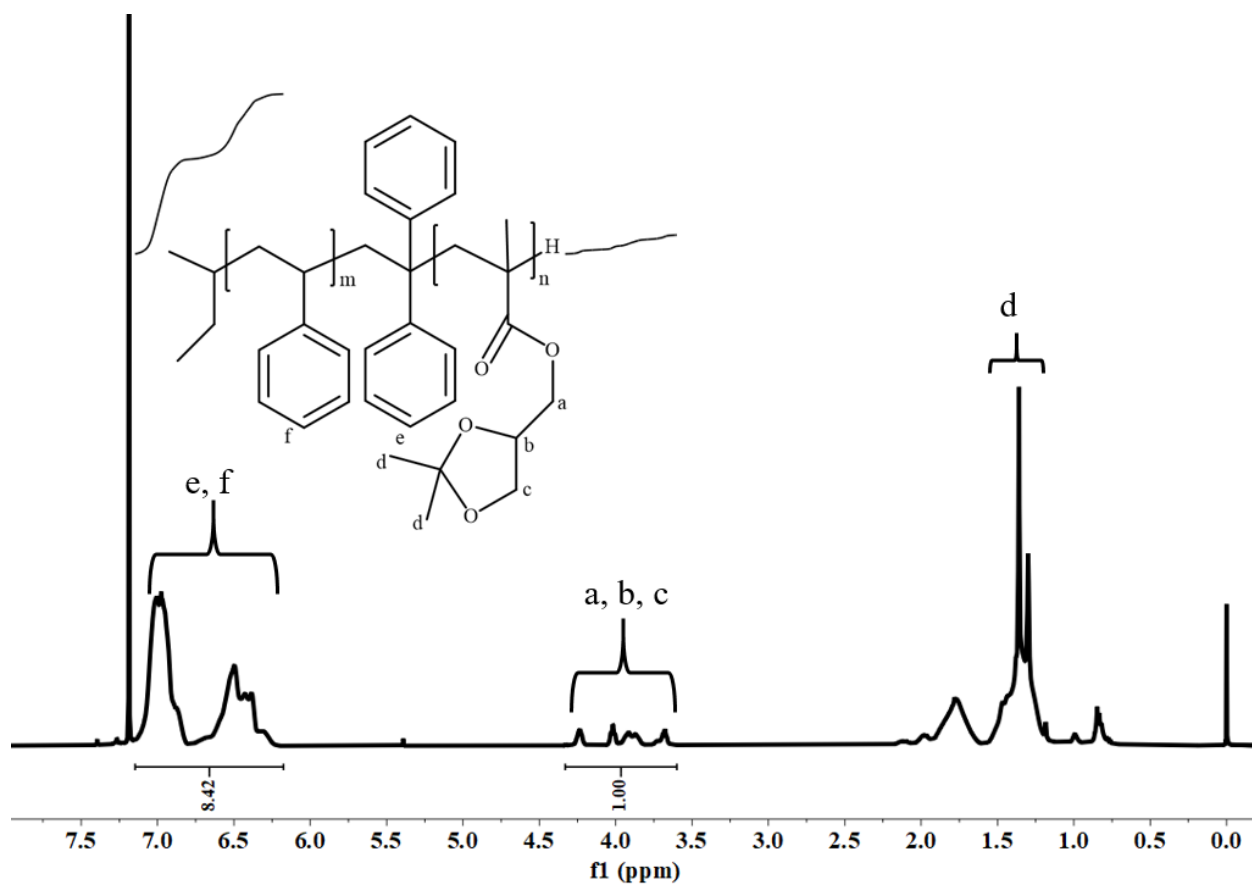


**Figure 4.1.3.**  $^1\text{H-NMR}$  spectrum of  $\text{PS}_{81}\text{-}b\text{-PSMA}_{19}^{170}$  in  $\text{CDCl}_3$

$^1\text{H-NMR}$  ( $\text{CDCl}_3$ ,  $20\text{ }^\circ\text{C}$ ,  $300\text{ MHz}$ , TMS):

$\delta$  [ppm] = 7.07-6.57(m', 15H, H-11, H-12, H-13, H-14, H-15, arom. H (DPE)), 5,4 (s', DPE), 4.23 (m', 1H, H-9), 4.03 (t', 1H, H10-a), 3.92 (m', 2H, H-8), 3.67 (m', 1H, H-10b), 2.1-1.41(m', 26H, H-1, H-2, H-3, H-4, H-5, H-6, H-7, 2x  $\text{CH}_3$  (*s*-BuLi), 3x  $\text{CH}_3$  (PSMA))

In this work, we focus on the synthesis of diblock copolymers with PSMA content of 17-26 wt% since the cylindrical nanostructures are intended to form in this range. An exemplary molar mass distribution of a  $\text{PS}_{81}\text{-}b\text{-PSMA}_{19}^{170}$  derived from SEC measurements and the corresponding  $^1\text{H-NMR}$  spectrum are given in Figure 4.1.3, 4.1.4.

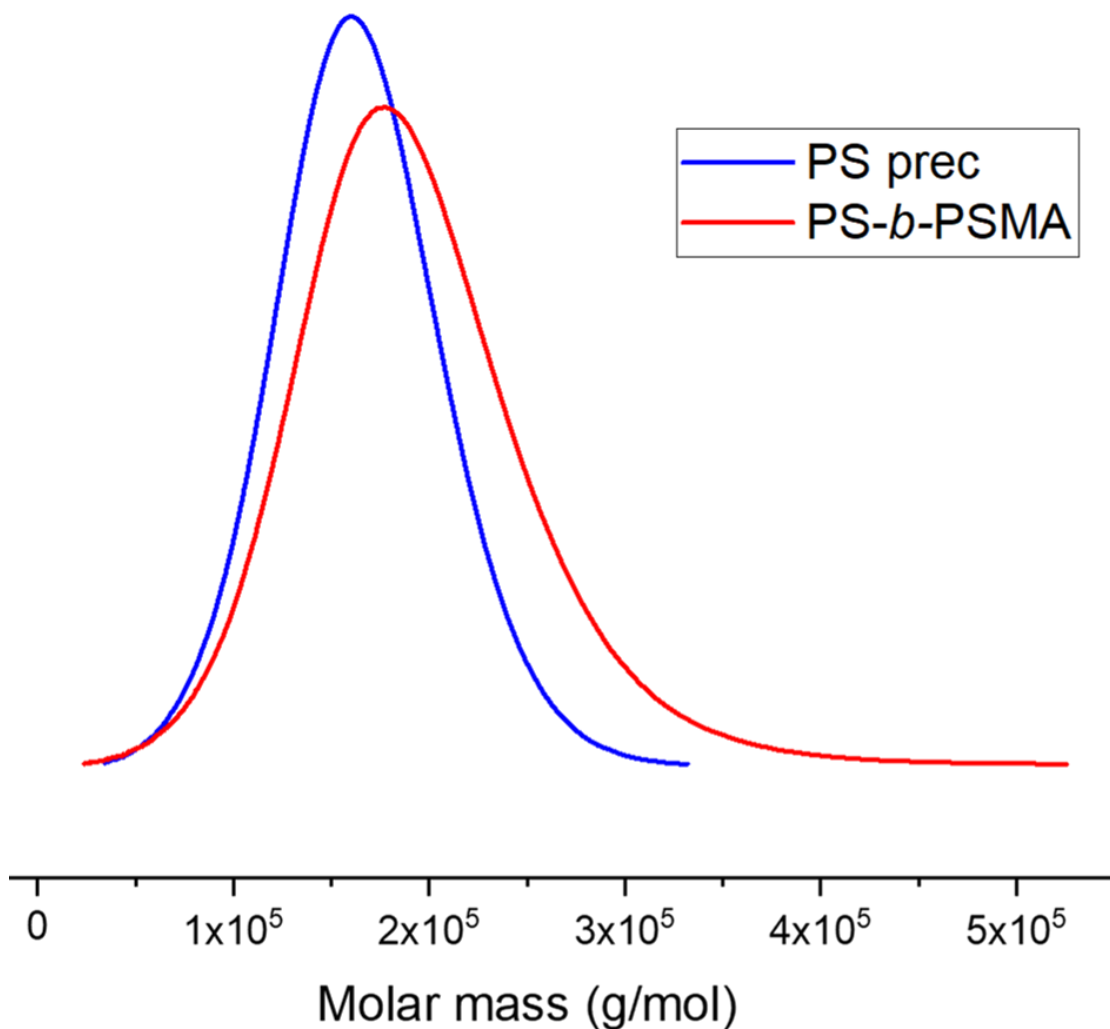


**Figure 4.1.4.** SEC traces of PS homopolymer and PS<sub>81</sub>-*b*-PSMA<sub>19</sub><sup>170</sup> diblock copolymer (measurement in THF at 30 °C using PS standards)

**Table 4. 3.** Characterization data of PS-*b*-PSMA diblock copolymers

Batch no	Polymer	M <sub>n</sub> (kg/mol)	PSMA (wt%)	<i>D</i>
SS-220816	PS <sub>76</sub> - <i>b</i> -PSMA <sub>24</sub>	135	24	1.03
SS-301015	PS <sub>81</sub> - <i>b</i> -PSMA <sub>19</sub>	170	19	1.04
SS-280616	PS <sub>76</sub> - <i>b</i> -PSMA <sub>24</sub>	200	24	1.03

SS-240918	PS <sub>76.5</sub> - <i>b</i> -PSMA <sub>23.5</sub>	55	23.5	1.01
SS-120916-1	PS <sub>82.5</sub> - <i>b</i> -PSMA <sub>17.5</sub>	176	17.5	1.02
SS-120916-2	PS <sub>82.8</sub> - <i>b</i> -PSMA <sub>17.2</sub>	187	17.2	1.01
SS-290916-1	PS <sub>78</sub> - <i>b</i> -PSMA <sub>22</sub>	132	22	1.04
SS-290916-2	PS <sub>81.5</sub> - <i>b</i> -PSMA <sub>18.5</sub>	319	18.5	1.04

The subscripts show weight percentage of the individual blocks, whereas the total number-averaged molecular weight  $M_n$  of the diblock copolymer was calculated from  $^1\text{H-NMR}$  and molecular weights of PS-precursors obtained from gel permeation chromatography (SEC, in THF calibrated with PS standards).

Very few kinetic and thermodynamic studies of PSMA and PGMA have been published. In this study, the Hoy method [155] was used to measure solubility parameters of homopolymers of PSMA and PGMA, as displayed in Table (4.4). Thermodynamic properties of polymer solution are described in terms of free energy change which occurs when a polymer is mixed with a solvent or mixture of solvents [156].

The equations used in Hoy's system for estimation of the solubility parameter and its components stated below where  $F_t$  is the molar attraction function,  $F_p$  is polar component,  $V$  is the molar volume of the solvent molecule or the structural unit of the polymer.  $\alpha$  is the molecular aggregation number, describing the association of the molecule;  $n$  is the number of repeating units per effective chain segment of the polymer and  $B$  is the base value.

$$\delta_t = (F_t + B/n) / V$$

$$\delta_p = \delta_t (1 / \alpha F_p / F_t + B)^{1/2}$$

$$\delta_h = \delta_t [ (\alpha - 1) / \alpha ]^{1/2}$$

$$\delta_d = (\delta_t^2 - \delta_p^2 - \delta_h^2)^{1/2}$$

**Table 4. 4.** Hansen solubility parameters ( $\delta$ ) of homopolymers, solvents and non-solvents [157]

Substance	$\delta_d$ (MPa <sup>0.5</sup> ) <sup>a</sup>	$\delta_p$ (MPa <sup>0.5</sup> ) <sup>a</sup>	$\delta_h$ (MPa <sup>0.5</sup> ) <sup>a</sup>	$\delta = \sqrt{\delta_d^2 + \delta_p^2 + \delta_h^2}$ (MPa <sup>0.5</sup> ) <sup>a</sup>
PS	18.5	4.5	2.9	19.3
P4VP	18.1	7.2	6.8	19.0
THF	16.8	5.7	8.0	19.5
DMF	17.4	13.7	11.3	24.8
DOX	17.5	1.8	9.0	19.8
Acetone	15.5	10.4	7.0	19.9
Water	15.6	16.0	42.3	47.8
Solubility parameters by the Hoy method [155]				
PSMA	16.76	9.35	5.54	19.9
PGMA	19.25	9.23	14.4	25.8

a) Dispersion solubility parameter  $\delta_d$ , Polar solubility parameter  $\delta_p$ , Hydrogen Bonding

solubility parameter  $\delta_h$ . The Hansen solubility parameter is given from the equation  $\delta = \sqrt{\delta_d^2 + \delta_p^2 + \delta_h^2}$

#### 4.1.4 Bulk Morphology of the PS-*b*-PSMA diblock copolymers

The bulk morphology of the block copolymers was studied by transmission electron microscopy following the commonly used preparation technique; *i.e.*, the formation of thick films by slow drying of a polymer solution and annealing at a temperature above the glass transition

temperatures of the blocks. Micelles of diblock copolymers were formed during film preparation. For PS-*b*-PSMA diblock copolymer, THF was chosen as it is a suitable solvent for both the blocks. Films were annealed very slowly from room temperature up to 120 °C (usually films are annealed up to 20 °C above the highest  $T_g$ ), and ultrathin sections of approximately 50 nm were obtained at room temperature by ultramicrotomy. Using solvent annealing method, thin films of block copolymers exhibiting surface-parallel or surface-perpendicular morphology or one with well-ordered hexagonally packed cylinders could be obtained [158, 159]. A TEM micrograph of the PS<sub>81</sub>-*b*-PSMA<sub>19</sub><sup>170</sup> diblock copolymer film is shown in Figure 4.1.5. Due to the sufficiently large electron density contrast between the two blocks, no staining was necessary. In this case hexagonally packed cylinder morphology was expected, however due to the smaller segregation strength parameter ( $\chi N$ ), where  $\chi$  is the Flory-Huggins segmental interaction parameter and  $N$  is the total number of block copolymer segments, a phase-mixed disordered morphology was observed.

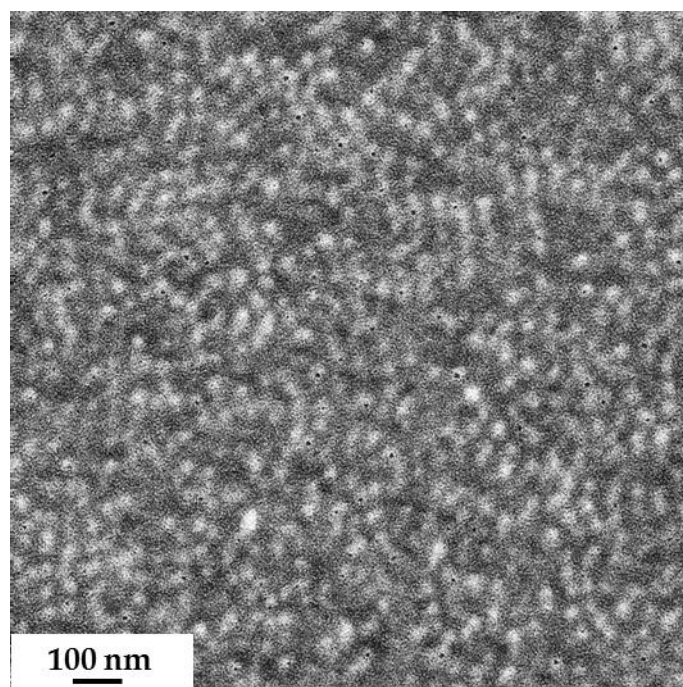


**Figure 4.1.5.** TEM image of an ultrathin section of PS<sub>81</sub>-*b*-PSMA<sub>19</sub><sup>170</sup>, film cast from 5 wt% polymer solution in THF, the diameter of the brighter spheres is approximately 25-30 nm

#### 4.1.5 Membrane fabrication via SNIPS

The formation of an intended integral asymmetric membrane with hexagonally oriented porous cylinders on top of the spongy structure via the SNIPS process is influenced by different parameters, such as the evaporation time, the solvent composition, and concentration of the casting solution, all of which have to be optimized. Different compositions of PS-*b*-PSMA block copolymers with varying concentration of solvents were studied and among them some of the selected results are chosen to represent microporous structure. In PS-*b*-PSMA block copolymer membranes, the PS blocks form the matrix of the membrane, whereas the inner surface of the pores and cylindrical domains are formed by PSMA in PS-*b*-PSMA block copolymer. The principle of this technique is based on the solidification of the already existing micellar assemblies of the cast polymer film by its immersion in the non-solvent, in our study water.

The cast film, and therefore membrane, morphology is partially driven from the tendency of the block copolymer to undergo microphase separation. Polystyrene-*b*-poly(solketal methacrylate) is an unknown system in the context of SNIPS process, so different compositions of solvent mixtures were investigated. In Figure 4.1.6, the surface structure of membranes prepared from 24 wt% PS<sub>76</sub>-*b*-PSMA<sub>24</sub><sup>200</sup> polymer solution in THF/DMF with solvent compositions 50/50 wt% and 40/60 wt% shows in both cases a rather poor organization of pores. The evaporation time before the immersion into the non-solvent bath was in both cases 10 s.

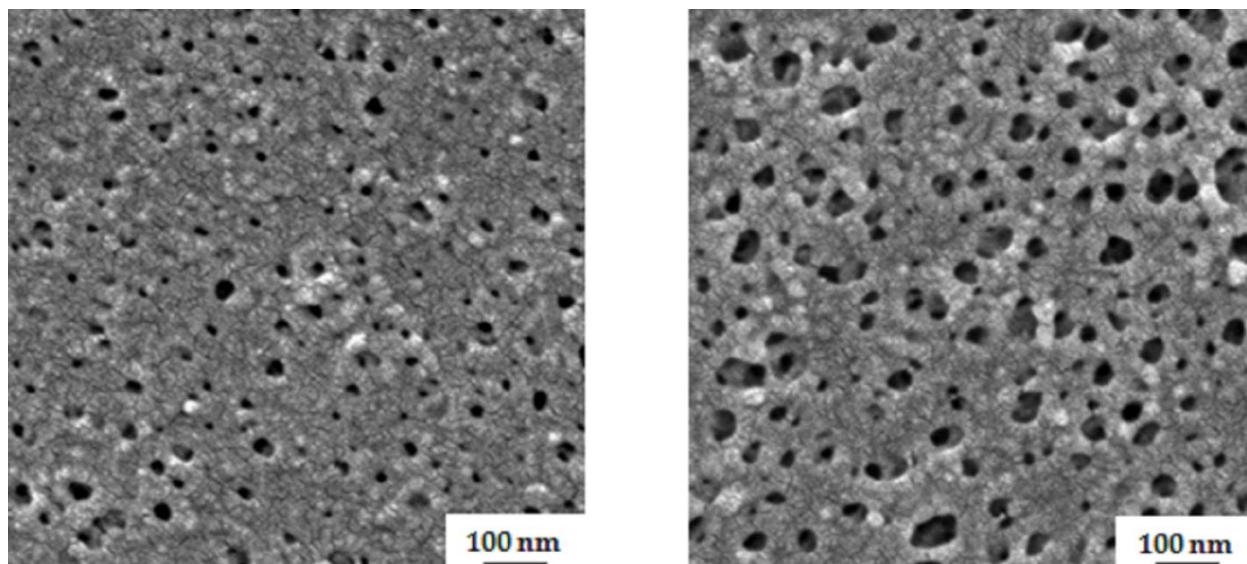


**Figure 4.1.6.** SEM images of the top surface of cast membranes from 24 wt% PS<sub>76</sub>-*b*-PSMA<sub>24</sub><sup>200</sup> from (left) THF/DMF 50/50 wt%, (right) THF/DMF 40/60 wt%. The time of evaporation before the immersion into the precipitant was 10 s.

In one case, concentration of more volatile solvent was reduced in the binary solvent mixture to check the effect on morphology. As shown in Figure 4.1.7 for an evaporation time of 10 s, a macroporous spongy-like structure formed by casting block copolymer solution in THF/DMF 30/70 wt%, whereas the surface structure of the membrane is getting more open with macropores which are not even interconnected at an evaporation time of 20 s.

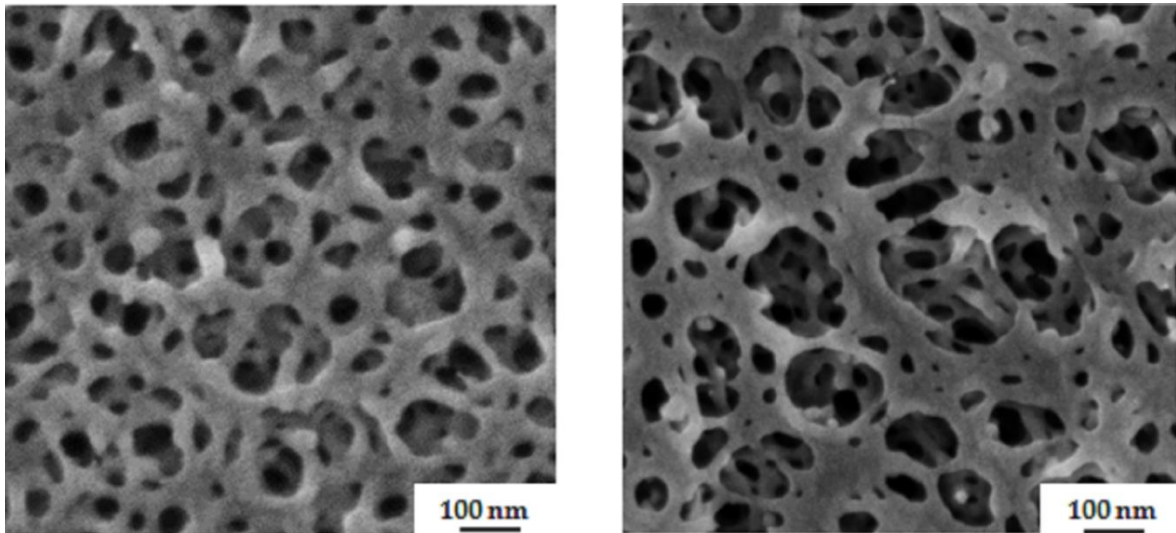


**Figure 4.1.7.** SEM topography images of the surface of the generated membrane from 25 wt%  $PS_{76}\text{-}b\text{-}PSMA_{24}^{200}$  in THF/DMF 30/70 wt% with evaporation time 10 s (left) and 20 s (right)

During the SNIPS process, the evaporation time before immersion into a non-solvent bath affects the top surface structure of the membrane. Figure 4.1.8 depicts the surfaces of the membranes prepared from a  $PS_{81}\text{-}b\text{-}PSMA_{19}^{170}$  solution in 50/50 wt% THF/DMF for different evaporation times, namely 5, 10 and 20, 25 s. With an increase in evaporation time, the top surface with a very small number of macropores appeared together with a rather dense structure.

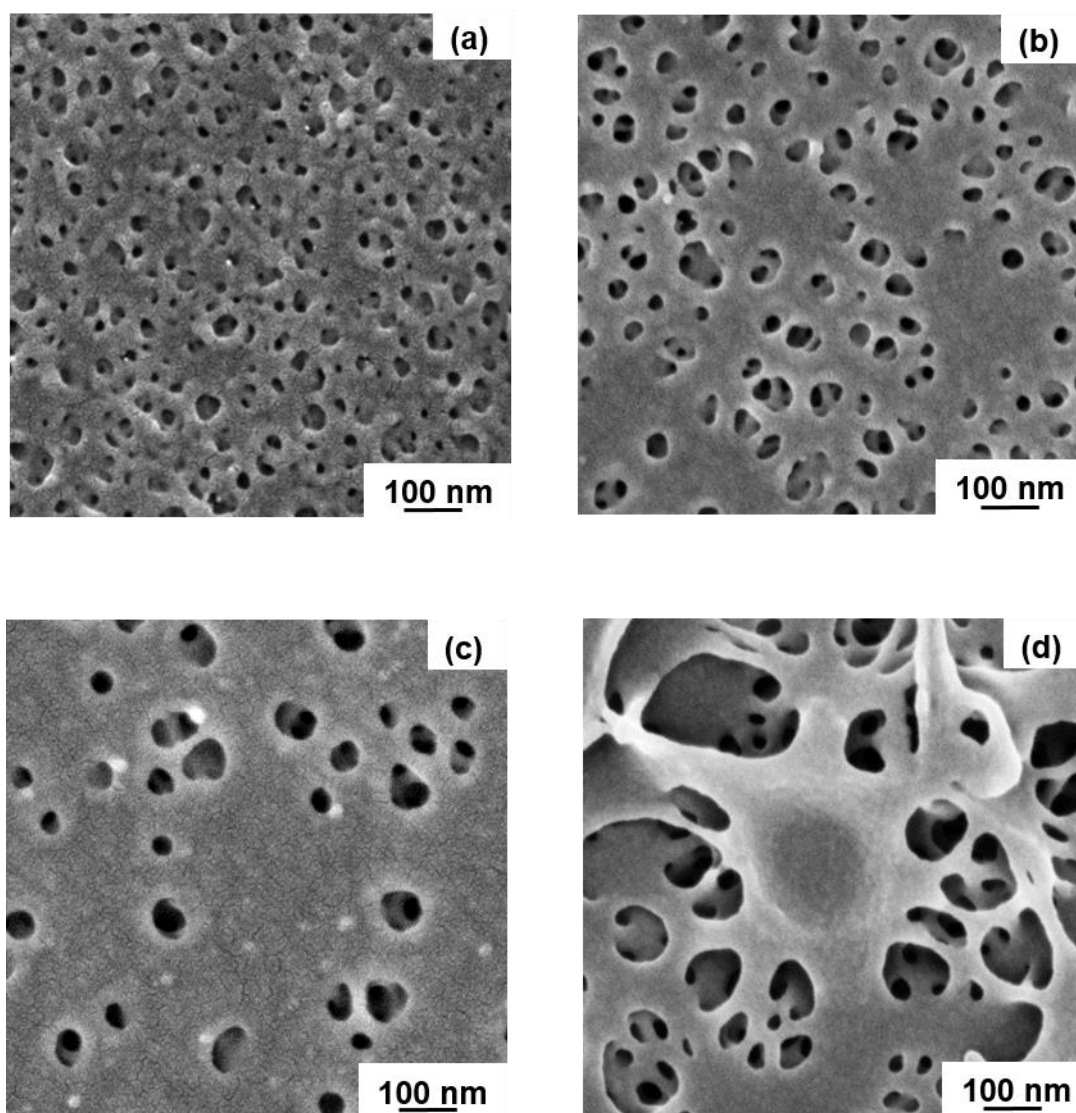


**Figure 4.1.8.** SEM images of surfaces of the membranes made from 24 wt% PS<sub>81</sub>-*b*-PSMA<sub>19</sub><sup>170</sup> in THF/DMF 50/50 wt%. Evaporation time before immersion: (a) 5 s, (b) 10 s, (c) 20 s, (d) 25 s.

The substructure of the PS<sub>81</sub>-PSMA<sub>19</sub><sup>170</sup> membrane shown in Figure 4.1.9-a exhibits finger-like structures through almost the entire substructure of the membrane. Open finger-like structure with large voids appeared due to an instantaneous demixing of polymer-poor phase [160]; however, the substructure becomes more dense with increasing evaporation time, as shown in Figure 4.1.9-b.

While increasing the evaporation time the casting solution becomes viscous before immersion into the non-solvent bath, due to evaporation of the more volatile THF. In addition, a longer evaporation time can lead to a decreasing concentration gradient of the diblock copolymer perpendicular to the surface, which also favors a parallel alignment of cylinders rather than the formation of standing cylindrical domains. An isoporous surface structure could not be obtained in any case, even by increasing the viscosity of the diblock copolymer solution. It can be concluded from surface and cross-sectional morphologies of these hydrophobic PS-*b*-PSMA diblock copolymers that this system still needs to be optimized with regard to self-assembly in combination with a non-solvent-induced phase separation process.

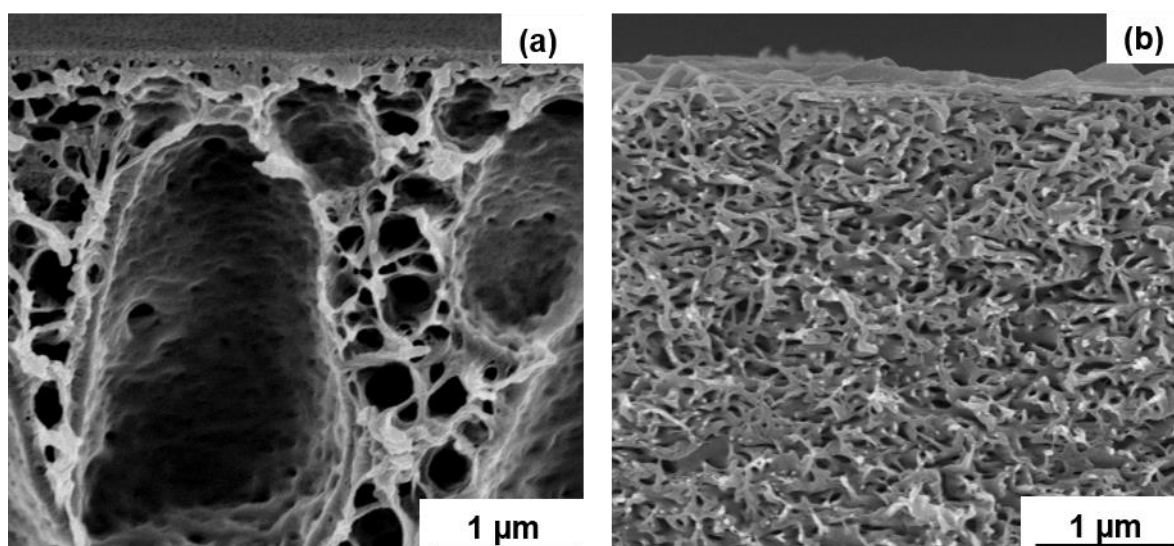


**Figure 4.1. 9.** SEM images of the cross-section of the membrane prepared from 24 wt% PS<sub>81</sub>-*b*-PSMA<sub>19</sub><sup>170</sup> in THF/DMF 50/50 wt% at (a) 5 s, (b) 25 s time of evaporation

In this chapter, we presented the synthesis of double hydrophobic diblock copolymers of PS-*b*-PSMA by anionic polymerization with low dispersity index ( $\mathcal{D}$ ). By utilizing the binary THF/DMF and ternary THF/DMF/DOX solvent system, only dense membranes with some macropores and dense sub-structure were obtained from PS-*b*-PSMA. Within this study, no

suitable solvents were found to prepare isoporous membranes from the hydrophobic PS-*b*-PSMA diblock copolymers. This will require a more subtle choice of solvents, as the level of selectivity of a solvent and also non-solvent is much less pronounced in a block copolymer composed of similar polar (or nonpolar) blocks.

## **4.2. A comparative study of amphiphilic polystyrene-*b*-poly(glyceryl methacrylate) (PS-*b*-PGMA) and hydrophobic polystyrene-*b*-poly(solketal methacrylate) (PS-*b*-PSMA) membranes**

### **4.2.1 Brief Introduction**

In this chapter, poly(solketal methacrylate) (PSMA) containing diblock copolymers were post-treated to get hydrophilic poly(glyceryl methacrylate) (PGMA). A comparative study of amphiphilic PS-*b*-PGMA and hydrophobic PS-*b*-PSMA diblock copolymers for the development of isoporous integral asymmetric membranes was conducted. In this way, the expected increase in hydrophilicity of the membrane was characterized by different methods. Moreover, the effect of addition of different nanofillers in the polymer solution was demonstrated.

### **4.2.2 Acidic hydrolysis of PS-*b*-PSMA and formation of PS-*b*-PGMA diblock copolymer**

As described in the previous chapter, a series of PS-*b*-PSMA diblock copolymers was employed to cast membranes, however, due to the hydrophobic nature of both blocks macro-porous and irregular structures were observed. The acidic hydrolysis of PS-*b*-PSMA was performed to convert the hydrophobic system (PS-*b*-PSMA) into an amphiphilic system (PS-*b*-PGMA). To deprotect the acetonide group of PSMA, 1N HCl was added drop-wise to a polymer dissolved in THF under continuous stirring. The reaction was stirred gently for 12 h and was precipitated

in methanol. The hydrolyzed polymer was dried at 40 °C under vacuum and was characterized by <sup>1</sup>H-NMR spectroscopy as shown in Figure 4.2.1.

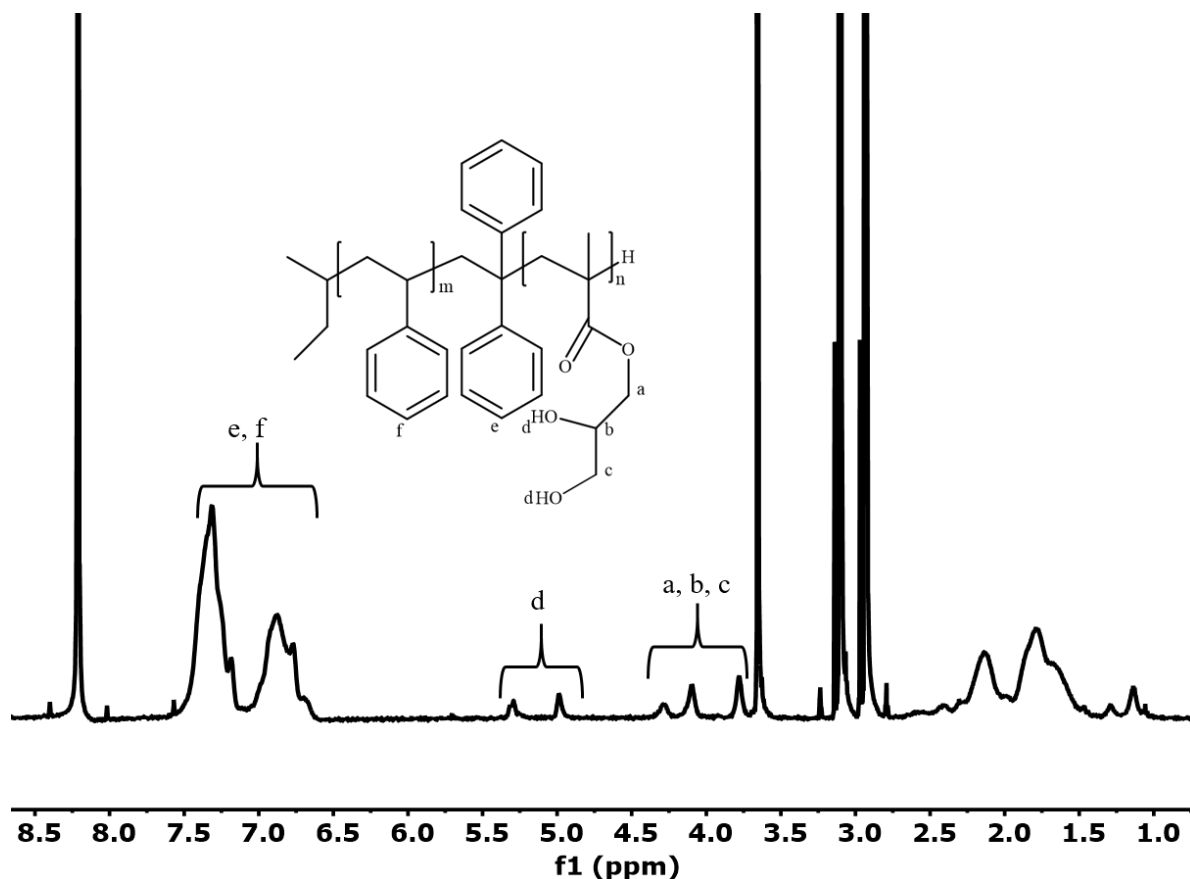


**Figure 4.2.1.** <sup>1</sup>H-NMR spectrum of PS-*b*-PGMA after the removal of 1, 3-dioxolane ring of PSMA block

**<sup>1</sup>H-NMR** (DMF-*d*<sub>7</sub>, 20 °C, 300 MHz, TMS):

$\delta$  [ppm] = 7.3-6.7(m', 15H, H-13, H-14, H-15, H-16, H-17, arom. H (DPE)), 5,7 (s', DPE), 5.2 (s', 1H, H-12), 4.9 (s', 1H, H-11), 4.28-3.7 (m', 5H, H-8, H-9, H-10), 2.1-1.41(m', 25H, H-1, H-2, H-3, H-4, H-5, H-6, H-7, 2x CH<sub>3</sub> (*s*-BuLi), 1x CH<sub>3</sub> (PGMA))

The amphiphilic nature of the block copolymers after hydrolysis did not permit SEC measurements using THF as an eluent, however; DMF offers sufficient solubility for block

copolymers after hydrolysis. Narrow monomodal molecular weight distributions were revealed by SEC using DMF as eluent. . This illustrates the completion of the reaction without any side reactions. An increase in the number average molecular weight observed in PS-*b*-PGMA as compared to PS-*b*-PSMA diblock copolymers by SEC—even though the acetonide moiety was removed—confirmed similar results reported before by Frey et al. [161]. The hydrodynamic volume of the chemically modified diblock copolymer PS-*b*-PGMA increases in comparison with the starting diblock copolymer (PS-*b*-PSMA). This is due to the stronger microphase separation tendency of the

PS-*b*-PGMA. In order to check the behavior of PS-*b*-PSMA and PS-*b*-PGMA in a common solvent, the hydroxyl groups of a PS-*b*-PGMA diblock copolymer were protected by the silylation reaction reported in literature by Hirao [162] described in the Section 4.2.5

#### **4.2.3 Protection of hydroxyl groups (-OH) of PGMA**

Due to the difference in solubility behavior of PS-*b*-PSMA and PS-*b*-PGMA (polystyrene-*block*-poly(glyceryl methacrylate), the hydroxyl groups (-OH) of the PS-*b*-PGMA diblock copolymers were protected by using two different chemical methods.

#### **4.2.4 Benzoylation of polystyrene-*block*-poly(glyceryl methacrylate) (PS-*b*-PGMA)**

0.25 g of PS-*b*-PGMA diblock copolymer in 3 mL dry pyridine was dissolved and later, 2.25 grams of benzoic anhydride at 0° C. The reaction mixture was stirred at room temperature for 48 h [163]. The reaction mixture was precipitated in methanol and dried at 40°C under vacuum. The dried polymer was characterized by <sup>1</sup>H-NMR.

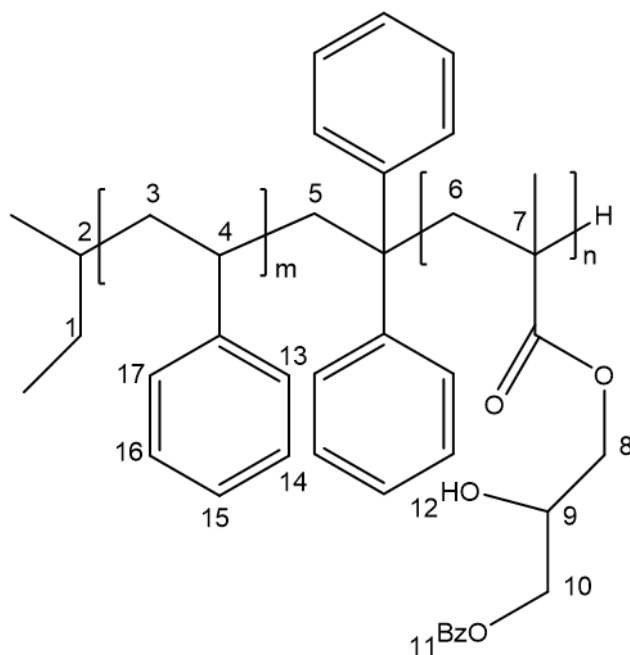


**Figure 4.2.2.** Structure of benzoylated PS-*b*-PGMA diblock copolymer

**<sup>1</sup>H-NMR** (CDCl<sub>3</sub>, 20 °C, 300 MHz, TMS):

δ [ppm] = 8.1-7.4 (m', 10H, H-11), 7.07-6.45 (m', 15H, H-13, H-14, H-15, H-16, H-17, arom. H (DPE)), 5.5 (m', 11H, H-9), 4.5-4.1 (m', 5H, H-8, H-9, H-10), 2.1-1.41 (m', 23H, H-1, H-2, H-3, H-4, H-5, H-6, H-7, 2x CH<sub>3</sub> (*s*-BuLi), 1x CH<sub>3</sub> (PSMA))

The results obtained from <sup>1</sup>H-NMR showed that only one hydroxyl group was protected by following this reaction path way. Therefore, an alternative method was used for complete protection of hydroxyl groups.

#### 4.2.5 Silylation of polystyrene-*block*-poly(glyceryl methacrylate) (PS-*b*-PGMA)

A mixture of polystyrene-*block*-poly(glyceryl methacrylate) PS-*b*-PGMA (0.1 g), imidazole (0.46g), *tert*-butyldimethylsilylchloride (0.54 g) and DMF (5 mL) was stirred for 18h at room temperature. The reaction was terminated with 5% NaOH solution and later polymer extracted with *n*-hexane. Methanol was used to precipitate the silylated polymer [162]. The resulting polymer was dried at 40°C under vacuum and characterized by <sup>1</sup>H-NMR.

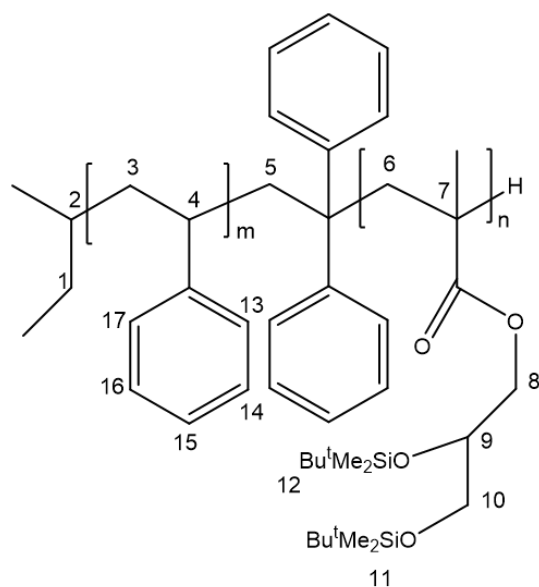


**Figure 4.2.3.** Silylation of PS-*b*-PGMA diblock copolymer

**<sup>1</sup>H-NMR** (CDCl<sub>3</sub>, 20 °C, 300 MHz, TMS):

$\delta$  [ppm] = 7.07-6.57(m', 15H, H-13, H-14, H-15, H-16, H-17, arom. H (DPE)), 4.23 (m', 1H, H-9), 4.03-3.5 (m', 5H, H-8, H-9, H-10), 2.1-1.41(m', 23H, H-1, H-2, H-3, H-4, H-5, H-6, H-7, 2x CH<sub>3</sub> (*s*-BuLi), 1x CH<sub>3</sub> (PSMA)), 0.91-0.1(m', 30H, H-11, H-12)

The (-OH) hydroxyl groups of PS-*b*-PGMA diblock copolymer were completely protected by following this procedure and the new polymer could be dissolved in THF.

The list of PS-*b*-PGMA diblock copolymers studied in this research work are shown in Table (4.5).

**Table 4. 5.** Characterization data of PS-*b*-PGMA diblock copolymers

<b>Batch no</b>	<b>Polymer</b>	<b><math>M_n</math></b> <b>(kg/mol)</b>	<b>PGMA</b> <b>(wt%)</b>	<b><math>\bar{D}</math></b>
SS-220816	PS <sub>81</sub> - <i>b</i> -PGMA <sub>19</sub>	128	19	1.06
SS-301015	PS <sub>85</sub> - <i>b</i> -PGMA <sub>15</sub>	163	15	1.04
SS-280616	PS <sub>76</sub> - <i>b</i> -PGMA <sub>19</sub>	190	19	1.03
SS-240918	PS <sub>88</sub> - <i>b</i> -PGMA <sub>12</sub>	51	12	1.1
SS-290916-1	PS <sub>82</sub> - <i>b</i> -PGMA <sub>18</sub>	126	18	1.1
SS-221118	PS <sub>79</sub> - <i>b</i> -PGMA <sub>21</sub>	120	21	1.1
SS-290916-2	PS <sub>85.2</sub> - <i>b</i> -PGMA <sub>14.8</sub>	307	14.8	1.1

#### 4.2.6 Analysis of bulk morphology of the PS-*b*-PGMA by TEM

The bulk morphology of the block copolymers was studied by transmission electron microscopy following the commonly used preparation technique as mentioned above in Section 4.1.4. An ultrathin section of PS<sub>81</sub>-*b*-PGMA<sub>19</sub><sup>128</sup> film was also analyzed without staining due to the sufficiently large difference in the electron density of the two blocks (Figure 4.2.4). In the case of PS<sub>81</sub>-*b*-PGMA<sub>19</sub><sup>128</sup>, a less-ordered morphology was observed with brighter spheres of PGMA in the darker polystyrene matrix. This may be due to the fact that DMF is a more selective solvent for PGMA, leading to a poorer solubility of the diblock copolymer.

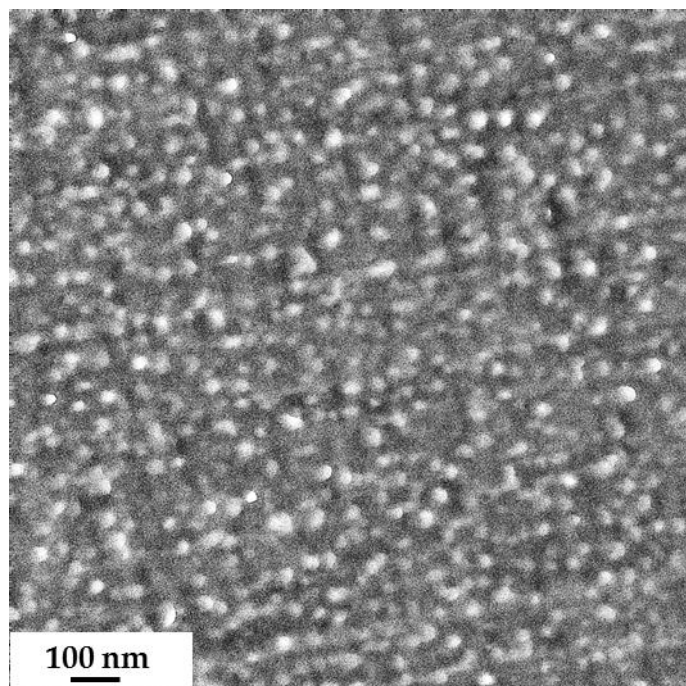


**Figure 4.2.4.** TEM image of an ultrathin section of  $\text{PS}_{81}\text{-}b\text{-PSMA}_{19}$ <sup>170</sup>, film cast from 5 wt% diblock copolymer solution in DMF, the diameter of the brighter spheres is approximately 30-35 nm

In one particular case,  $\text{PS}_{82}\text{-}b\text{-PSMA}_{18}$ <sup>126</sup> bulk morphology was analyzed by addition of binary solvent THF/DMF where THF was used in excess. An ultrathin section of  $\text{PS}_{82}\text{-}b\text{-PSMA}_{18}$ <sup>126</sup> film was analyzed by staining the polystyrene block with ruthenium tetroxide ( $\text{RuO}_4$ ). In this case a cylinder morphology was observed with very less distinguished contrast between the two blocks (Figure 4.2.5)

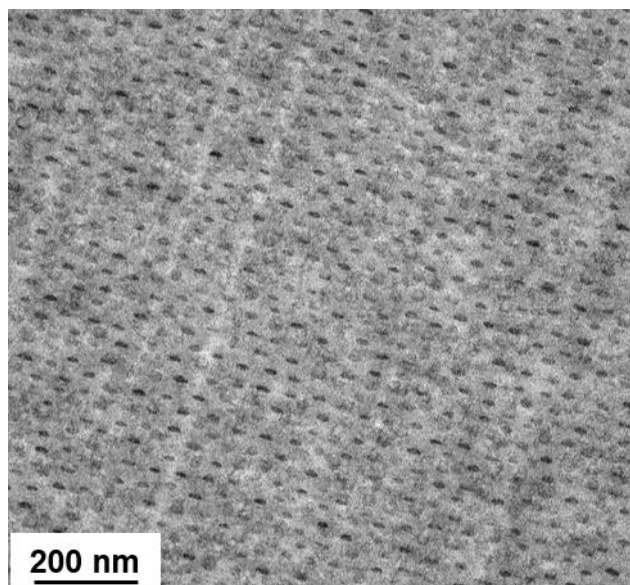


**Figure 4.2.5.** TEM image of an ultrathin section of PS<sub>82</sub>-*b*-PSMA<sub>18</sub><sup>126</sup>, film cast from diblock copolymer in THF and DMF solution, stained with RuO<sub>4</sub> (20min)

#### **4.2.7 Fabrication of PS-*b*-PGMA membranes via SNIPS**

In this work, amphiphilic PS-*b*-PGMA diblock copolymers were used for casting integral asymmetric membranes via the SNIPS process. In Figure 4.2.6, SEM images of the surface of a membrane prepared from 23 wt% PS<sub>81</sub>-*b*-PGMA<sub>19</sub><sup>128</sup> in THF/DMF 50/50 wt% using a blade height of 200 μm show a regular pattern of hexagonally-oriented open pores with a sponge-like structure underneath.

The time of evaporation before immersion into the non-solvent bath was 10 s. The pore diameter in this case was approximately  $33 \pm 2$  nm. An ordered perpendicular cylindrical morphology was observed for an evaporation time window from 5–15 s; however, the isoporous structure of the block copolymer membrane disappeared after an evaporation time of 20 s.

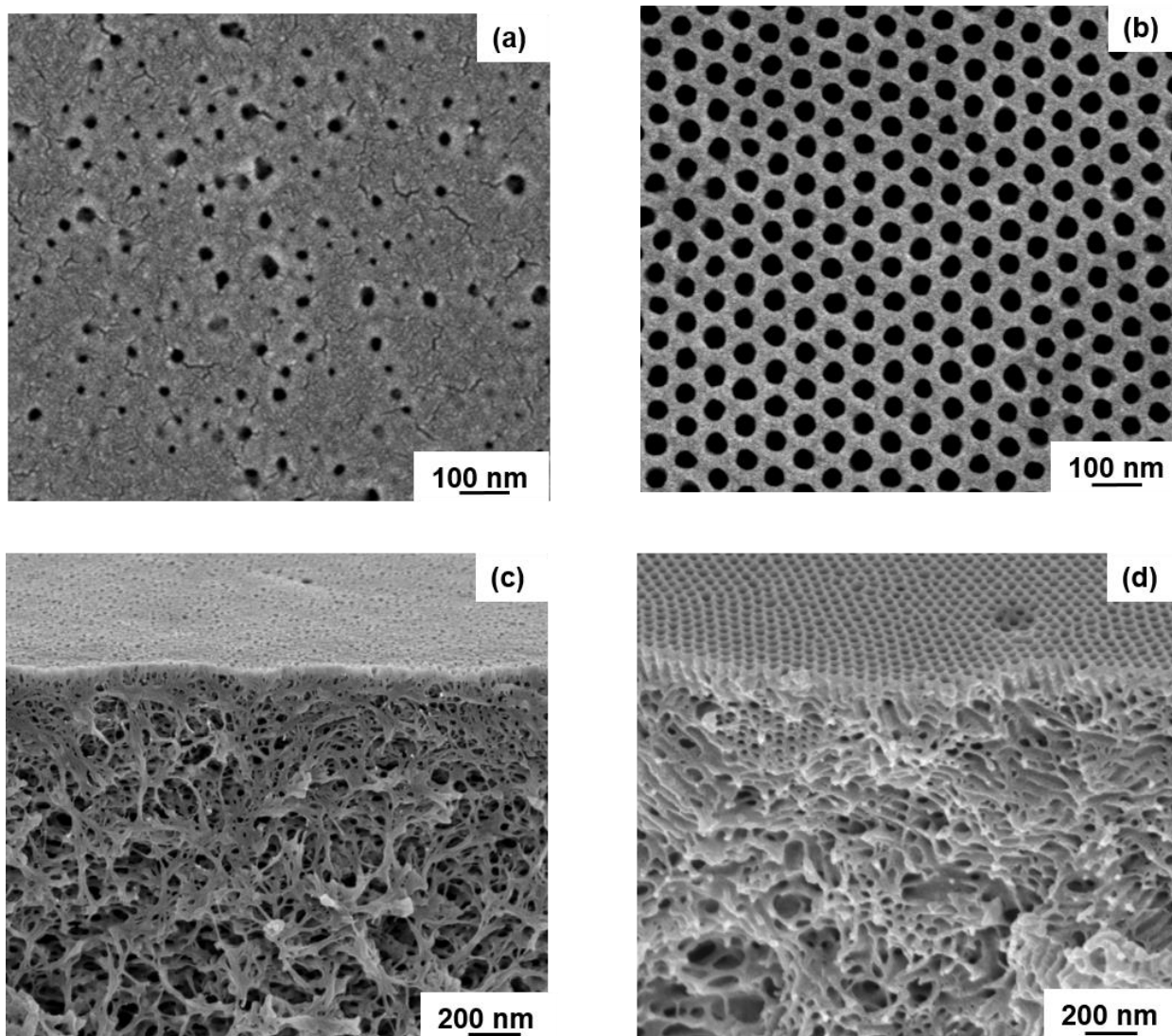


**Figure 4.2.6.** SEM topography images of membranes prepared from (a) 23 wt% PS<sub>76</sub>-*b*-PSMA<sub>24</sub><sup>135</sup> and (b) 23 wt% PS<sub>81</sub>-*b*-PGMA<sub>19</sub><sup>128</sup> in THF/DMF 50/50 wt%. The corresponding cross-section views for each case are shown in (c) and (d) images, respectively. The time of evaporation was 10s.

At this point, it should be mentioned that the open porous membrane surface structure is a combined result of the strongly amphiphilic character of the block copolymer, which is a prerequisite to be very selective in the interaction with the involved solvents and the solvent-induced phase separation. Specifically for a solution system with two solvents, the less volatile but more polar solvent swells the polar minority block, while the more volatile but less polar solvent is selective for the less polar matrix-forming block, which is the one which vitrifies at

the surface first due to the fast evaporation of this more volatile solvent. In the case we deal with a double hydrophobic block copolymer and using the aforementioned solvent system, we no longer have such a strong selectivity of the solvents, and therefore the formation of an isoporous surface structure is unlikely to occur. The incompatibility of the different blocks is the product of segmental interaction parameter and the degree of polymerization. Similarly it is expected that a larger degree of polymerization would be required to give the same degree of incompatibility for the unhydrolyzed diblock copolymer as compared to the hydrolyzed one. Therefore, if for a given hydrolyzed diblock copolymer a hexagonally ordered porous membrane structure can be obtained, for the unhydrolyzed diblock copolymer a micro-phase separation is expected for higher degrees of polymerization. On the contrary, the viscosity would increase due to the higher molecular weight and this would also lead to other requirements for the evaporation time, again affecting the necessary solvent concentration gradient which is built up by the evaporation of the faster-evaporating solvent.

It has been reported in the literature that the addition of dioxane (DOX) in the mixture of THF-DMF reduces the solvent quality of the polar block [22]. Therefore, ternary solvent mixtures THF/DMF/DOX for ratios 1/1/1 and 2/1/1, respectively, were studied for their effect on the membrane formation of the  $PS_{81}\text{-}b\text{-}PGMA_{19}^{128}$  diblock copolymers.

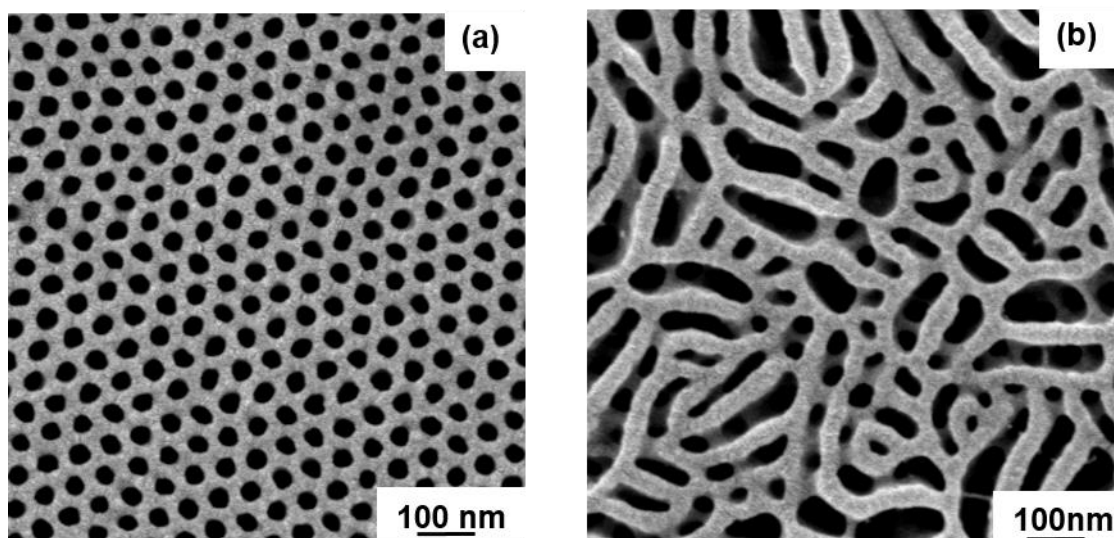


**Figure 4.2.7.** SEM images of surface of the membranes prepared from 22 wt % PS<sub>81</sub>-*b*-PGMA<sub>19</sub><sup>128</sup> in THF/DMF/DOX (1:1:1); time of evaporation (a) 10 s (b) 20 s.

In Figure 4.2.7, SEM images are shown of a membrane obtained from a block copolymer solution in THF/DMF/DOX (1/1/1) cast by using a blade height of 200  $\mu\text{m}$ . The viscosity of the ternary solvent polymer solution was approximately comparable to the binary solvent polymer solution, as a lower concentration of diblock copolymer was used. At an evaporation time of 10 s, regular patterns of hexagonally oriented cylindrical pores were observed which changes to thermodynamically more favorable laying cylindrical morphology by increasing evaporation time for the same reasons as discussed before.

Several solutions of PS-*b*-PGMA diblock copolymers with different compositions were studied and among them some of the representative results are chosen to demonstrate an isoporous morphology. An increase in pore size of the membrane was observed from PS<sub>79</sub>-*b*-PGMA<sub>21</sub><sup>120</sup> diblock copolymer with higher PGMA content as shown in Figure 4.2.8 which was in agreement with previous findings [123].

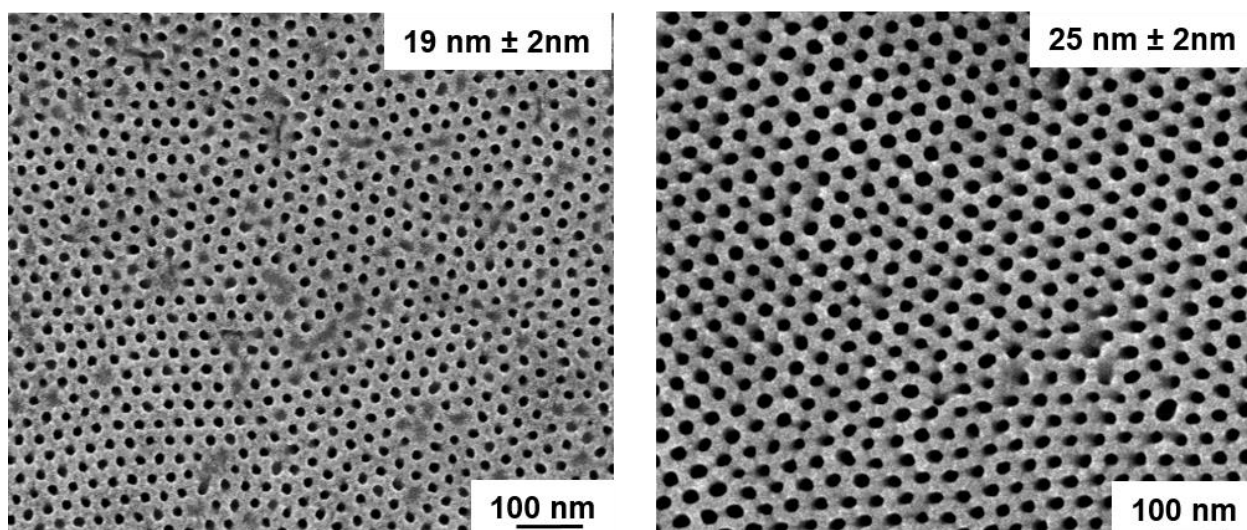


**Figure 4.2.8.** SEM images of surface of the membranes prepared from 23 wt% (left) PS<sub>82</sub>-*b*-PGMA<sub>18</sub><sup>126</sup> (right) PS<sub>79</sub>-*b*-PGMA<sub>21</sub><sup>120</sup> in THF/DMF/DOX (2:1:1); time of evaporation 20 s.

#### 4.2.8 Addition of nano-fillers

As already mentioned many additives have been used to improve the membrane structure formation. The kinetics of the phase separation and self-assembly is tremendously influenced by the viscosity of the polymer solution and additives. Transition metals like (copper (II), nickel (II), cobalt (II) and iron (II)) containing salts were utilized for stabilization of the PS-*b*-P4VP micelles in solution and as a result pore order of the membranes was improved [125, 128, 164]. However, transition metals suffer clear disadvantages due to their toxic behavior in biological membrane application. Similar positive effects were observed with magnesium acetate as an additive in a PS-*b*-P4VP block copolymer membrane solution [164]. Biocompatible carbohydrate (glucose and saccharose) were also reported as efficient additives for the membrane formation from PS-*b*-P4VP polymeric solution. An increase in viscosity of the polymeric solution was observed probably due to the hydrogen bonding interaction between hydroxyl groups of carbohydrate and pyridine units of block copolymer [139]. In the same context, during the last decade, graphene oxide (GO) based membranes have attracted a lot of

attention due to their fouling resistance and easy chemical functionalization behavior [165-167]. The combination of inherent physical and chemical properties sets up GO an excellent nanofiller material for hybrid membranes. The incorporation of GO in the membrane solution could change the morphology and enhanced the performance of the membranes [168-170]. In this study, GO nanosheets were prepared by Hummers method, as described previously [171, 172]. GO nanosheets contains oxides (C–O–C), phenolic hydroxyl (–OH), carboxylic (–COOH) and other carbonyl functional groups (C=O) and is considered polar and hydrophilic. Strong intermolecular hydrogen bonding is expected between PS-*b*-PGMA diblock copolymer hydroxyl (–OH) and GO functional groups. The chemical structure of graphene oxide layers is shown in Figure 4.2.9

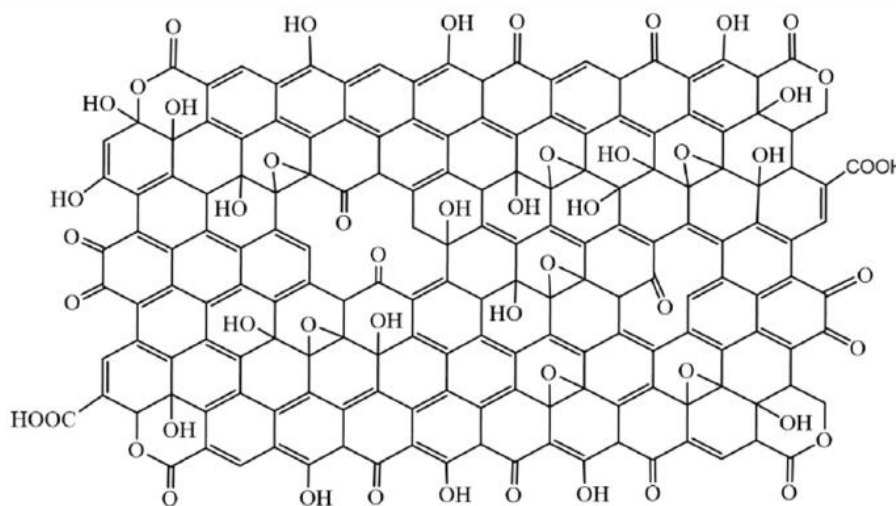


**Figure 4.2.9.** Structure of graphene oxide layer.[171]

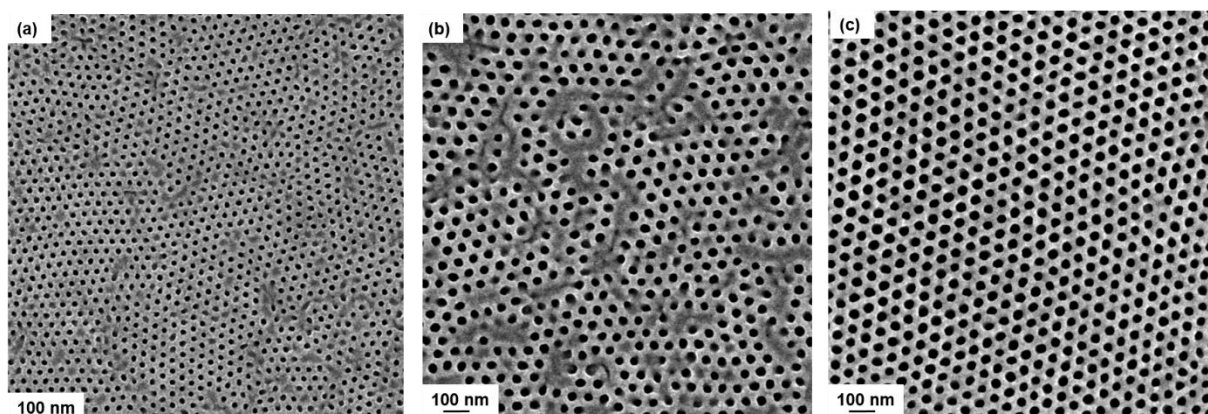


**Figure 4.2.10.** SEM images of surface of the membranes prepared from 23 wt% PS<sub>82</sub>-*b*-PGMA<sub>18</sub><sup>126</sup> (a) pristine membrane, time of evaporation 20 s. (b) 0.5 (c) 1 wt% GO nanosheets in THF/DMF/DOX (2:1:1); time of evaporation 10 s.

To investigate the effect of GO nanosheets on the structure of membranes, different GO contents were added into the PS-*b*-PGMA block copolymer solution. A comparison of SEM micrographs of pristine membrane of PS<sub>82</sub>-*b*-PGMA<sub>18</sub><sup>126</sup> and PS-*b*-PGMA/GO membranes with 0.5 and 1 wt% GO were given in Figure 4.2.10.

To conserve the isoporous morphology of membranes after the addition of additives (graphene oxide) in the membrane solution is the greatest challenge. The addition of 1 wt % GO nanosheets in PS<sub>82</sub>-*b*-PGMA<sub>18</sub><sup>126</sup> membrane solution results into a typical isoporous membrane with larger pores  $30 \pm 2$  nm diameter as compared to the pristine membrane ( $19 \pm 2$  nm) present on top of a sponge-like sublayer. The viscosity of the solution increases along with the added amount of GO nanosheets. The evaporation time of isoporous membrane obtained from the addition of 1 wt% GO was shifted to 10 seconds due to an increase in the viscosity of the casting solution. The difference in pore size can be interpreted as follows. The GO nanosheets as a hydrophilic material accelerate the diffusion of non-solvent and solvents during phase separation process, due to the existing interaction between components in the casting solution [168, 173]. However, along with the porous structure some defects were observed on the membrane surface as shown

in Figure 4.2.11. The final membrane applications are affected by the presence of defects. The dispersion of GO was hindered in the membrane solution due to hydrogen bonding interaction between different functional groups on GO and water molecules within interlayer cavities, thus restricting its solution process ability during membrane formation [174, 175].

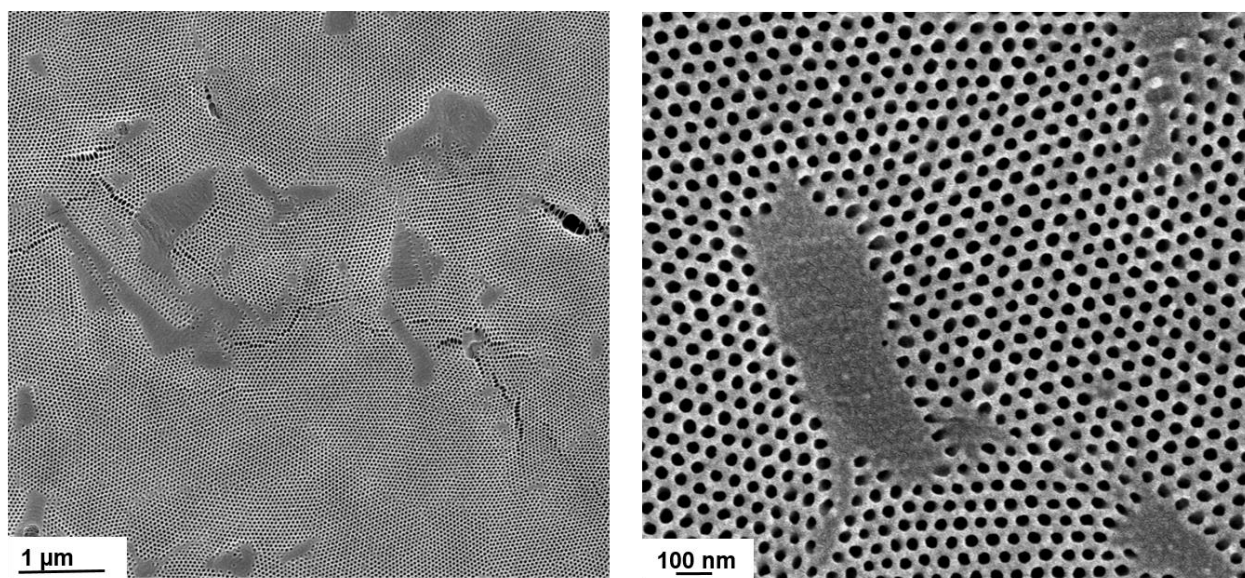


**Figure 4.2.11.** Surface SEM images of the membranes prepared from 23 wt% PS<sub>82</sub>-*b*-PGMA<sub>18</sub><sup>126</sup> 1 wt% GO nanosheets in THF/DMF/DOX (2:1:1); time of evaporation 10 s.

The comparison of the cross-sectional morphology of membranes fabricated from PS<sub>82</sub>-*b*-PGMA<sub>18</sub><sup>126</sup> and GO-PS<sub>82</sub>-*b*-PGMA<sub>18</sub><sup>126</sup> is shown in Figure 4.2.12. Clusters or agglomerates of the GO nanosheets were observed in the substructure of GO-PS<sub>82</sub>-*b*-PGMA<sub>18</sub><sup>126</sup> membranes, supporting the assumption of low dispersion of the GO nanosheets in the casting solution. Nevertheless, the length of cylindrical pores increased by the addition of hydrophilic 1 wt% GO as compared to the pristine membrane.

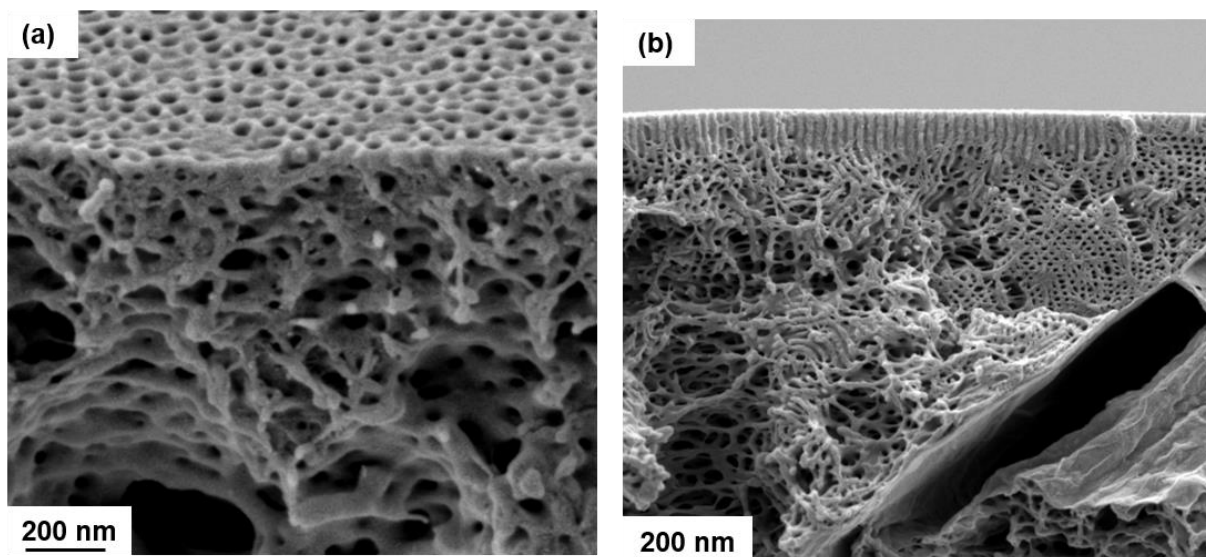


**Figure 4.2.12.** The cross-sectional SEM images of pristine (a) 23 wt% PS<sub>82</sub>-*b*-PGMA<sub>18</sub><sup>126</sup> (b) 1 wt% GO in PS<sub>82</sub>-*b*-PGMA<sub>18</sub><sup>126</sup> in THF/DMF/DOX (2:1:1). The evaporation time after addition of GO was shifted to 10 s.

#### 4.2.9 Addition of PDEA-GO to the PS-*b*-PGMA polymer solution

The chemical functionalization of GO is expected to improve the poor dispersion of GO in organic media. Numerous efforts have been made to increase the dispersibility or solubility of GO nanosheets in common organic solvents [176-178]. In this context, surface initiated atom transfer radical polymerization (SI-ATRP), “grafting from” technique, is considered convenient as it allows the propagation of polymer chains of controlled molecular weights from various substrates. Polymer brushes have been extensively used to modify the physical and chemical properties of interfaces. In this work, 2-diethylaminoethyl methacrylate (DEAEMA) monomer was selected for grafting on the surface of GO nanosheets via SI-ATRP [179]. PDEAEMA is an example of weak polybasic polymer that demonstrates the pH responsive behavior due to the presence of tertiary amine group [180-182]. It also demonstrates an antibacterial response due to the spontaneous protonation of tertiary amine groups. PDEA brushes have received rather less attention as compared to 2-dimethylaminoethyl methacrylate (DMA), therefore we begun

by experimenting with the growth of PDEA brushes by surface initiated ATRP, and further decided to fabricate isoporous membrane impregnated with PDEA-grafted GO nanosheets to check the enhanced performance of the hybrid isoporous membrane. Recently, the hydrophilic poly(*N,N*-dimethylamino ethyl methacrylate) (PDMAEMA) was grafted on the GO surface. The addition of these modified nanosheets into a PS-*b*-P4VP diblock copolymer solution enhanced the hydrophilicity and antifouling behavior of the hybrid isoporous membranes [140].

#### **4.2.10 Membrane morphology and functional group characterization**

The formation of the intended integral asymmetric membranes with hexagonally oriented porous cylinders on top of the spongy structure via SNIPS process is influenced by different parameters, such as evaporation time, solvent composition, and polymer concentration of the casting solution as mentioned before. At the same time, the addition of nanofillers in the block copolymer solution has a great influence on the morphological and functional behavior of the membrane. The functional groups of the PDEA-GO nanofiller are capable of making supramolecular interactions with the PGMA block of the block copolymer (BC) in solution and stabilizing the micellar assembly to conserve the isoporous morphology. A block copolymer solution containing PDEA-GO nanosheets was prepared by following two steps; the calculated amount of ternary solvents (THF/DMF/DOX) and PDEA-GO nanosheets were sonicated in the ultra-sonication bath followed by the addition of the block copolymer to the suspension. The prepared viscous solution was directly hand cast with a doctor blade (blade gap 200  $\mu\text{m}$ ) on a glass plate.

To compare the influence of PDEA-GO nanosheets addition into the PS-*b*-PGMA block copolymer solution with GO nanosheets, the same parameters (e.g., concentration of polymer solution, evaporation window before immersion into the non-solvent bath, solvent composition) were followed to cast the membrane *via* SNIPS. 0.5, 1.0 and 1.5 (w/w)% of PDEA-GO was added separately to the block copolymer solution and the best reproducible results in the form

of the most uniform pores were obtained from 1.5 wt% at 10s evaporation time. The resulting membrane showed vertically aligned nanochannels with a larger pore diameter of  $27 \pm 3$  nm as compared to the pristine membrane. Figure 4.2.13 shows surface and cross-sectional images of pristine membrane.

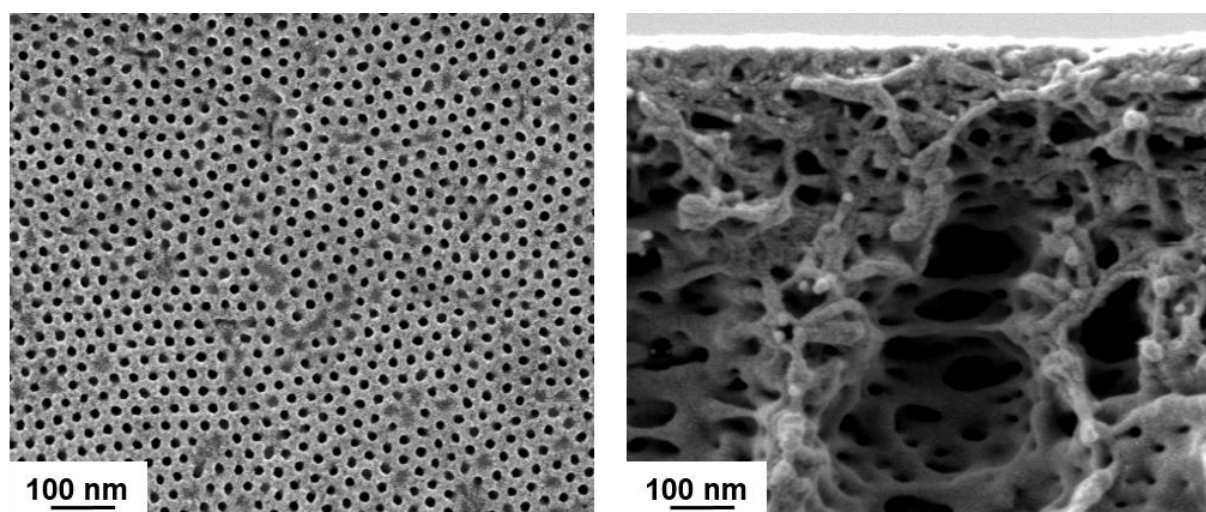


**Figure 4.2.13.** SEM images of surface and cross-section of the membranes prepared from 23 wt% PS<sub>82</sub>-*b*-PGMA<sub>18</sub><sup>126</sup> in THF/DMF/DOX (2:1:1); time of evaporation 20 s.

The surface and cross sectional scanning electron microscope images revealed isoporous morphology without defects or agglomeration of PDEA-GO nanosheets on the skin or sublayer. Scanning electron micrograph images of cross section and surface (from left to right) with 1.5 % (w/w) PDEA-GO content are shown in Figure 4.2.14.

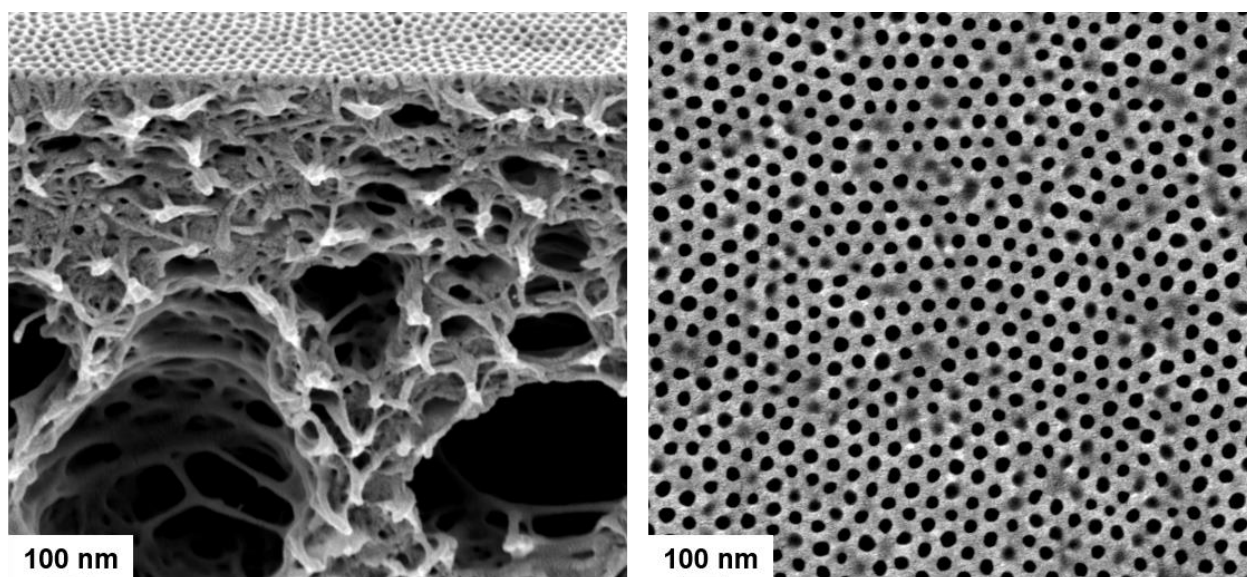


**Figure 4.2.14.** Scanning electron micrograph images of cross section and surface (from left to right) with 1.5 % (w/w) PDEA-GO in THF/DMF/DOX (2:1:1). The evaporation time after addition of PDEA-GO nanosheets was shifted to 10 s.

This indicates that the grafting of PDEAEMA to graphene oxide supports the well dispersion of PDEA-GO nanosheets throughout the membrane solution and prevents aggregation in the substructure. It is assumed that hydrogen bonding interaction between PDEA-GO nanosheets and hydroxyl groups of PS-*b*-PGMA diblock copolymer stabilizes the micellar assembly.

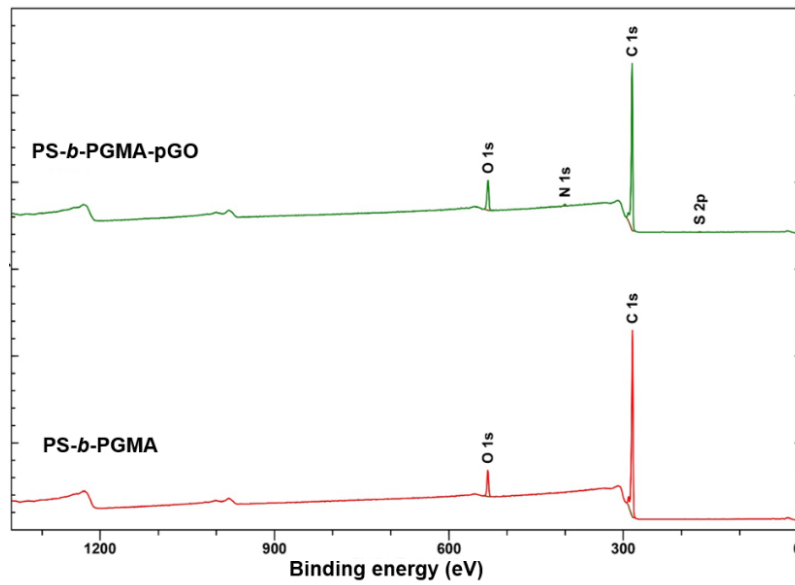


**Figure 4.2.15.** XPS analysis of PS-*b*-PGMA diblock copolymer membrane and hybrid membranes of PS-*b*-PGMA/PDEA-GO nanosheets

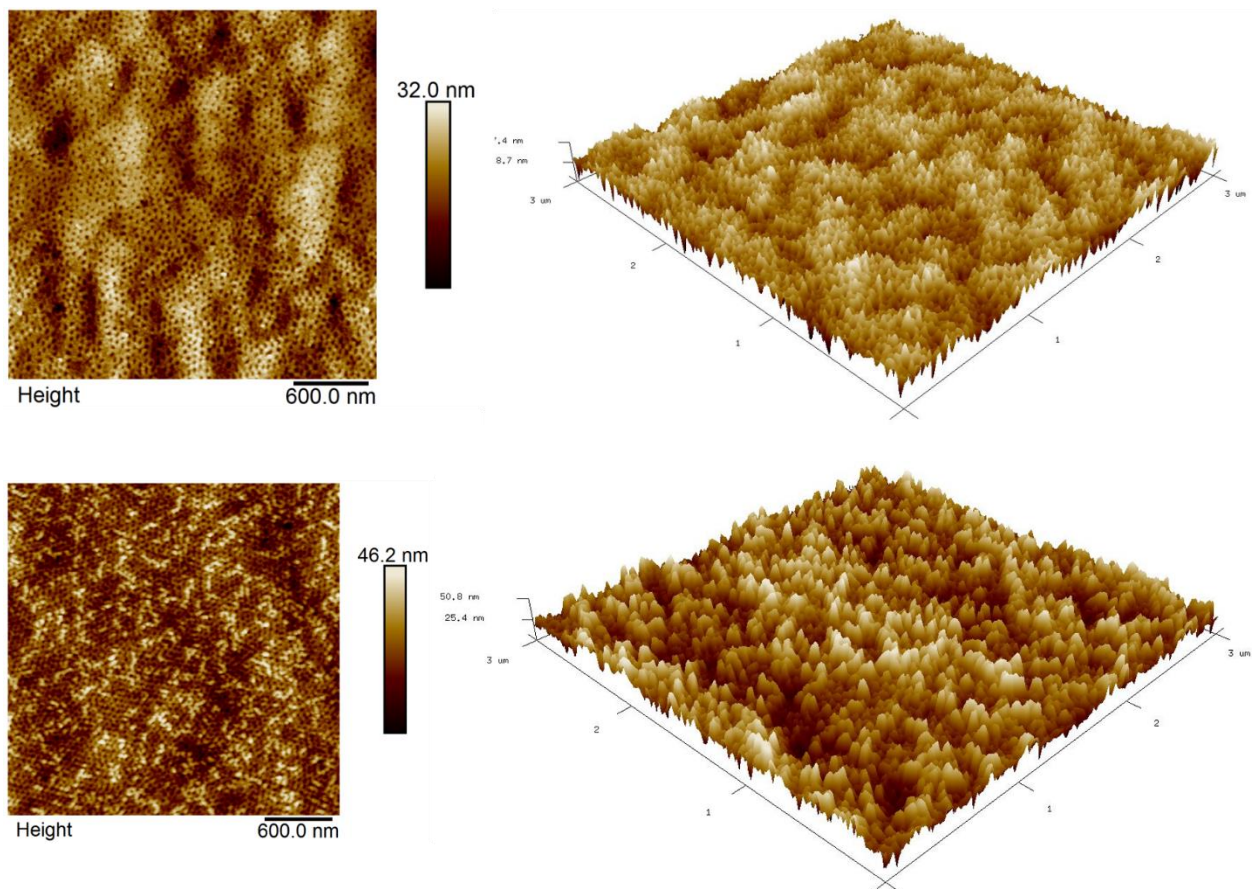


**Figure 4.2.16.** Atomic force micrograph of the surface and three dimensional images of membranes (a) PS-*b*-PGMA (b) 1.5 wt% PS-*b*-PGMA/PDEA-GO nanosheets

Above 1.5 wt% PDEA-GO nanosheets concentration in the polymeric solution resulted in a highly viscous solution and it was very difficult to cast membrane on a glass plate. The surface chemistry of pristine PS-*b*-PGMA and hybrid PS-*b*-PGMA/PDEA-GO membranes were characterized through X-ray photoelectron spectroscopy. Figure 4.2.15 shows comparison of the results of pristine membrane and hybrid membrane impregnated with 1.5 wt% PDEA-GO nanosheets. The appearance of a nitrogen signal in the hybrid membrane confirmed the presence of PDEA grafted nanosheets on the surface of the membrane.

The roughness parameters of the hybrid membrane PS-*b*-PGMA/PDEA-GO nanosheets are given in Table (4.6). Figure 4.2.16 shows a comparison of the three dimensional surface images of PS-*b*-PGMA and PS-*b*-PGMA/PDEA-GO nanosheets membranes by atomic force microscopy. The roughness parameters ( $R_a$  and  $R_q$ ) were calculated from AFM analysis software where ( $R_a$ ) (mean roughness) stands for arithmetic average of the surface height deviations measured from the mean value and ( $R_q$ ) for root mean square average of height deviations taken from the mean plane. It was observed that the roughness values of PS-*b*-PGMA/PDEA-GO nanosheets membrane were larger than the pristine PS-*b*-PGMA membrane (as shown in Table 4.6). The surface roughness of membrane influences its wettability and fouling properties. According to the Wenzel model [183], an increase in surface roughness improves hydrophilicity due to low water/polymer contact angle. At the same time an increase in water permeance of  $200 \pm 20 \text{ L m}^{-2} \text{ bar}^{-1} \text{ h}^{-1}$  was observed for PS-*b*-PGMA/PDEA-GO nanosheets membranes than pristine PS-*b*-PGMA membrane  $24 \pm 10 \text{ L m}^{-2} \text{ bar}^{-1}$ . It is well known that higher surface roughness of the membrane increases the surface area as well as permeation. [184]. Another possible reason for the increase in the water flux values was larger pore diameter of the hybrid membranes. The presence of tertiary amine groups of the (PDEAEMA) grafted on the GO nanosheets are also capable of binding more water molecules to form a stable hydration layer on the surface of the membrane.

**Table 4. 6.** Roughness parameters for membranes PS-*b*-PGMA and PS-*b*-PGMA/PDEA-GO nanosheets

Scanning Area	Membranes	<u>Roughness</u>	
		R <sub>a</sub> (nm)	R <sub>q</sub> (nm)
3μm × 3 μm	PS- <i>b</i> -PGMA	4.1	5.1
3μm × 3 μm	PS- <i>b</i> -PGMA/PDEA-GO	5.8	7.3

#### 4.2.11 Comparison of static adsorption of proteins/antifouling behavior

The static protein adsorption behavior of an ultrafiltration membrane can be a valuable indication of its fouling properties [185, 186]. The adsorption of protein on the membrane surface causes a reduction in the effective pore diameter to a complete blocking which influences the performance of the membrane negatively. To check the effect of the hydrophilic nature of the membranes on the antifouling behavior, static proteins adsorption experiments were conducted. For a comparison between two different systems, diblock copolymers PS<sub>82</sub>-*b*-PGMA<sub>18</sub><sup>126</sup> and PS<sub>81</sub>-P4VP<sub>19</sub><sup>123</sup> of relatively similar compositions were synthesized by anionic polymerization. Afterwards, the polymers were employed to cast isoporous membranes via SNIPS. The membrane surface and their cross sectional view are shown in Figure 4.2.17. The pore size of the PS<sub>82</sub>-*b*-PGMA<sub>18</sub><sup>126</sup>, PS<sub>81</sub>-*b*-P4VP<sub>19</sub><sup>123</sup> isoporous membranes is relatively comparable 19 ± 2 nm and 18 ± 2nm, respectively.

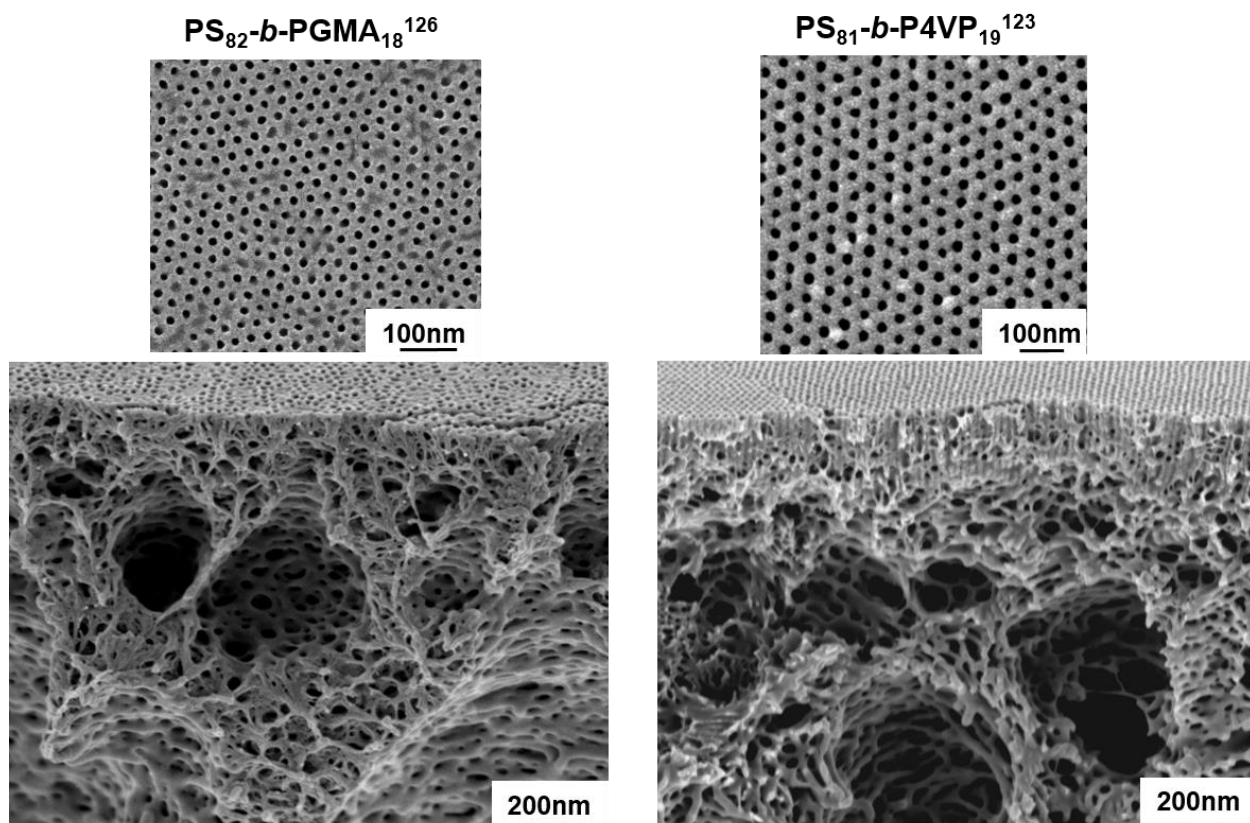


**Figure 4.2.17.** SEM topography and cross-section images of membranes prepared from (left) 23 wt% PS<sub>82</sub>-*b*-PGMA<sub>18</sub><sup>126</sup> in THF/DMF/DOX (2:1:1) and (right) 28 wt% PS<sub>81</sub>-P4VP<sub>19</sub><sup>123</sup> in THF/DMF 50/50 wt%. The corresponding cross-section views for each case are shown under the surface images (left) and (right), respectively. The time of evaporation was 10 s (left) and 5 s (right)

The change in adsorption behavior will not be affected by the topography of the membrane as the pore size of both the membranes is quite similar, however the nature/chemistry of pore forming block is different in both cases.

The adsorption of proteins was performed to evaluate the fouling resistant ability of both the membranes. Figure 4.2.18 presents the protein adsorption amount of membranes using BSA,  $\gamma$ -globulin and hemoglobin. The results demonstrated that the protein adsorption capacity of the PS<sub>82</sub>-*b*-PGMA<sub>18</sub><sup>126</sup> diblock copolymer membrane exhibited a significant decline in comparison to PS<sub>81</sub>-*b*-P4VP<sub>19</sub><sup>123</sup> membranes, which evidenced the more hydrophilic behavior of the PS<sub>82</sub>-*b*-PGMA<sub>18</sub><sup>126</sup> block copolymer membrane. The presence of two hydroxyl groups (-

OH) per repeating unit of PGMA block, provides a strong hydration on the surface that prevents fouling. It also indicates that more hydrophilic membrane surfaces hinder the attachment and adsorption of foulants by developing strong interactions with the ambient water molecules [187].

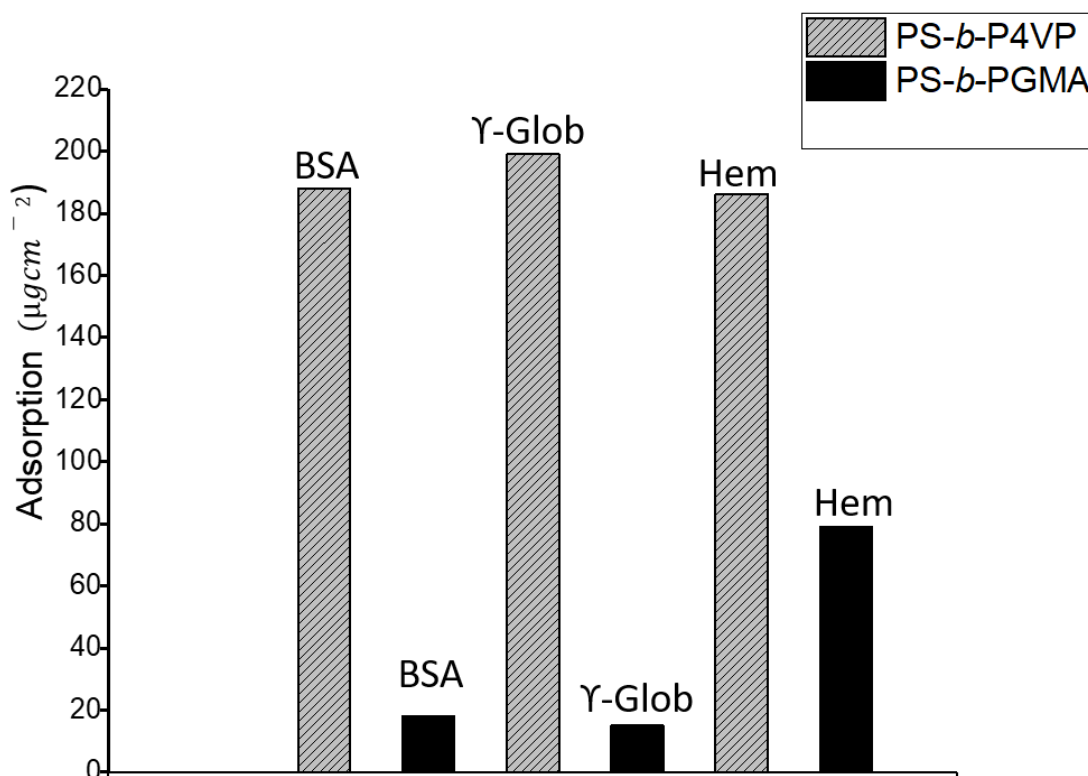


**Figure 4.2.18.** Adsorbed amount of foulants bovine serum albumin (BSA), gamma globulin ( $\gamma$ -Glob), hemoglobin (Hem) at pH 7.4 for PS<sub>82</sub>-*b*-PGMA<sub>18</sub><sup>126</sup> and PS<sub>81</sub>-*b*-P4VP<sub>19</sub><sup>123</sup> membranes

#### 4.2.12 Comparison of dynamic contact angle measurements

Hydrophilic and hydrophobic surface properties of block copolymer membranes were characterized by contact angle measurements. Figure 4.2.19 shows the variation of the dynamic contact angle with time of 5  $\mu$ L water droplets on the surface of PS<sub>81</sub>-*b*-PGMA<sub>19</sub><sup>128</sup> and PS<sub>76</sub>-*b*-PSMA<sub>24</sub><sup>135</sup> membranes. In case of the PS<sub>81</sub>-*b*-PGMA<sub>19</sub><sup>128</sup> membrane, the water droplet penetrates into the membrane within 120 s, whereas PS<sub>76</sub>-*b*-PSMA<sub>24</sub><sup>135</sup> membranes showed no

sinking of a water droplet at all, even after 120 s. These results proved that the inner surface of pores is covered by PGMA blocks in the case of  $\text{PS}_{81}\text{-}b\text{-PGMA}_{19}^{128}$  membranes, which are more hydrophilic than PSMA.

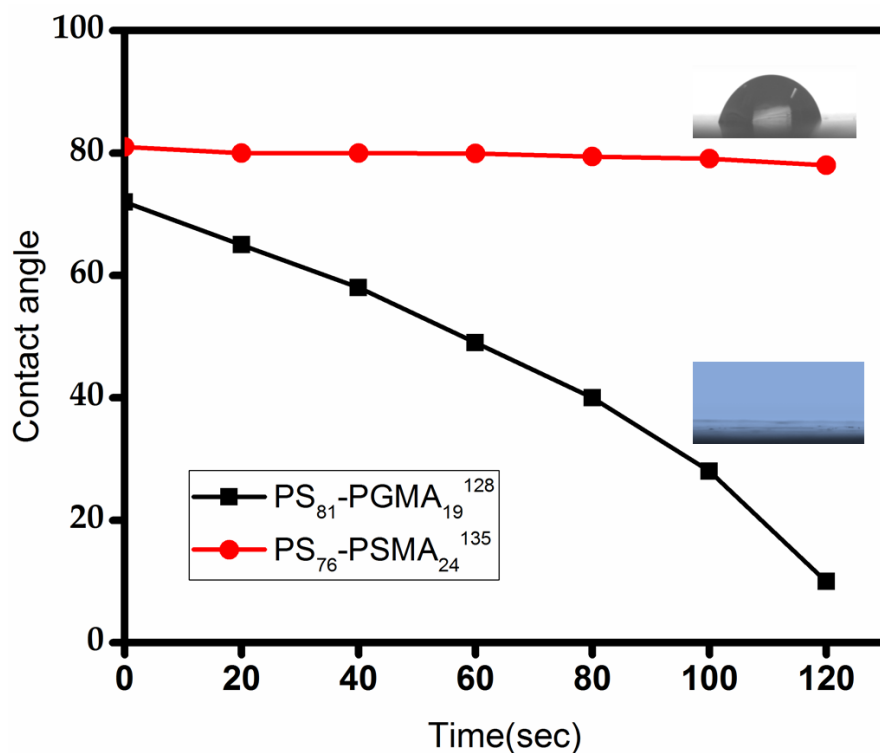


**Figure 4.2.19.** Graphical representation of the dynamic contact angle measurement of water droplets (5  $\mu\text{L}$ ) onto membrane surfaces developed from block copolymers  $\text{PS}_{76}\text{-}b\text{-PSMA}_{24}^{135}$  and  $\text{PS}_{81}\text{-}b\text{-PGMA}_{19}^{128}$  (previously shown in Figure 4.2.6 a, b)

### 4.2.13 Water flux measurements

To check the performance of the  $\text{PS}\text{-}b\text{-PGMA}$  membranes time-dependent water flux measurements were carried out in dead-end mode at room temperature as shown in Figure 4.2.20. The isoporous membrane showed low but constant water flux, even after 15 h. This indicates a rather fast swelling of the pore-forming hydrophilic blocks in water, which then hinder the water flux. An additional reason for the low water flux may be the rather dense

substructure of the membrane. Membranes of PS-*b*-PSMA showed almost no flux due to a completely closed morphology.

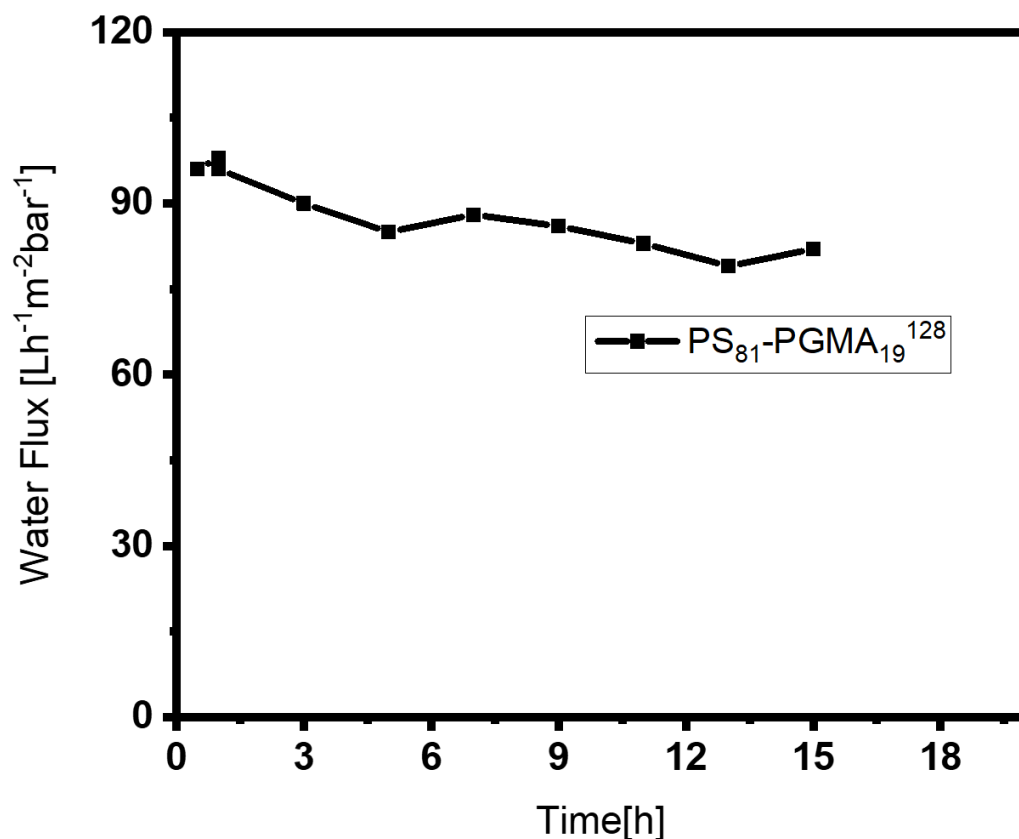


**Figure 4.2.20.** Time dependent water flux measurements of PS<sub>81</sub>-*b*-PGMA<sub>19</sub><sup>128</sup> membrane

In this chapter, a series of amphiphilic PS-*b*-PGMA diblock copolymers were prepared by acidic hydrolysis of PSMA block and were employed to cast integral asymmetric membranes via SNIPS. Different compositions of binary and ternary solvent systems were investigated to find the optimum composition for the fabrication of isoporous membranes. The hydrophilic behavior of PS-*b*-PGMA membranes was confirmed by contact angle measurements and the measurement of static adsorption of proteins. Later, hybrid membranes of PS-*b*-PGMA/PDEA-GO nanosheets were fabricated by the addition of nanofillers and were characterized through SEM, AFM and XPS.



## Chapter 5

### Isoporous membranes from novel polystyrene-*b*-poly(4-vinylpyridine)-*b*-poly(solketal methacrylate) (PS-*b*-P4VP-*b*-PSMA) triblock terpolymers and their post-modification

#### 5.1. Brief Introduction

In this chapter, we report the synthesis of a series of amphiphilic triblock terpolymers PS-*b*-P4VP-*b*-PSMA, by living anionic polymerization, followed by the exploration of triblock terpolymer membrane formation in varying polymer concentrations, solvent compositions and evaporation times. The motivation behind the synthesis of triblock terpolymer is as follows:

- 1) PS-*b*-PSMA/PS-*b*-PGMA diblock copolymers membranes were non-stimuli responsive, however, introduction of PSMA to PS-*b*-P4VP could lead to pH responsive membranes due to the 4-vinylpyridine (P4VP) block
- 2) PSMA is hydrophobic in nature and therefore the addition of this hydrophobic block to PS-*b*-P4VP could possibly reduce the amphiphilicity of the whole system, consequently affect the morphology of the membrane
- 3) Compared to PS-*b*-P4VP membranes, PS-*b*-P4VP-*b*-PGMA membranes could potentially enhance the fouling resistance due to the presence of two additional hydroxyl groups per repeating units present in poly(glyceryl methacrylate) (PGMA) block
- 4) The addition of third block could also enhance the structure formation of the membrane as reported before [45].
- 5) The third functional block added to the PS-*b*-P4VP system could broaden the window of possible post-modification

### 5.1.1 Synthesis and characterization of polystyrene-*block*-poly(4-vinylpyridine)-*block*-poly(solketal methacrylate) (PS-*b*-P4VP-*b*-PSMA) triblock terpolymer

A three-step sequential living anionic copolymerization procedure was employed for the synthesis of PS-*b*-P4VP-*b*-PSMA triblock terpolymers. The compositions of triblock terpolymers were determined by  $^1\text{H-NMR}$  spectroscopy. The molecular weight and dispersity index ( $\bar{D}$ ) determined by (SEC) using DMAc as solvent and polystyrene as standard.

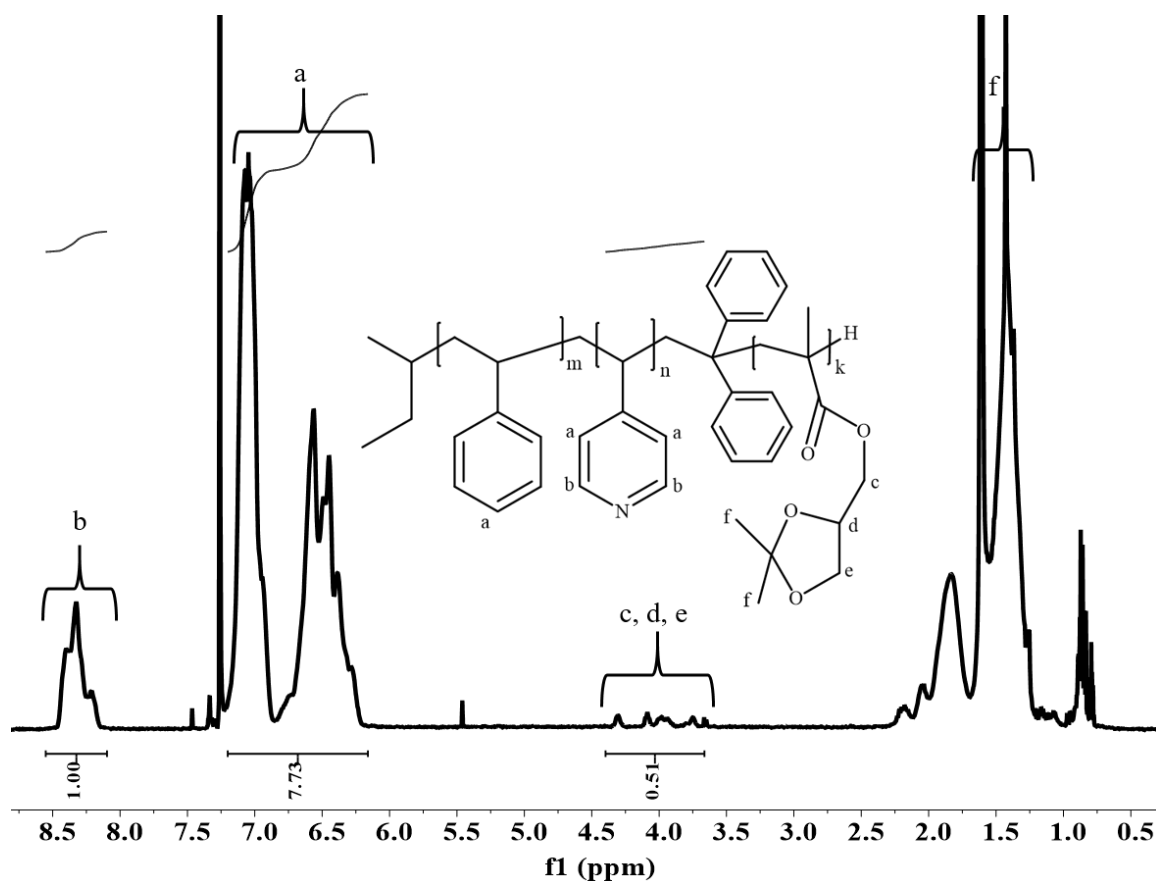


**Figure 5.1.1.**  $^1\text{H-NMR}$  spectra of PS<sub>71</sub>-*b*-P4VP<sub>26</sub>-*b*-PSMA<sub>3</sub><sup>145</sup> in  $\text{CDCl}_3$

$\delta$  [ppm] = 8.3 (m', 2H, H-14, H-15), 7.07-6.56 (m', 18H, H-13, H16, H17, H-18, H-19, arom. H(DPE)), 5.46 (s', DPE), 4.30 (m', 1H, H-11), 4.08 (t', 1H, H-12a), 3.98 (m', 2H, H-10), 3.74

(m', 1H, H-12b), 2.15-1.43 (m', 29H, H-1, H-2, H-3, H-4, H-5, H-6, H-7, H-8, H-9, 2x CH<sub>3</sub> (s-BuLi), 3x CH<sub>3</sub> (PSMA)).

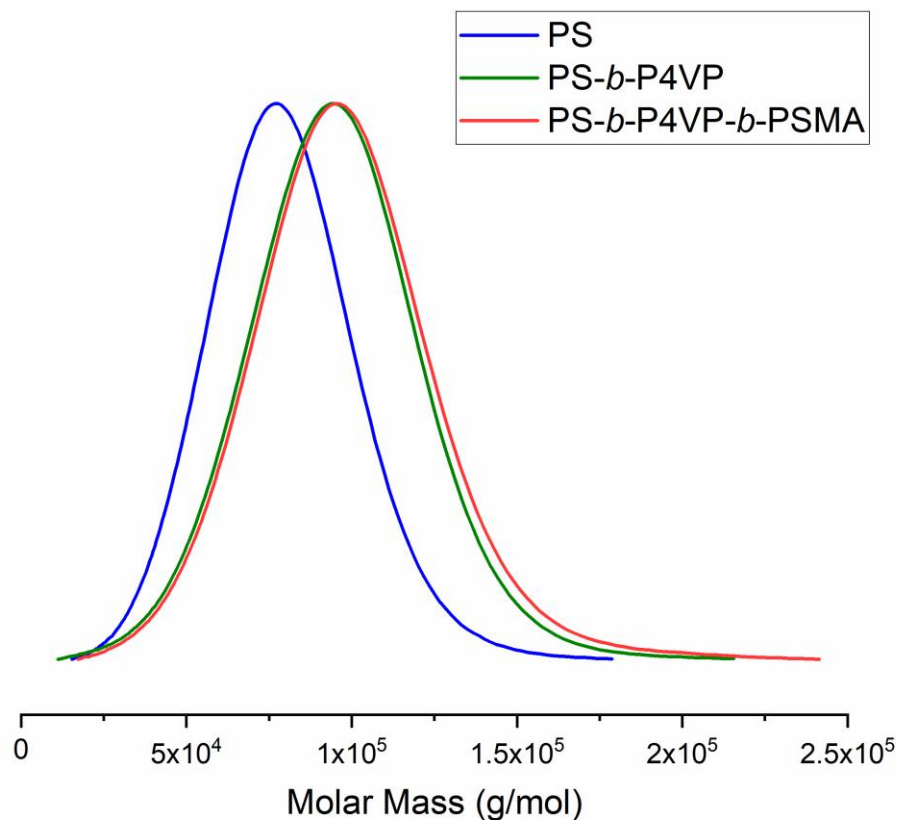


**Figure 5.1.2.** SEC chromatogram of PS homopolymer, PS-*b*-P4VP and PS<sub>72</sub>-*b*-P4VP<sub>17</sub>-*b*-PSMA<sub>11</sub><sup>91</sup> triblock terpolymer (measurement in THF at 30 °C using PS standards)

Figure 5.1.1 shows <sup>1</sup>H-NMR spectra of PS<sub>71</sub>-*b*-P4VP<sub>26</sub>-*b*-PSMA<sub>3</sub><sup>145</sup> where (c, d, e) peaks at 3.6 - 4.3 ppm correspond to five characteristic protons of PSMA. The length of the PS block was calculated from <sup>1</sup>H-NMR spectra by comparing the signal integral areas of the aromatic PS peaks at 6.3 - 7.2, 4VP peaks at 8.1 - 8.3 ppm and PSMA peak at 3.6 - 4.3 ppm. Peaks denoted by (f) are assigned to the two methyl groups present in the isopropylidene ring.

The evidence of NMR spectroscopy in Figure 5.1.1 and SEC measurements in Figure 5.1.2 support the formation of a triblock terpolymer. By using this method a series of triblock

terpolymers with varying molecular weights and narrow molecular weight distributions were successfully obtained as shown in Table 5.1. The yields range between 75-93 %. The polymers are sorted in ascending order according to their PSMA content.

**Table 5. 1.** Composition and molecular weights of PS-*b*-P4VP-*b*-PSMA triblock terpolymer

<b>Batch number</b>	<b>Polymer</b>	<b><math>M_n</math> (kg/mol)</b>	<b>P4VP (wt%)</b>	<b>PSMA (wt%)</b>	<b><math>\bar{D}</math></b>
300816-2	PS <sub>71</sub> - <i>b</i> -P4VP <sub>26</sub> - <i>b</i> - PSMA <sub>3</sub>	145	26	3	1.05
190122	PS <sub>70</sub> - <i>b</i> -P4VP <sub>25</sub> - <i>b</i> - PSMA	143	25	5	1.03
181128	PS <sub>69.3</sub> - <i>b</i> -P4VP <sub>25.5</sub> - <i>b</i> - PSMA <sub>5.2</sub>	128	25.5	5.2	1.04
300816-1	PS <sub>73</sub> - <i>b</i> -P4VP <sub>20</sub> - <i>b</i> - PSMA <sub>7</sub>	170	20	7	1.07
160816-2	PS <sub>73</sub> - <i>b</i> -P4VP <sub>19</sub> - <i>b</i> - PSMA <sub>8</sub>	154	19	8	1.02
191015	PS <sub>71</sub> - <i>b</i> -P4VP <sub>17</sub> - <i>b</i> - PSMA <sub>12</sub>	91	17	11	1.12
160816-1	PS <sub>69</sub> - <i>b</i> -P4VP <sub>20</sub> - <i>b</i> - PSMA <sub>11</sub>	103	20	11	1.03
270716	PS <sub>64.8</sub> - <i>b</i> -P4VP <sub>23.6</sub> - <i>b</i> - PSMA <sub>11.6</sub>	179	23.6	11.6	1.08

### 5.1.2 Bulk morphology of the triblock terpolymers

Annealed films obtained from solution casting were used to study the bulk morphology of the triblock terpolymers. TEM analysis of PS-*b*-P4VP-*b*-PSMA triblock terpolymers (PS<sub>71</sub>-*b*-P4VP<sub>26</sub>-*b*-PSMA<sub>3</sub><sup>145</sup>, PS<sub>71</sub>-*b*-P4VP<sub>17</sub>-*b*-PSMA<sub>12</sub><sup>91</sup>) was performed by preparing ultrathin sections of the respective triblock terpolymer film. For this purpose, a 7.5 wt% solution of polymer was prepared in CHCl<sub>3</sub>, which is a common rather non-selective solvent for all the three blocks. The solution dried for a week in a porcelain crucible under a constant vapor atmosphere in a desiccator. The films were further annealed slowly from room temperature to 150°C. Figure 5.1.3-a shows the TEM micrograph of a PS<sub>71</sub>-*b*-P4VP<sub>17</sub>-*b*-PSMA<sub>12</sub><sup>91</sup> triblock terpolymer film in which only PS block was stained with RuO<sub>4</sub>. In this case, no typical or well-defined block copolymer morphology could be evidenced, however, some bright domains of PSMA could be observed in the darker PS matrix. Later the P4VP blocks of the same ultrathin section were stained with iodine vapor. The result is depicted in Figure 5.1.3-b. In the presence of iodine staining the PSMA block remains unstained, grey features demonstrate the PS block which are distributed in the darker phase constituted by P4VP. Regular hexagonally packed cylindrical structures predominate in PS<sub>71</sub>-*b*-P4VP<sub>26</sub>-*b*-PSMA<sub>3</sub><sup>145</sup> with no clear differentiation of the phase composition as shown in Figure 5.1.4-a.

Figure 5.1.4-b shows an AFM image of a thin film of PS<sub>71</sub>-*b*-P4VP<sub>26</sub>-*b*-PSMA<sub>3</sub><sup>145</sup> prepared by spin coated on a silicon wafer from a solution in chloroform and the long-range ordered morphology was confirmed.

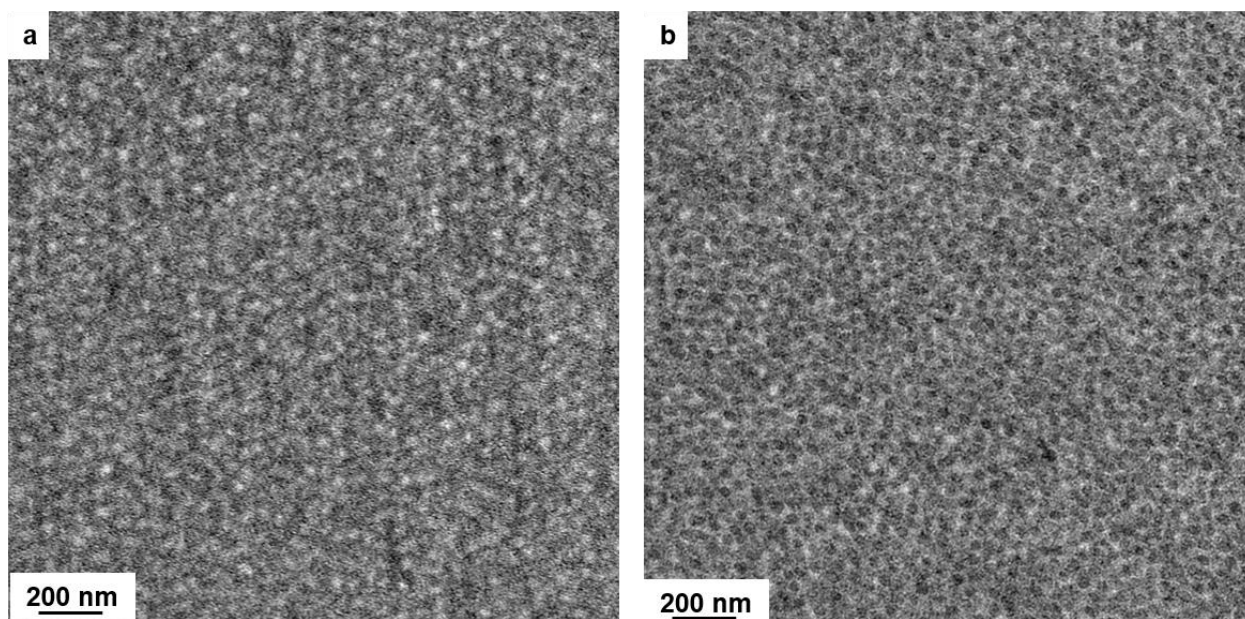


**Figure 5.1.3.** TEM micrographs of PS-*b*-P4VP-*b*-PSMA triblock terpolymer cast from chloroform (a) PS<sub>71</sub>-*b*-P4VP<sub>17</sub>-*b*-PSMA<sub>12</sub><sup>91</sup> stained with RuO<sub>4</sub> (b), with RuO<sub>4</sub> and I<sub>2</sub>

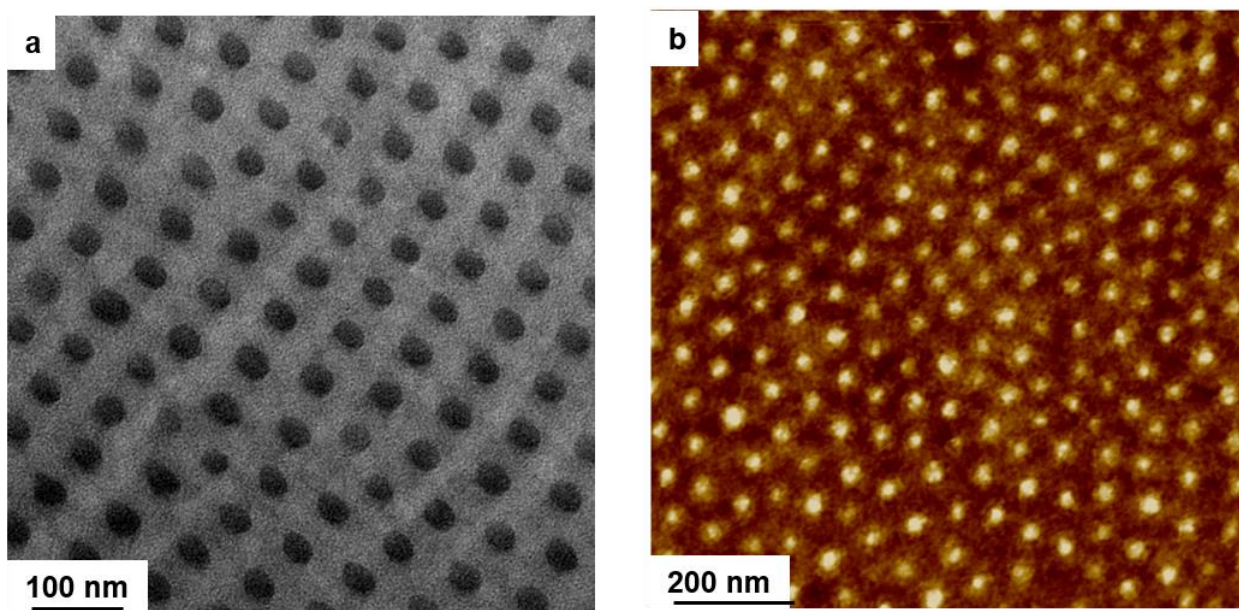


**Figure 5.1. 4.** (a) TEM image of PS<sub>71</sub>-*b*-P4VP<sub>26</sub>-*b*-PSMA<sub>3</sub><sup>145</sup> stained with I<sub>2</sub> (b) AFM height image (in tapping mode) of the film surface of the asymmetric PS<sub>71</sub>-*b*-P4VP<sub>26</sub>-*b*-PSMA<sub>3</sub><sup>145</sup> triblock terpolymer

### 5.1.3 Preparation of the membrane by SNIPS

Among the parameters influencing the nanostructure of a membrane prepared by SNIPS the (mixed) solvent interactions to different blocks and the concentration of the polymer are the most important ones [188, 189].

Rational design of the selective solvent mixture plays a decisive role in the SNIPS process for the desired morphology of block copolymer membranes. Solutions of block copolymer with binary or ternary mixtures of solvents varying from volatile to non-volatile were prepared. The volatile solvents THF and acetone are suitable for both PS and PSMA blocks, whereas DMF is the preferred solvent for P4VP blocks according to the solubility parameters of the solvents and blocks of the block copolymers.

Initially, we prepared membranes using different concentrations of binary solvent mixtures THF/DMF: 50/50, 60/40, 70/30 wt%, however, the morphologies of the PS<sub>71</sub>-*b*-P4VP<sub>26</sub>-*b*-PSMA<sub>3</sub><sup>145</sup> membranes did not show ordered pore structures, but rather dense regions with random macropores were obtained (Figure 5.1.5).

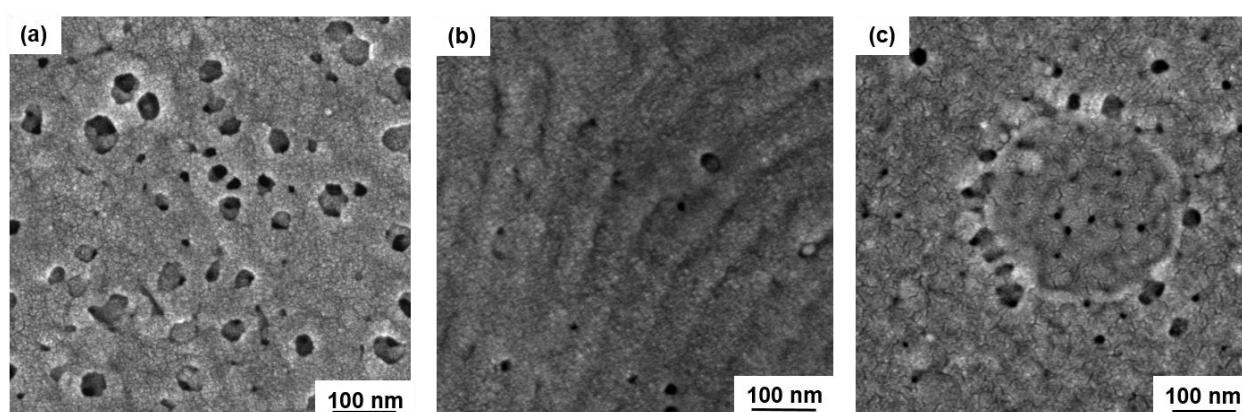


**Figure 5.1.5.** SEM images of PS<sub>71</sub>-*b*-P4VP<sub>26</sub>-*b*-PSMA<sub>3</sub><sup>145</sup> membrane surfaces prepared from different solutions: 22 wt% copolymer at 10 sec evaporation time in (a) 60/40 THF/DMF; (b) 50/50 THF/DMF; (c) 70/30 THF/DMF

Therefore, two types of ternary solvent mixtures THF/DMF/DOX and THF/DMF/acetone were used for membrane casting. Self-assembly of the triblock terpolymer was not successful in different compositions of THF/DMF/DOX (Figure 5.1.6).

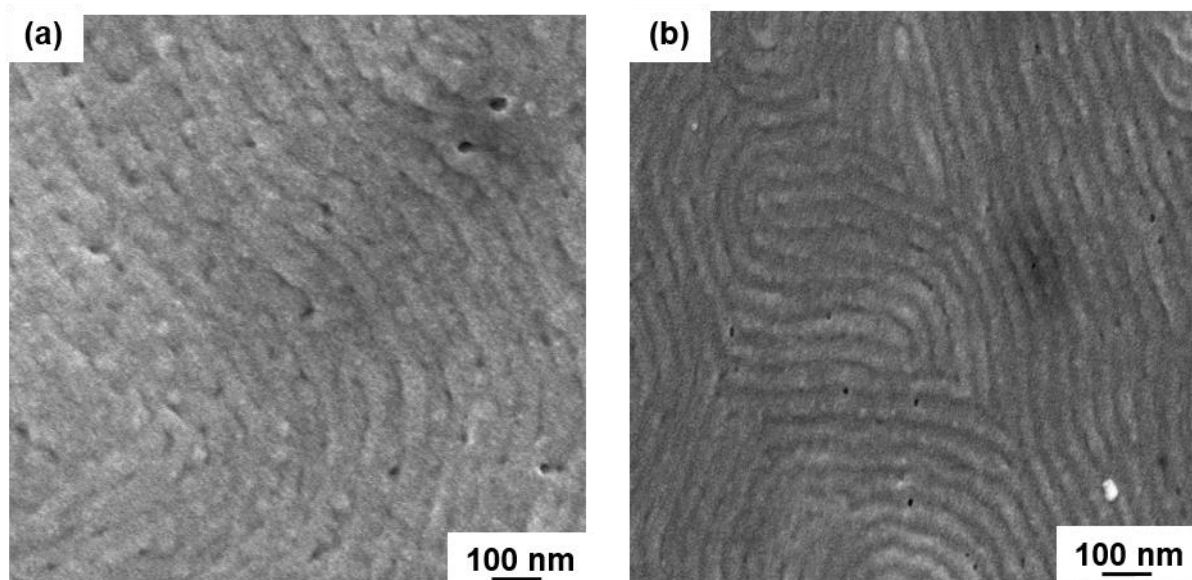


**Figure 5.1.6.** SEM images of the  $PS_{71}\text{-}b\text{-}P4VP_{26}\text{-}b\text{-}PSMA_3$ <sup>145</sup> membranes cast from a 22 wt% copolymer solution in (a) THF/DMF/DOX 1/1/1 (b) THF/DMF/DOX 40/30/30. The evaporation time before immersion into the precipitant was 10 seconds.

However, the addition of acetone to the THF/DMF mixture directs the self-assembly of the triblock terpolymer into highly ordered hexagonally packed cylinders with perpendicular orientation. Different combinations of THF/DMF/acetone were examined, but only the mixture of THF/DMF/acetone (50/30/20 wt%) leads to the desired nanostructure containing a narrow pore size distribution with 10 s evaporation time as shown in Figure 5.1.7-a. THF and acetone are selective volatile solvents for PS and PSMA while DMF is a more selective and much less volatile solvent for P4VP. The abrupt change in the polymer solution concentration due to the fast evaporation of acetone and THF favors the perpendicular ordering of the microdomains and this differs from the solvent mixture containing less volatile DOX instead of acetone. Phillip et al. [133] reported that fast evaporation conditions on the top layer can form perpendicular

cylinders templated by the copolymer self-assembly, while the underlying porous structure is controlled by the polymer precipitation. The cross-section of the triblock terpolymer membrane was imaged by SEM in Figure 5.1.7-b. The mean pore diameter of the integral asymmetric membrane is  $26 \pm 3$  nm. It is advantageous to have a volatile co-solvent to study the effect of evaporation time for  $PS_{71}-b-P4VP_{26}-b-PSMA_3$ <sup>145</sup> membranes.

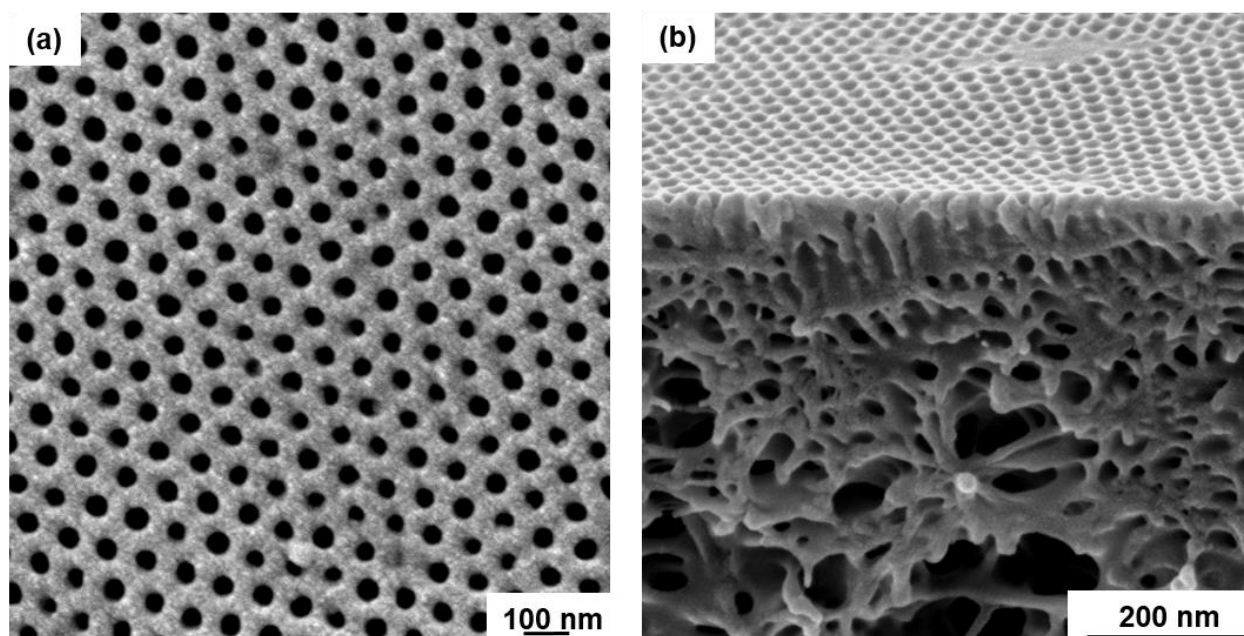


**Figure 5.1.7.** SEM images of (a) top view and (b) cross-section of  $PS_{71}-b-P4VP_{26}-b-PSMA_3$ <sup>145</sup> membranes cast from 22 wt% solution in a THF/DMF/acetone: 50/30/20 wt%. Evaporation time was 10 seconds before immersion in water

By increasing the evaporation time to 30 seconds, membrane regularity was partially destroyed and a dense structure was formed predominately with only few open pores. Due to the longer evaporation time the very well-ordered hexagonal cylindrical structure disappeared. The lying cylindrical structure is much less porous and thus retards the solvent/non-solvent exchange. (Figure 5.1.8)

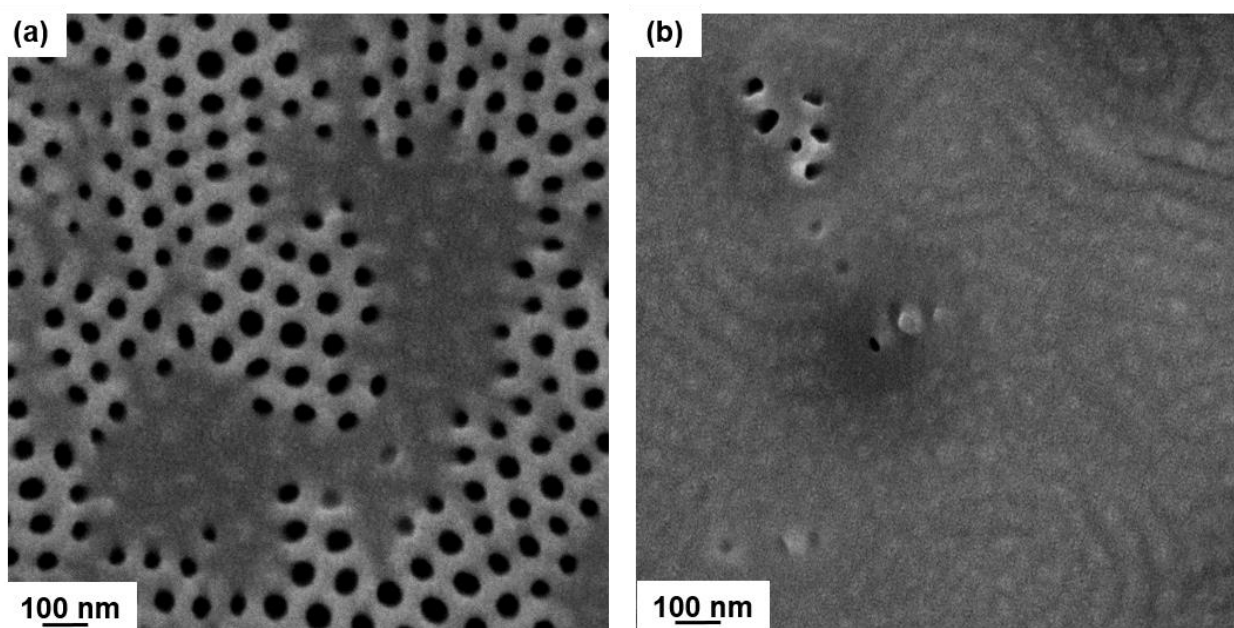


**Figure 5.1.8.** Surface SEM images of  $PS_{71}\text{-}b\text{-}P4VP_{26}\text{-}b\text{-}PSMA_3^{145}$  membranes cast from solutions THF/DMF/Acetone: 50/30/20 wt%. (a) 20 seconds (b) 30 seconds evaporation time before immersion into non-solvent bath.

It is observed that in-diffusion of non-solvent and out-diffusion of co-solvent becomes more difficult by increasing the polymer concentration of the casting solution from 21-24 wt%. The concentration of  $PS_{71}\text{-}b\text{-}P4VP_{26}\text{-}b\text{-}PSMA_3^{145}$  was varied by keeping all the other parameters constant. Membranes with a top isoporous layer (with cylindrical channels of approximately 220 nm length) followed by the spongy structure underneath, were obtained as shown in Figure 5.1.7 The high viscosity of the more concentrated casting solutions restricts the movement of the polymeric chains due to the higher amount of the polymer and perhaps influences the final membrane morphology. (Figure 5.1.9)

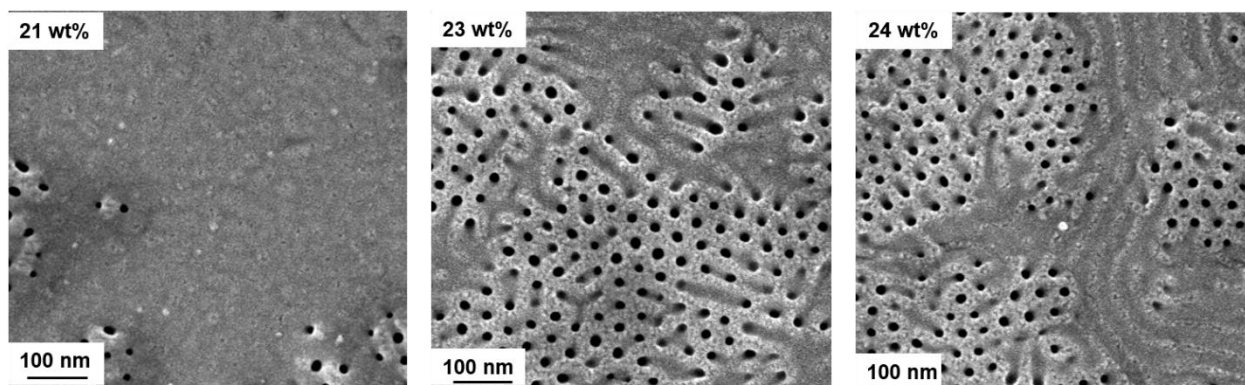


**Figure 5.1.9.** Surface SEM images of  $\text{PS}_{71}\text{-}b\text{-P4VP}_{26}\text{-}b\text{-PSMA}_3$ <sup>145</sup> membranes cast from 21 wt%, 23 wt%, and 24 wt% terpolymer solutions in THF/DMF/Acetone: 50/30/20 wt%. The evaporation time before immersion into the precipitant was 10 s.

#### 5.1.4 Post-modification of $\text{PS}_{71}\text{-}b\text{-P4VP}_{17}\text{-}b\text{-PSMA}_{12}$ <sup>91</sup> triblock terpolymer

The triblock terpolymers synthesized in this study with a longer third hydrophobic block (PSMA) suffer difficulties for membrane formation via SNIPS. Based on previous findings [45, 190], this is probably due to the shorter hydrophilic P4VP block, which cannot compensate for the hydrophobic nature of the PSMA block.

The  $\text{PS}_{71}\text{-}b\text{-P4VP}_{17}\text{-}b\text{-PSMA}_{12}$ <sup>91</sup> triblock terpolymer was treated with 1M HCl solution at 50 °C for 3 days to remove the acetonide moiety of PSMA blocks. The acid treated polymer was stirred in 0.1M NaOH solution for 45 minutes to completely deprotonate the quaternized P4VP blocks. Finally, the triblock terpolymer was treated with deionized water and dried in a vacuum oven at 50 °C. The procedure was monitored by <sup>1</sup>H-NMR to ensure the removal of the isopropylidene acetal group. After each step the polymers were re-dissolved in deuterated solvents and spectra were recorded. Quaternization of the P4VP was monitored by the solubility of the polymer in  $\text{CDCl}_3$  (quaternized polymers were not dissolved in  $\text{CDCl}_3$ ). The complete acidic hydrolysis of the ketal moiety of PSMA block shown in the Section 3.3.2.

$^1\text{H-NMR}$  spectra of  $\text{PS}_{71}\text{-}b\text{-P4VP}_{17}\text{-}b\text{-PGMA}_{12}^{91}$  is shown in Figure 5.1.10 after acidic hydrolysis of the PSMA block. The appearance of two signals at (f) corresponds to two hydroxyl groups (-OH) of GMA units whereas peaks at c, d, e represent five protons of the solketal moiety, which are shifted up field due to the replacement of the carbon atom with a hydrogen atom.  $\text{PS}_{71}\text{-}b\text{-P4VP}_{17}\text{-}b\text{-PGMA}_{12}^{91}$  was also protonated by HCL during the acidic hydrolysis of the ketal moieties of the PSMA block, resulting in temporarily charged  $\text{PS-}b\text{-PQ4VP-}b\text{-PGMA}$  (PQ4VP stands for quarternized P4VP) because of quaternization of the 4-vinyl pyridine moiety. However, the temporary quarternized P4VP block was deprotonated successfully by stirring the polymer in 0.1 M sodium hydroxide solution.

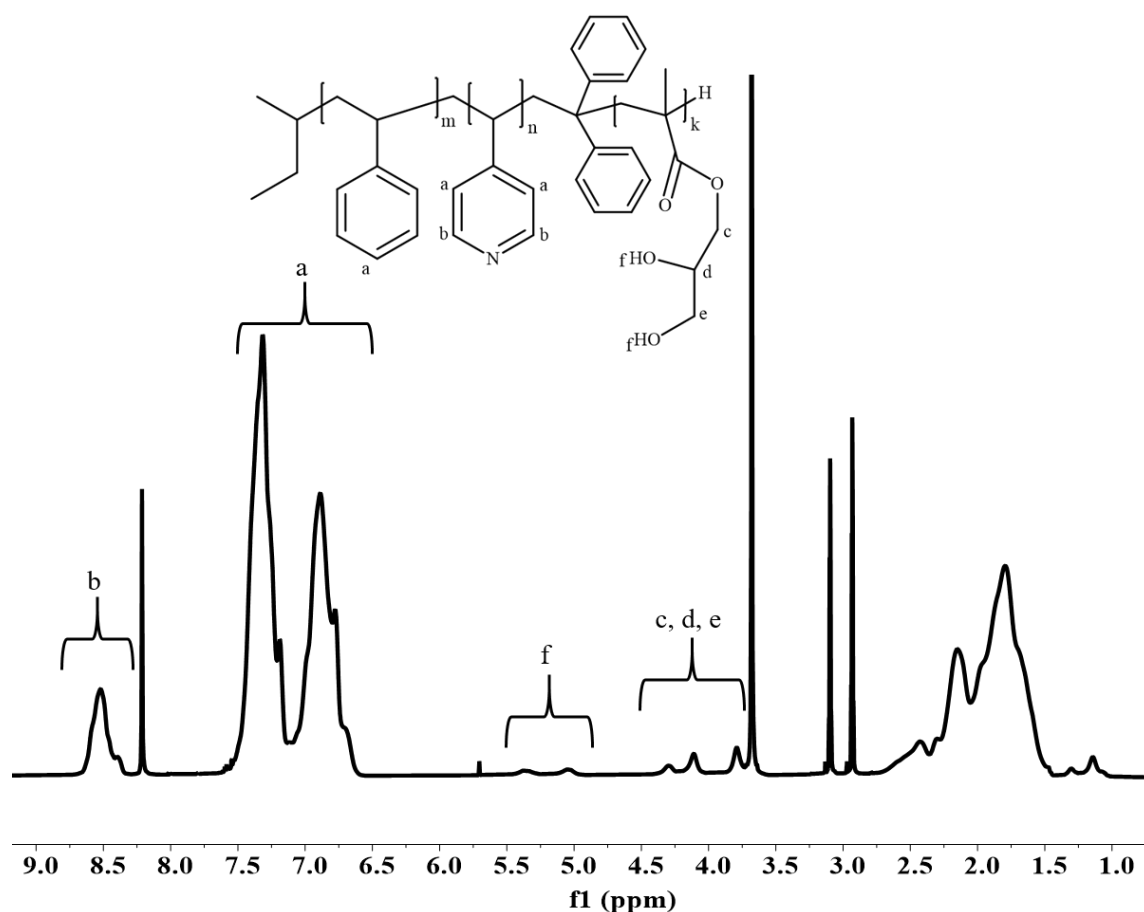


**Figure 5.1.10.**  $^1\text{H-NMR}$  spectrum of the linear triblock terpolymer  $\text{PS}_{71}\text{-}b\text{-P4VP}_{17}\text{-}b\text{-PGMA}_{12}^{91}$  in  $\text{DMF-}d_7$

**<sup>1</sup>H-NMR** (DMF-*d*<sub>7</sub>, 20 °C, 300 MHz, TMS)

$\delta$  [ppm] = 8.3 (m', 2H, H-14, H-15), 7.4-6.7 (m', 18H, H-13, H16, H17, H-18, H-19, arom. H(DPE)), 5.7 (s', DPE), 5.3 (s', 1H, H-14), 5.04 (s', 1H, H-13), 4.28-3.7 (m', 5H, H-10, H-11, H-12), 2.15-1.43 (m', 23H, H-1, H-2, H-3, H-4, H-5, H-6, H-7, H-8, H-9, 2x CH<sub>3</sub> (*s*-BuLi), 1 x CH<sub>3</sub> (PGMA)).

### **5.1.5 Membrane fabrication after post-modification of triblock terpolymer**

Apparently, the amphiphilic behavior plays a crucial role in the self-assembly and pore formation during the phase inversion process. After the acidic hydrolysis of PS<sub>71</sub>-*b*-P4VP<sub>17</sub>-*b*-PSMA<sub>12</sub><sup>91</sup> triblock terpolymer, the amphiphilicity of the whole polymer increased due to the appearance of hydroxyl groups in PS<sub>71</sub>-*b*-P4VP<sub>17</sub>-*b*-PGMA<sub>12</sub><sup>91</sup>, resulting into a hexagonally oriented cylindrical porous membrane as shown in Figure 5.1.11. It is assumed that the hydrophilic short block at the end of the pore-forming block (P4VP) enhances the formation of a good membrane structure, while the addition of a hydrophobic block tends to suppress the formation of a porous membrane structure. Only if the P4VP block is large enough it can overcome the influence of the hydrophobic PSMA block and a membrane with highly oriented pores can be obtained.

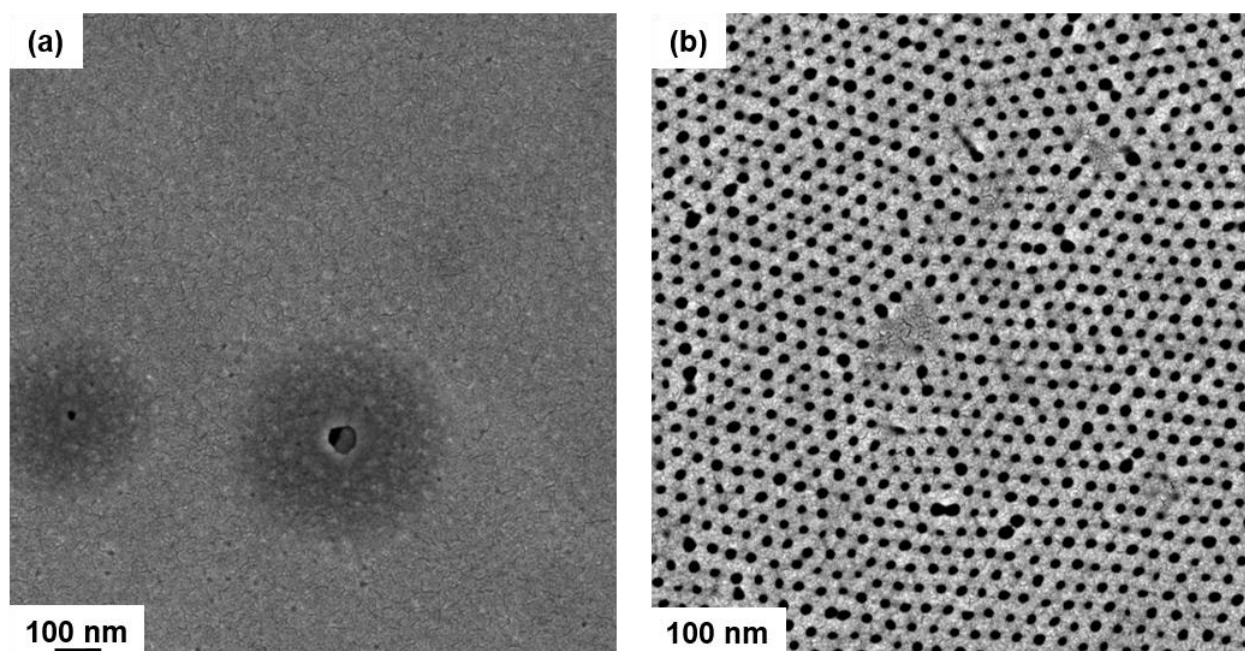


**Figure 5.1.11.** SEM images of (a)  $\text{PS}_{71}\text{-}b\text{-P4VP}_{17}\text{-}b\text{-PSMA}_{12}^{91}$  membrane (b)  $\text{PS}_{71}\text{-}b\text{-P4VP}_{17}\text{-}b\text{-PGMA}_{12}^{91}$  membrane obtained after acidic hydrolysis. The evaporation time before immersion into water bath was 10 s.

This is in agreement with our previous results for a  $\text{PS-}b\text{-PSMA}$  and the corresponding hydrolyzed  $\text{PS-}b\text{-PGMA}$  diblock copolymer, where only the latter one yielded the isoporous membranes by applying SNIPS [190].

### 5.1.6 Post-modification of $\text{PS}_{71}\text{-}b\text{-P4VP}_{26}\text{-}b\text{-PSMA}_3^{145}$ membranes.

The same procedure mentioned in Section 5.1.4 was followed for the post-modification of PSMA block of  $\text{PS}_{71}\text{-}b\text{-P4VP}_{26}\text{-}b\text{-PSMA}_3^{145}$  triblock terpolymer membranes (in solid state).

## 5.2 Comparison of the performance of membranes

In this chapter, a comparison of the performance of the membranes prepared before ( $\text{PS-}b\text{-P4VP-}b\text{-PSMA}$ ) and after acidic hydrolysis ( $\text{PS-}b\text{-P4VP-}b\text{-PGMA}$ ) will be discussed.

## 5.2.1 Comparison of contact angle measurements

The hydrophilicity of the membrane is characterized by water contact angle. The sessile drop method was used to investigate the dynamic contact angle of  $\text{PS}_{71}\text{-}b\text{-P4VP}_{26}\text{-}b\text{-PSMA}_3^{145}$  and  $\text{PS}_{71}\text{-}b\text{-P4VP}_{26}\text{-}b\text{-PGMA}_3^{145}$  membranes. Figure 5.2.1 shows the contact angles or sinking of a water droplet with time on/into the membrane surfaces before and after hydrolysis of PSMA blocks. It can be seen that the water contact angle of  $\text{PS}_{71}\text{-}b\text{-P4VP}_{26}\text{-}b\text{-PSMA}_3^{145}$  membrane surface is definitely higher as compared to the  $\text{PS}_{71}\text{-}b\text{-P4VP}_{26}\text{-}b\text{-PGMA}_3^{145}$  membranes. The lower contact angle value for  $\text{PS}_{71}\text{-}b\text{-P4VP}_{26}\text{-}b\text{-PGMA}_3^{145}$  membranes surfaces indicates the presence of hydroxyl ( $\text{-OH}$ ) groups.

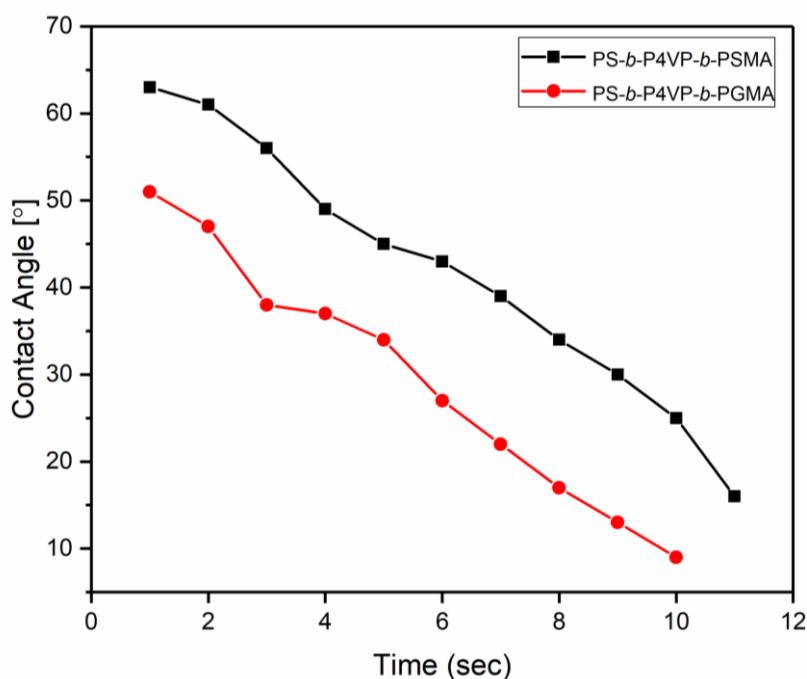


**Figure 5.2.1.** Dynamic contact angle measurements of water droplets ( $2\mu\text{L}$  each) onto the  $\text{PS}_{71}\text{-}b\text{-P4VP}_{26}\text{-}b\text{-PSMA}_3^{145}$  (black squares) and  $\text{PS}_{71}\text{-}b\text{-P4VP}_{26}\text{-}b\text{-PGMA}_3^{145}$  (red circles) membranes

### 5.2.2 Water permeation and pH responsive behavior

Block copolymer membranes with high porosity, homogeneous pore size, and tunable chemical properties hold tremendous potential as robust, efficient, and highly selective separation membranes. We tested the integral asymmetric  $\text{PS}_{71}\text{-}b\text{-P4VP}_{26}\text{-}b\text{-PGMA}_3^{145}$  membrane for ultrafiltration and analyzed the separation performance of the hexagonally organized isoporous structure by comparing it with the pristine  $\text{PS}_{71}\text{-}b\text{-P4VP}_{26}\text{-}b\text{-PSMA}_3^{145}$  membrane. The permeance of the membranes before and after hydrolysis was measured in dead-end mode at 2 bar trans-membrane pressure. It is reported in the literature that improvement of hydrophilicity has an influence on the pure water flux [191].

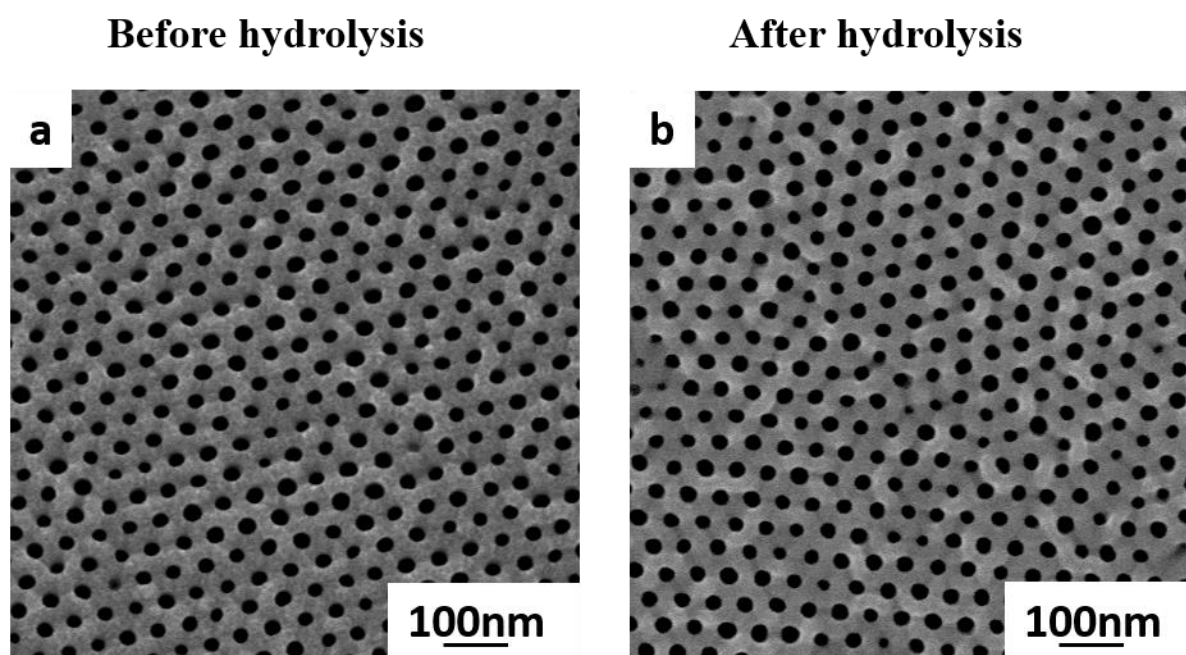


**Figure 5.2.2.** SEM images of pristine  $\text{PS}_{71}\text{-}b\text{-P4VP}_{26}\text{-}b\text{-PSMA}_3^{145}$  membrane before acidic hydrolysis and (b)  $\text{PS}_{71}\text{-}b\text{-P4VP}_{26}\text{-}b\text{-PGMA}_3^{145}$  membrane.

The initial permeance of the pristine  $\text{PS}_{71}\text{-}b\text{-P4VP}_{26}\text{-}b\text{-PSMA}_3^{145}$  and hydrolyzed  $\text{PS}_{71}\text{-}b\text{-P4VP}_{26}\text{-}b\text{-PGMA}_3^{145}$  membrane is  $390 \pm 25 \text{ L m}^{-2} \text{ bar}^{-1} \text{ h}^{-1}$  and  $485 \pm 10 \text{ L m}^{-2} \text{ bar}^{-1} \text{ h}^{-1}$ , respectively. Compared to the pristine membrane, the hydrolyzed membrane decorated with

hydrophilic PGMA not only has a higher flux, but also appears to have stable permeance. The pore diameters of both the membranes before and after hydrolysis are rather similar (Figure 5.2.2). These increased permeability results are in accordance with the contact angle measurements, the more hydrophilic surfaces lead to an increased wetting of the porous structure [192].

The stimuli responsive behavior of the triblock terpolymer membrane  $PS_{71}\text{-}b\text{-}P4VP_{26}\text{-}b\text{-}PGMA_3^{145}$  was investigated by the influence of the pH value on water flux. Since P4VP can be protonated at low pH, due to the swelling of the positively charged P4VP blocks, a decrease in the size of the pores was observed whereas the highest water flux was observed at pH 7. The P4VP block behaves like a polyelectrolyte at low pH (Figure 5.2.3).

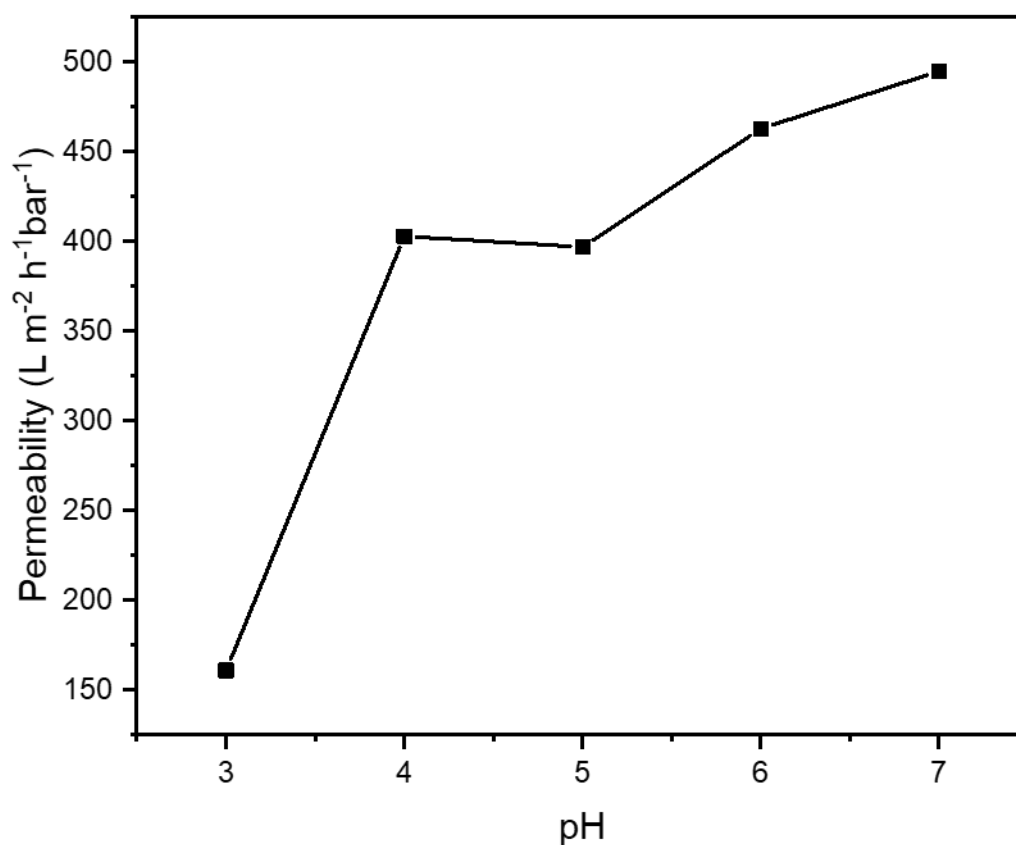


**Figure 5.2.3.** Water permeability of  $PS_{71}\text{-}b\text{-}P4VP_{26}\text{-}b\text{-}PGMA_3^{145}$  membrane measured at various pH, at pH > 4 high water permeability was observed, due to deswelling of the deprotonated P4VP blocks at larger pH, leading to their collapse on the pore walls

### 5.2.3 BSA retention measurements

Ultrafiltration membranes suffer from organic and biological fouling, which impede the performance in long-term use [41, 193, 194]. For studying the properties of our membranes, retention and adsorption measurements were carried out. The retention measurements were carried out by using 1 mg/1 mL bovine serum albumin (BSA, Sigma-Aldrich, USA) solution at pH 7.4. The isoelectric point is at pH 5.2. BSA shows a negative overall charge at the given pH when taking into account the isoelectric point of the protein. The hydrodynamic diameter of BSA (7.6 nm as stated by the supplier) is much below the pore size; its retention depends mainly on the interaction with the membrane, rather than being a size effect. The results in Table 5.2 show that the retention rate of BSA for PS<sub>71</sub>-*b*-P4VP<sub>26</sub>-*b*-PSMA<sub>3</sub><sup>145</sup> membrane was 90% whereas only 24% retention was observed for hydrolyzed PS<sub>71</sub>-*b*-P4VP<sub>26</sub>-*b*-PGMA<sub>3</sub><sup>145</sup> membrane. The low retention rate to the protein demonstrates that increasing the membrane hydrophilicity by incorporating hydroxyl groups containing PGMA results in a decreased fouling [195].

**Table 5. 2.** Retention results from experiments in a 1 mg/1 mL BSA solution in (PBS buffer pH = 7.4).

Membrane/BSA	% BSA retention	Average pore diameter/size (nm)
PS <sub>71</sub> - <i>b</i> -P4VP <sub>26</sub> - <i>b</i> -PSMA <sub>3</sub> <sup>145</sup>	90	26 ± 3 <sup>a</sup>
PS <sub>71</sub> - <i>b</i> -P4VP <sub>26</sub> - <i>b</i> -PGMA <sub>3</sub> <sup>145</sup>	24	26 ± 4 <sup>a</sup>
BSA	–	7.6 [196]

<sup>a</sup> determined by using the software analysis (Olympus Soft Imaging Solutions) of the SEM surface images

### 5.2.4 Static adsorption of hemoglobin

Further on, the high hydrophilicity and the antifouling behavior of PS-*b*-P4VP, pristine PS<sub>71</sub>-*b*-P4VP<sub>26</sub>-*b*-PSMA<sub>3</sub><sup>145</sup>, and modified PS<sub>71</sub>-*b*-P4VP<sub>26</sub>-*b*-PGMA<sub>3</sub><sup>145</sup> membranes were confirmed by static hemoglobin adsorption experiments at 25 °C in PBS buffer (pH 7.4). The hydrodynamic diameter of hemoglobin (IEP = 6.8) is 6.4 nm as stated by the supplier. The results of the adsorption experiments are shown in Figure 5.2.4. The modified surfaces were tested in comparison to the untreated triblock terpolymer surfaces.

The highest hemoglobin adsorption found for PS<sub>74</sub>-*b*-P4VP<sub>26</sub><sup>162</sup> membranes can be attributed to chelation of the iron ions from hemoglobin by the free electron pair of the P4VP nitrogen atom [197, 198], whereas a decrease in adsorption value was observed when P4VP pores were covered with a hydrophobic PSMA block. At the given pH value, hemoglobin is not significantly charged (IEP = 6.8) and the membranes are also neutral, which allows the adsorption of hemoglobin to occur because of the hydrophobic/hydrophilic balance of the membranes. PS-*b*-P4VP-*b*-PGMA membranes decorated with hydrophilic PGMA block showed the smallest hemoglobin adsorption among all tested membranes due to strong hydration of the surface, which gives the surface an antifouling property [199]. This significant improvement in the protein adsorption resistance has a profound effect on the long-term filtration of proteins.

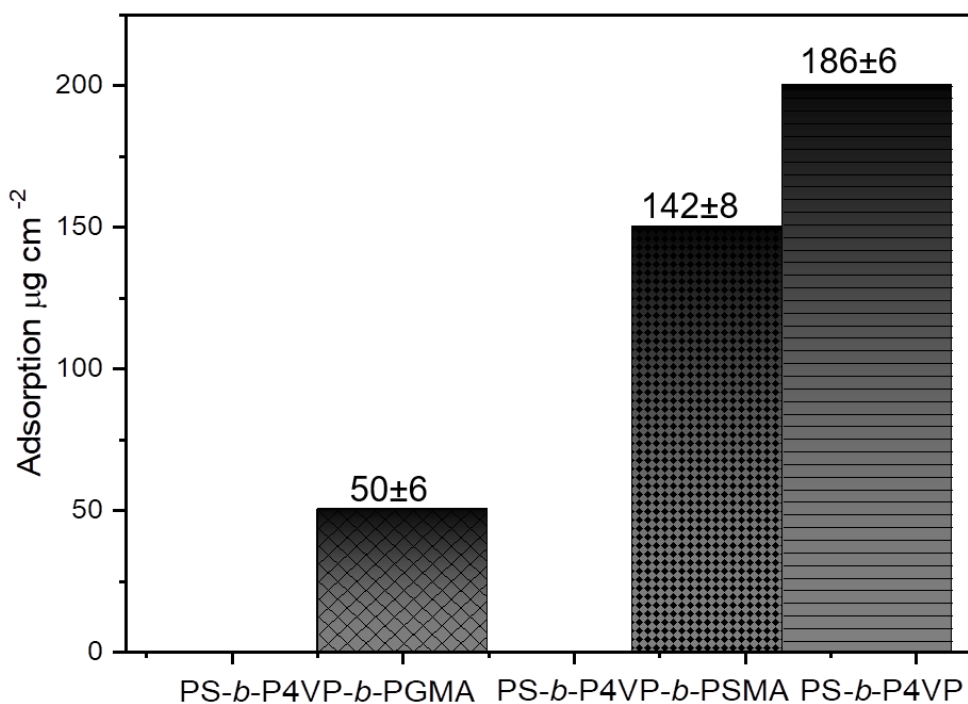


**Figure 5.2.4.** Protein adsorption of hemoglobin of PS<sub>74</sub>-*b*-P4VP<sub>26</sub><sup>162</sup>, PS<sub>71</sub>-*b*-P4VP<sub>26</sub>-*b*-PSMA<sub>3</sub><sup>145</sup> and PS<sub>71</sub>-*b*-P4VP<sub>26</sub>-*b*-PGMA<sub>3</sub><sup>145</sup> membranes at pH 7.4

In this chapter, a series of novel triblock terpolymers of PS-*b*-P4VP-*b*-PSMA with varying compositions were synthesized by living sequential anionic polymerization with low dispersity values ( $\bar{D} = 1.06 - 1.12$ ). It was demonstrated that isoporous integral asymmetric membranes could be prepared successfully via SNIPS, if the hydrophobic PSMA block was not too long with respect to the P4VP block by using the ternary solvent system (THF/DMF/acetone) for this novel PS-*b*-P4VP-*b*-PSMA triblock terpolymer. The conversion of PSMA into PGMA block by acidic hydrolysis did not affect the membrane morphology. The amphiphilic PS-*b*-P4VP-*b*-PGMA triblock terpolymer membranes showed a significant decrease in retention and adsorption of proteins as compared to more hydrophobic PS-*b*-P4VP-*b*-PSMA membranes and PS-*b*-P4VP membranes. The results of contact angle and water flux measurements also confirm the more hydrophilic behavior of PS-*b*-P4VP-*b*-PGMA triblock terpolymer membranes. This

indicates the strong and positive influence of the third hydrophilic block on the membrane properties.

## Chapter 6: Summary and outlook

### 6.1. Summary and outlook

The aim of this work was to develop integral asymmetric membranes via self-assembly and non-solvent induced phase inversion process from novel diblock and triblock copolymers. Diblock copolymers of polystyrene-*block*-poly(solketal methacrylate) (PS-*b*-PSMA) of different composition were successfully synthesized by sequential living anionic polymerization whereas polystyrene-*b*-poly(glyceryl methacrylate) (PS-*b*-PGMA) were obtained by acid hydrolysis of the acetone groups of the poly(solketal methacrylate) (PSMA) blocks into poly(glyceryl methacrylate) (PGMA). By utilizing the binary THF/DMF and ternary THF/DMF/DOX solvent system, integral asymmetric membranes of PS-*b*-PGMA via self-assembly and non-solvent-induced phase separation process could be achieved. Later, a comparative study of amphiphilic PS-*b*-PGMA and hydrophobic PS-*b*-PSMA diblock copolymers for the development of isoporous integral asymmetric membranes was presented. Within this study, no suitable solvents were found to prepare isoporous membranes from the PS-*b*-PSMA diblock copolymer. This will require a more subtle choice of solvents, as the level of selectivity of a solvent and non-solvent is much less pronounced in a block copolymer composed of similar polar (or nonpolar) blocks.

Further, static protein adsorption measurements were performed to analyze the increase in hydrophilic behavior of isoporous membranes of PS-*b*-PGMA and were compared with a PS-*b*-P4VP system of similar molecular weight and block ratio. Different nanofillers were added to the PS-*b*-PGMA diblock copolymer system and the hybrid membranes fabricated via SNIPS.

For the first time, PS-*b*-P4VP-*b*-PSMA triblock terpolymers with varying compositions were successfully synthesized by sequential living anionic polymerization. Composite membranes of PS-*b*-P4VP-*b*-PSMA and PS-*b*-P4VP-*b*-PGMA triblock terpolymers with ordered hexagonally packed cylindrical pores were developed. The morphology of the membranes was studied with

scanning electron microscopy (SEM) and atomic force microscopy (AFM). PS-*b*-P4VP-*b*-PSMA triblock terpolymer membranes were further treated with acid to get polystyrene-*b*-poly(4-vinylpyridine)-*block*-poly(glyceryl methacrylate) (PS-*b*-P4VP-*b*-PGMA). An increase in the hydrophilicity was observed after treatment of isoporous membranes from PS-*b*-P4VP-*b*-PSMA, through acidic hydrolysis of the hydrophobic poly(solketal methacrylate) PSMA block into a hydrophilic poly(glyceryl methacrylate) PGMA block, which contains two neighbored hydroxyl (–OH) groups per repeating unit. Notably, the pristine porous membrane structure could be maintained even after acidic hydrolysis. The membrane properties were analyzed further by contact angle, protein retention, and adsorption measurements. It was found that membranes containing hydroxyl groups (PS-*b*-P4VP-*b*-PGMA) show a stable and higher water permeance than membranes without hydroxyl groups (PS-*b*-P4VP-*b*-PSMA), what is due to the increase in hydrophilicity.

The new functional triblock terpolymer PS-*b*-P4VP-*b*-PGMA showed significantly lower (cut off) retention and fouling compared to the more hydrophobic PS-*b*-P4VP-*b*-PSMA precursor membrane and also compared to a PS-*b*-P4VP membrane, indicating a strong and positive influence of the third hydrophilic block on the membrane properties. Thus, the introduction of a highly functional and hydrophilic block containing repeating units with two hydroxyl groups could be carried out, which allows for a large variety of further post-modification reactions.

## 6.2. Zusammenfassung und Ausblick

Das Ziel dieser Arbeit war die Entwicklung integraler asymmetrischer Membranen durch Self-assembly und nicht lösungsmittelinduzierte Phaseninversion aus neuartigen Diblock und Triblockcopolymeren. Diblockcopolymeren aus Polystyrol-*block*-poly(solketalmethacrylat) (PS-*b*-PSMA) unterschiedlicher Zusammensetzung wurden erfolgreich durch sequentielle lebende anionische Polymerisation synthetisiert, Polystyrol-*b*-poly(glyceryl methacrylat) (PS-*b*-PGMA) wurde durch anschließende Säurehydrolyse der Acetonidgruppen der Polysolketal methacrylat (PSMA)-Blöcke zu (PGMA) erhalten. Unter Verwendung des binären THF/DMF- und ternären THF/DMF/DOX-Lösungsmittelsystems konnten integrale asymmetrische Membranen von PS-*b*-PGMA mittels Self-assembly und Nicht-lösemitte linduzierten Phaseninversionsprozess erfolgreich hergestellt werden. Im Folgenden wurden amphiphiles PS-*b*-PGMA und hydrophobes PS-*b*-PSMA Diblockcopolymeren zur Entwicklung isoporöser integraler asymmetrischer Membranen untersucht und charakterisiert. Innerhalb dieser Studie wurden keine geeigneten Lösungsmittel gefunden, zur Herstellung von isoporösen Membranen aus PS-*b*-PSMA-Diblockcopolymer. Dies erfordert weitere Untersuchungen, da die Wahl eines passenden Lösemittels und eines Nichtlösemittels für ein nicht-amphiphiles Blockcopolymer, das aus ähnlichen polaren (oder unpolaren) Blöcken besteht, wenig untersucht ist und eine Vielzahl an möglichen Kombinationen aus Nicht- und Lösemitteln gibt.

Des Weiteren wurden statische Proteinadsorptionsmessungen durchgeführt, um die Zunahme des hydrophilen Verhaltens von isoporösen Membranen von PS-*b*-PGMA zu analysieren, diese Ergebnisse wurden mit dem PS-*b*-P4VP-System mit ähnlichem Molekulargewicht und Blockverhältnis verglichen. Dem PS-*b*-PGMA-Diblockcopolymerensystem und den über SNIPS hergestellten Hybridmembranen wurden verschiedene Nanofüllstoffe zugesetzt. Erstmals wurden PS-*b*-P4VP-*b*-PSMA-Triblockterpolymere mit unterschiedlichen Zusammensetzungen erfolgreich durch sequentielle lebende anionische Polymerisation synthetisiert.

Verbundmembranen von *PS-b-P4VP-b-PSMA* und *PS-b-P4VP-b-PGMA* Triblockterpolymeren mit geordneten hexagonal gepackten zylindrischen Poren konnten erfolgreich hergestellt werden. Die Morphologie der Membranen wurde per Rasterelektronenmikroskopie (REM) und Rasterkraftmikroskopie (AFM) untersucht. *PS-b-P4VP-b-PSMA* Triblockterpolymer Membranen wurden zusätzlich mit Säure behandelt, um *Polystyrol-b-poly(4-vinylpyridin)-block-Poly(glyceryl methacrylat) (PS-b-P4VP-b-PGMA)* zu erhalten. Eine Zunahme der Hydrophilie wurde nach Behandlung von isoporösen Membranen aus *PS-b-P4VP-b-PSMA* durch saure Hydrolyse des hydrophoben *Poly(solketal methacrylat) PSMA*-Blocks zu einem hydrophilen *Poly(glyceryl methacrylat) PGMA*-Block beobachtet, welches zwei benachbarte Hydroxylgruppen (-OH) pro Wiederholungseinheit enthält. Die Membraneigenschaften wurden durch Kontaktwinkel-, Proteinrückhaltungs- und Adsorptionsmessungen charakterisiert. Bemerkenswert ist, dass die isoporöse Membranstruktur auch nach der sauren Hydrolyse beibehalten werden. Für Membranen mit Hydroxylgruppen (*PS-b-P4VP-b-PGMA*) wurde eine stabilere und höhere Permeanz gemessen im Vergleich zu Membranen ohne Hydroxylgruppen (*PS-b-P4VP-b-PSMA*), Dies kann auf die Zunahme der Hydrophilie zurückgeführt werden.

Das neue funktionelle Triblockterpolymer *PS-b-P4VP-b-PGMA* zeigte im Vergleich zur hydrophoberen *PS-b-P4VP-b-PSMA*-Vorläufermembran eine signifikant bessere Rückhaltung und reduziertes Fouling, und im Vergleich zu einer *PS-b-P4VP*-Membran ebenfalls, was auf den positiven Einfluss des dritten hydrophilen Blocks in die Membran zurückzuführen ist. Die erfolgreiche Integration eines hochfunktionellen und hydrophilen Blocks, mit wiederholenden Einheiten aus zwei Hydroxylgruppen, ermöglicht eine große Vielfalt weiterer Postmodifizierungsreaktionen.

## Chapter 7: References

- [1] M.A. Shannon, P.W. Bohn, M. Elimelech, J.G. Georgiadis, B.J. Mariñas, A.M. Mayes, Science and technology for water purification in the coming decades, *Nature* 452(7185) (2008) 301-310.
- [2] M. Elimelech, The global challenge for adequate and safe water, *Journal of Water Supply: Research and Technology-Aqua* 55(1) (2006) 3-10.
- [3] G.M. Geise, H.-S. Lee, D.J. Miller, B.D. Freeman, J.E. McGrath, D.R. Paul, Water purification by membranes: The role of polymer science, *Journal of Polymer Science Part B: Polymer Physics* 48(15) (2010) 1685-1718.
- [4] M. Elimelech, W.A. Phillip, The Future of Seawater Desalination: Energy, Technology, and the Environment, *Science* 333(6043) (2011) 712-717.
- [5] S.P. Nunes, P.Z. Culfaz-Emecen, G.Z. Ramon, T. Visser, G.H. Koops, W. Jin, M. Ulbricht, Thinking the future of membranes: Perspectives for advanced and new membrane materials and manufacturing processes, *Journal of Membrane Science* 598 (2020) 117761.
- [6] X. Yu, Y. Zhu, C. Cheng, T. Zhang, X. Wang, B.S. Hsiao, Novel thin-film nanofibrous composite membranes containing directional toxin transport nanochannels for efficient and safe hemodialysis application, *Journal of Membrane Science* 582 (2019) 151-163.
- [7] J.R. Werber, C.O. Osuji, M. Elimelech, Materials for next-generation desalination and water purification membranes, *Nature Reviews Materials* 1(5) (2016) 16018.
- [8] H.K. Lonsdale, U. Merten, R.L. Riley, Transport properties of cellulose acetate osmotic membranes, *Journal of Applied Polymer Science* 9(4) (1965) 1341-1362.
- [9] K.T. Sanders, M.E. Webber, Evaluating the energy consumed for water use in the United States, *Environmental Research Letters* 7(3) (2012) 034034.
- [10] U. Merten, Flow Relationships in Reverse Osmosis, *Industrial & Engineering Chemistry Fundamentals* 2(3) (1963) 229-232.
- [11] W.R. Bowen, A.W. Mohammad, Characterization and Prediction of Nanofiltration Membrane Performance—A General Assessment, *Chemical Engineering Research and Design* 76(8) (1998) 885-893.
- [12] W.R. Bowen, A.W. Mohammad, N. Hilal, Characterisation of nanofiltration membranes for predictive purposes — use of salts, uncharged solutes and atomic force microscopy, *Journal of Membrane Science* 126(1) (1997) 91-105.
- [13] R. van Reis, A. Zydney, Bioprocess membrane technology, *Journal of Membrane Science* 297(1) (2007) 16-50.
- [14] Y. Zhang, J.L. Sargent, B.W. Boudouris, W.A. Phillip, Nanoporous membranes generated from self-assembled block polymer precursors: Quo Vadis?, *Journal of Applied Polymer Science* 132(21) (2015).

- [15] C.G. Gamys, J.-M. Schumers, C. Mugemana, C.-A. Fustin, J.-F. Gohy, Pore-Functionalized Nanoporous Materials Derived from Block Copolymers, *Macromolecular Rapid Communications* 34(12) (2013) 962-982.
- [16] M. Tasaka, T. Okano, T. Fujimoto, Mass transport through charge-micromosaic membranes, *Journal of Membrane Science* 19(3) (1984) 273-288.
- [17] Z. Zhang, M.M. Rahman, C. Abetz, A.-L. Höhme, E. Sperling, V. Abetz, Chemically Tailored Multifunctional Asymmetric Isoporous Triblock Terpolymer Membranes for Selective Transport, *Advanced Materials* n/a(n/a) 1907014.
- [18] Z. Zhang, M.M. Rahman, C. Abetz, V. Abetz, High-performance asymmetric isoporous nanocomposite membranes with chemically-tailored amphiphilic nanochannels, *Journal of Materials Chemistry A* 8(19) (2020) 9554-9566.
- [19] Y. Zhang, N.E. Almodovar-Arbelo, J.L. Weidman, D.S. Corti, B.W. Boudouris, W.A. Phillip, Fit-for-purpose block polymer membranes molecularly engineered for water treatment, *npj Clean Water* 1(1) (2018) 2.
- [20] E.A. Jackson, M.A. Hillmyer, Nanoporous Membranes Derived from Block Copolymers: From Drug Delivery to Water Filtration, *ACS Nano* 4(7) (2010) 3548-3553.
- [21] J. Hahn, J.I. Clodt, V. Filiz, V. Abetz, Protein separation performance of self-assembled block copolymer membranes, *RSC Advances* 4(20) (2014) 10252-10260.
- [22] B. Sutisna, G. Polymeropoulos, E. Mygiakis, V. Musteata, K.V. Peinemann, D.M. Smilgies, N. Hadjichristidis, S.P. Nunes, Artificial membranes with selective nanochannels for protein transport, *Polymer Chemistry* 7(40) (2016) 6189-6201.
- [23] M. Barboiu, A. Gilles, From Natural to Bioassisted and Biomimetic Artificial Water Channel Systems, *Accounts of Chemical Research* 46(12) (2013) 2814-2823.
- [24] D.J. Miller, D.R. Dreyer, C.W. Bielawski, D.R. Paul, B.D. Freeman, Surface Modification of Water Purification Membranes, *Angewandte Chemie International Edition* 56(17) (2017) 4662-4711.
- [25] W. Fu, T. Pei, Y. Mao, G. Li, Y. Zhao, L. Chen, Highly hydrophilic poly(vinylidene fluoride) ultrafiltration membranes modified by poly(N-acryloyl glycine) hydrogel based on multi-hydrogen bond self-assembly for reducing protein fouling, *Journal of Membrane Science* 572 (2019) 453-463.
- [26] S. Rajesh, A. Jayalakshmi, S. Senthikumar, H.S.H. Sankar, D.R. Mohan, Performance Evaluation of Poly(amide-imide) Incorporated Cellulose Acetate Ultrafiltration Membranes in the Separation of Proteins and Its Fouling Propensity by AFM Imaging, *Industrial & Engineering Chemistry Research* 50(24) (2011) 14016-14029.
- [27] E. Ostuni, R.G. Chapman, R.E. Holmlin, S. Takayama, G.M. Whitesides, A Survey of Structure–Property Relationships of Surfaces that Resist the Adsorption of Protein, *Langmuir* 17(18) (2001) 5605-5620.

- [28] S. Kang, A. Asatekin, A.M. Mayes, M. Elimelech, Protein antifouling mechanisms of PAN UF membranes incorporating PAN-g-PEO additive, *Journal of Membrane Science* 296(1) (2007) 42-50.
- [29] S. Saleem, S. Rangou, C. Abetz, V. Filiz, V. Abetz, Isoporous Membranes from Novel Polystyrene-b-poly(4-vinylpyridine)-b-poly(solketal methacrylate) (PS-b-P4VP-b-PSMA) Triblock Terpolymers and Their Post-Modification, *Polymers* 12(1) (2019).
- [30] A. Lee, J.W. Elam, S.B. Darling, Membrane materials for water purification: design, development, and application, *Environmental Science: Water Research & Technology* 2(1) (2016) 17-42.
- [31] M. Ulbricht, Advanced functional polymer membranes, *Polymer* 47(7) (2006) 2217-2262.
- [32] G. Tealdo, G. Castello, G. D'Amato, S. Munari, Water—glycerol permeation through styrene-grafted and sulphonated PTFE membranes, *Journal of Membrane Science* 11(1) (1982) 3-9.
- [33] H. Yamagishi, J.V. Crivello, G. Belfort, Development of a novel photochemical technique for modifying poly (arylsulfone) ultrafiltration membranes, *Journal of Membrane Science* 105(3) (1995) 237-247.
- [34] A.V.R. Reddy, D.J. Mohan, A. Bhattacharya, V.J. Shah, P.K. Ghosh, Surface modification of ultrafiltration membranes by preadsorption of a negatively charged polymer: I. Permeation of water soluble polymers and inorganic salt solutions and fouling resistance properties, *Journal of Membrane Science* 214(2) (2003) 211-221.
- [35] T.-H. Bae, T.-M. Tak, Preparation of TiO<sub>2</sub> self-assembled polymeric nanocomposite membranes and examination of their fouling mitigation effects in a membrane bioreactor system, *Journal of Membrane Science* 266(1) (2005) 1-5.
- [36] B.C. Johnson, İ. Yilgör, C. Tran, M. Iqbal, J.P. Wightman, D.R. Lloyd, J.E. McGrath, Synthesis and characterization of sulfonated poly(acrylene ether sulfones), *Journal of Polymer Science: Polymer Chemistry Edition* 22(3) (1984) 721-737.
- [37] T. Matsuda, S. Ito, Surface coating of hydrophilic-hydrophobic block co-polymers on a poly(acrylonitrile) haemodialyser reduces platelet adhesion and its transmembrane stimulation, *Biomaterials* 15(6) (1994) 417-422.
- [38] D. Rana, T. Matsuura, R.M. Narbaitz, Novel hydrophilic surface modifying macromolecules for polymeric membranes: Polyurethane ends capped by hydroxy group, *Journal of Membrane Science* 282(1) (2006) 205-216.
- [39] M. Radjabian, V. Abetz, Tailored Pore Sizes in Integral Asymmetric Membranes Formed by Blends of Block Copolymers, *Advanced Materials* 27(2) (2015) 352-355.
- [40] X. Ma, Y. Su, Q. Sun, Y. Wang, Z. Jiang, Preparation of protein-adsorption-resistant polyethersulfone ultrafiltration membranes through surface segregation of amphiphilic comb copolymer, *Journal of Membrane Science* 292(1) (2007) 116-124.

- [41] L.F. Hancock, S.M. Fagan, M.S. Ziolo, Hydrophilic, semipermeable membranes fabricated with poly(ethylene oxide)–polysulfone block copolymer, *Biomaterials* 21(7) (2000) 725-733.
- [42] J. Hahn, V. Filiz, S. Rangou, J. Clodt, A. Jung, K. Buhr, C. Abetz, V. Abetz, Structure formation of integral-asymmetric membranes of polystyrene-block-Poly(ethylene oxide), *Journal of Polymer Science Part B: Polymer Physics* 51(4) (2013) 281-290.
- [43] C. Burguière, C. Chassenieux, B. Charleux, Characterization of aqueous micellar solutions of amphiphilic block copolymers of poly(acrylic acid) and polystyrene prepared via ATRP. Toward the control of the number of particles in emulsion polymerization, *Polymer* 44(3) (2003) 509-518.
- [44] S. Schöttner, H.-J. Schaffrath, M. Gallei, Poly(2-hydroxyethyl methacrylate)-Based Amphiphilic Block Copolymers for High Water Flux Membranes and Ceramic Templates, *Macromolecules* 49(19) (2016) 7286-7295.
- [45] A. Jung, V. Filiz, S. Rangou, K. Buhr, P. Merten, J. Hahn, J. Clodt, C. Abetz, V. Abetz, Formation of Integral Asymmetric Membranes of AB Diblock and ABC Triblock Copolymers by Phase Inversion, *Macromolecular Rapid Communications* 34(7) (2013) 610-615.
- [46] H. Mori, A. Hirao, S. Nakahama, K. Senshu, Synthesis and Surface Characterization of Hydrophilic-Hydrophobic Block Copolymers Containing Poly(2,3-dihydroxypropyl methacrylate), *Macromolecules* 27(15) (1994) 4093-4100.
- [47] H. Zhang, E. Ruckenstein, A Novel Successive Route to Well-Defined Water-Soluble Poly(2,3-dihydroxypropyl methacrylate) and Amphiphilic Block Copolymers Based on an Osmylation Reaction, *Macromolecules* 33(13) (2000) 4738-4744.
- [48] M.F. Refojo, Glyceryl methacrylate hydrogels, *Journal of Applied Polymer Science* 9(9) (1965) 3161-3170.
- [49] J. Hahn, J.I. Clodt, C. Abetz, V. Filiz, V. Abetz, Thin Isoporous Block Copolymer Membranes: It Is All about the Process, *ACS Applied Materials & Interfaces* 7(38) (2015) 21130-21137.
- [50] K. Hong, D. Uhrig, J.W. Mays, Living anionic polymerization, *Current Opinion in Solid State and Materials Science* 4(6) (1999) 531-538.
- [51] N. Hadjichristidis, H. Iatrou, S. Pispas, M. Pitsikalis, Anionic polymerization: High vacuum techniques, *Journal of Polymer Science Part A: Polymer Chemistry* 38(18) (2000) 3211-3234.
- [52] M. Szwarc, M. Levy, R. Milkovich, POLYMERIZATION INITIATED BY ELECTRON TRANSFER TO MONOMER. A NEW METHOD OF FORMATION OF BLOCK POLYMERS<sup>1</sup>, *Journal of the American Chemical Society* 78(11) (1956) 2656-2657.
- [53] T.R. Darling, T.P. Davis, M. Fryd, A.A. Gridnev, D.M. Haddleton, S.D. Ittel, R.R. Matheson Jr., G. Moad, E. Rizzardo, Living polymerization: Rationale for uniform terminology, *Journal of Polymer Science Part A: Polymer Chemistry* 38(10) (2000) 1706-1708.
- [54] R.P.Q. H.L. Hsieh, *Anionic Polymerization: Principles and Practical Applications*, New York, 1996.

- [55] O.W. Webster, *Living Polymerization Methods*, Science 251(4996) (1991) 887.
- [56] K.V. Peinemann, Nunes. S.P, *Membrane Technology in the Chemical Industry*, WILEY-VCH verlag GmbH & Co. KGaA, Weinheim, Germany, 2006.
- [57] R.P. Quirk, B. Lee, Adducts of Polymeric Organolithiums with 1,1-Diphenylethylene. Rates of Formation and Crossover to Styrene and Diene Monomers, *Macromolecular Chemistry and Physics* 204(14) (2003) 1719-1737.
- [58] D.M. Wiles, S. Bywater, Polymerization of methyl methacrylate initiated by 1,1-diphenylhexyl lithium, *Transactions of the Faraday Society* 61(0) (1965) 150-158.
- [59] T. Fox, B. Garrett, W. Goode, S. Gratch, J. Kincaid, A. Spell and. J. D. Stroupe, *J. Am. Chem. Soc* 80 (1958) 1768.
- [60] S. Antoun, P. Teyssié, R. Jérôme, Lithium Diisopropylamide as Initiator for the Anionic Polymerization of Methacrylates, *Macromolecules* 30(6) (1997) 1556-1561.
- [61] K.M. A.H.E. Müller, "Structure of Carbanion", in *Controlled and Living Polymerizations*, Wiley-VCH, 2009.
- [62] R.M. Fuoss, Ionic Association. III. The Equilibrium between Ion Pairs and Free Ions, *Journal of the American Chemical Society* 80(19) (1958) 5059-5061.
- [63] S. Winstein, E. Clippinger, A.H. Fainberg, G.C. Robinson, SALT EFFECTS AND ION-PAIRS IN SOLVOLYSIS1, *Journal of the American Chemical Society* 76(9) (1954) 2597-2598.
- [64] C.A. Finch, *Encyclopedia of polymer science and engineering*, 2nd edition volume 2, anionic polymerisation to cationic polymerisation editor-in-chief Jacqueline I. Kroschwitz, Editors H. F. Mark, N. M. Bikales, C. G. Overberger and G. Menges, Wiley-Interscience, New York, 1985. , *British Polymer Journal* 17(4) (1985) 377-377.
- [65] P.J. Flory, *Principles of Polymer Chemistry*, Cornell University Press, Ithaca, London, 1953.
- [66] S. Nakahama, A. Hirao, Protection and polymerization of functional monomers: Anionic living polymerization of protected monomers, *Progress in Polymer Science* 15(2) (1990) 299-335.
- [67] A. Hirao, S. Nakahama, Anionic living polymerization of monomers with functional silyl groups, *Progress in Polymer Science* 17(3) (1992) 283-317.
- [68] A. Hirao, S. Loykulant, T. Ishizone, Recent advance in living anionic polymerization of functionalized styrene derivatives, *Progress in Polymer Science* 27 (2002) 1399-1471.
- [69] A. Matsuo, T. Watanabe, A. Hirao, Synthesis of Well-Defined Dendrimer-like Branched Polymers and Block Copolymer by the Iterative Approach Involving Coupling Reaction of Living Anionic Polymer and Functionalization, *Macromolecules* 37(17) (2004) 6283-6290.
- [70] R. Advincula, Q. Zhou, M. Park, S. Wang, J. Mays, G. Sakellariou, S. Pispas, N. Hadjichristidis, Polymer Brushes by Living Anionic Surface Initiated Polymerization on Flat Silicon (SiOx) and Gold Surfaces: Homopolymers and Block Copolymers, *Langmuir* 18(22) (2002) 8672-8684.

- [71] Q. Zhou, X. Fan, C. Xia, J. Mays, R. Advincula, Living Anionic Surface Initiated Polymerization (SIP) of Styrene from Clay Surfaces, *Chemistry of Materials* 13(8) (2001) 2465-2467.
- [72] Z. Wojnarowska, H. Feng, Y. Fu, S. Cheng, B. Carroll, R. Kumar, V.N. Novikov, A.M. Kisiuk, T. Saito, N.-G. Kang, J.W. Mays, A.P. Sokolov, V. Bocharova, Effect of Chain Rigidity on the Decoupling of Ion Motion from Segmental Relaxation in Polymerized Ionic Liquids: Ambient and Elevated Pressure Studies, *Macromolecules* 50(17) (2017) 6710-6721.
- [73] W.-B. Zhang, B. Sun, H. Li, X. Ren, J. Janoski, S. Sahoo, D.E. Dabney, C. Wesdemiotis, R.P. Quirk, S.Z.D. Cheng, Synthesis of In-Chain-Functionalized Polystyrene-block-poly(dimethylsiloxane) Diblock Copolymers by Anionic Polymerization and Hydrosilylation Using Dimethyl-[4-(1-phenylvinyl)phenyl]silane, *Macromolecules* 42(19) (2009) 7258-7262.
- [74] J. Kim, S. Kwak, K.U. Kim, K.H. Kim, J.C. Cho, W.H. Jo, D. Lim, D. Kim, Synthesis of a diphenylethylene derivative carrying aromatic tertiary amine groups and its use in chain end functionalization of alkyllithium-initiated polymerizations, *Macromolecular Chemistry and Physics* 199(10) (1998) 2185-2191.
- [75] A. Hanisch, H. Schmalz, A.H.E. Müller, A Modular Route for the Synthesis of ABC Miktoarm Star Terpolymers via a New Alkyne-Substituted Diphenylethylene Derivative, *Macromolecules* 45(20) (2012) 8300-8309.
- [76] E. Giebler, R. Stadler, ABC triblock polyampholytes containing a neutral hydrophobic block, a polyacid and a polybase, *Macromolecular Chemistry and Physics* 198(12) (1997) 3815-3825.
- [77] M. Szwarc, 'Living' Polymers, *Nature* 178(4543) (1956) 1168-1169.
- [78] H.-C. Kim, S.-M. Park, W.D. Hinsberg, Block Copolymer Based Nanostructures: Materials, Processes, and Applications to Electronics, *Chemical Reviews* 110(1) (2010) 146-177.
- [79] J.K. Kim, S.Y. Yang, Y. Lee, Y. Kim, Functional nanomaterials based on block copolymer self-assembly, *Progress in Polymer Science* 35(11) (2010) 1325-1349.
- [80] A. Kishimura, A. Koide, K. Osada, Y. Yamasaki, K. Kataoka, Encapsulation of Myoglobin in PEGylated Polyion Complex Vesicles Made from a Pair of Oppositely Charged Block Ionomers: A Physiologically Available Oxygen Carrier, *Angewandte Chemie International Edition* 46(32) (2007) 6085-6088.
- [81] M.T. Zarka, O. Nuyken, R. Weberskirch, Amphiphilic Polymer Supports for the Asymmetric Hydrogenation of Amino Acid Precursors in Water, *Chemistry – A European Journal* 9(14) (2003) 3228-3234.
- [82] M.A.C. Stuart, W.T.S. Huck, J. Genzer, M. Müller, C. Ober, M. Stamm, G.B. Sukhorukov, I. Szleifer, V.V. Tsukruk, M. Urban, F. Winnik, S. Zauscher, I. Luzinov, S. Minko, Emerging applications of stimuli-responsive polymer materials, *Nature Materials* 9 (2010) 101.
- [83] F.H. Schacher, P.A. Rugar, I. Manners, Functional Block Copolymers: Nanostructured Materials with Emerging Applications, *Angewandte Chemie International Edition* 51(32) (2012) 7898-7921.

- [84] X. Qiang, R. Chakroun, N. Janoszka, A.H. Gröschel, Self-Assembly of Multiblock Copolymers, *Israel Journal of Chemistry* 59(10) (2019) 945-958.
- [85] F.S. Bates, Polymer-Polymer Phase Behavior, *Science* 251(4996) (1991) 898.
- [86] F.S. Bates, G.H. Fredrickson, Block copolymers--designer soft materials, *Physics Today* 52 (1999) 32-38.
- [87] L. Leibler, Theory of Microphase Separation in Block Copolymers, *Macromolecules* 13(6) (1980) 1602-1617.
- [88] G.H. Fredrickson, E. Helfand, Fluctuation effects in the theory of microphase separation in block copolymers, *The Journal of Chemical Physics* 87(1) (1987) 697-705.
- [89] F.S. Bates, J.H. Rosedale, G.H. Fredrickson, C.J. Glinka, Fluctuation-induced first-order transition of an isotropic system to a periodic state, *Physical Review Letters* 61(19) (1988) 2229-2232.
- [90] D.J. Meier, Theory of block copolymers. I. Domain formation in A-B block copolymers, *Journal of Polymer Science Part C: Polymer Symposia* 26(1) (1969) 81-98.
- [91] T.S. Bailey, H.D. Pham, F.S. Bates, Morphological Behavior Bridging the Symmetric AB and ABC States in the Poly(styrene-*b*-isoprene-*b*-ethylene oxide) Triblock Copolymer System, *Macromolecules* 34(20) (2001) 6994-7008.
- [92] T.S. Bailey, C.M. Hardy, T.H. Epps, F.S. Bates, A Noncubic Triply Periodic Network Morphology in Poly(isoprene-*b*-styrene-*b*-ethylene oxide) Triblock Copolymers, *Macromolecules* 35(18) (2002) 7007-7017.
- [93] A. Wolf, A. Walther, A.H.E. Müller, Janus Triad: Three Types of Nonspherical, Nanoscale Janus Particles from One Single Triblock Terpolymer, *Macromolecules* 44(23) (2011) 9221-9229.
- [94] U. Breiner, U. Krappe, R. Stadler, Evolution of the "knitting pattern" morphology in ABC triblock copolymers, *Macromolecular Rapid Communications* 17(8) (1996) 567-575.
- [95] U. Breiner, U. Krappe, E.L. Thomas, R. Stadler, Structural Characterization of the "Knitting Pattern" in Polystyrene-block-poly(ethylene-co-butylene)-block-poly(methyl methacrylate) Triblock Copolymers, *Macromolecules* 31(1) (1998) 135-141.
- [96] U. Krappe, R. Stadler, I. Voigt-Martin, Chiral Assembly in Amorphous ABC Triblock Copolymers. Formation of a Helical Morphology in Polystyrene-block-polybutadiene-block-poly(methyl methacrylate) Block Copolymers, *Macromolecules* 28(13) (1995) 4558-4561.
- [97] U. Breiner, U. Krappe, V. Abetz, R. Stadler, Cylindrical morphologies in asymmetric ABC triblock copolymers, *Macromolecular Chemistry and Physics* 198(4) (1997) 1051-1083.
- [98] S. Brinkmann, R. Stadler, E.L. Thomas, New Structural Motif in Hexagonally Ordered Cylindrical Ternary (ABC) Block Copolymer Microdomains, *Macromolecules* 31(19) (1998) 6566-6572.
- [99] C.-A. Fustin, V. Abetz, J.-F. Gohy, Triblock terpolymer micelles: A personal outlook, *The European Physical Journal E* 16(3) (2005) 291-302.

- [100] C. Auschra, R. Stadler, New ordered morphologies in ABC triblock copolymers, *Macromolecules* 26(9) (1993) 2171-2174.
- [101] R. Stadler, C. Auschra, J. Beckmann, U. Krappe, I. Voight-Martin, L. Leibler, Morphology and Thermodynamics of Symmetric Poly(A-block-B-block-C) Triblock Copolymers, *Macromolecules* 28(9) (1995) 3080-3097.
- [102] V. Abetz, T. Goldacker, Formation of superlattices via blending of block copolymers, *Macromolecular Rapid Communications* 21(1) (2000) 16-34.
- [103] D.E. Discher, A. Eisenberg, Polymer Vesicles, *Science* 297(5583) (2002) 967.
- [104] P. Lim Soo, A. Eisenberg, Preparation of block copolymer vesicles in solution, *Journal of Polymer Science Part B: Polymer Physics* 42(6) (2004) 923-938.
- [105] J.N. Israelachvili, *Intermolecular and surface forces*, third ed., London, 1992.
- [106] I.L. Atanase, G. Riess, Self-Assembly of Block and Graft Copolymers in Organic Solvents: An Overview of Recent Advances, *Polymers* 10(1) (2018).
- [107] Y. Mai, A. Eisenberg, Self-assembly of block copolymers, *Chemical Society Reviews* 41(18) (2012) 5969-5985.
- [108] R.C. Hayward, D.J. Pochan, Tailored Assemblies of Block Copolymers in Solution: It Is All about the Process, *Macromolecules* 43(8) (2010) 3577-3584.
- [109] A.H. Gröschel, A.H.E. Müller, Self-assembly concepts for multicompartment nanostructures, *Nanoscale* 7(28) (2015) 11841-11876.
- [110] A. Blanazs, S.P. Armes, A.J. Ryan, Self-Assembled Block Copolymer Aggregates: From Micelles to Vesicles and their Biological Applications, *Macromolecular Rapid Communications* 30(4-5) (2009) 267-277.
- [111] A. Blanazs, J. Madsen, G. Battaglia, A.J. Ryan, S.P. Armes, Mechanistic Insights for Block Copolymer Morphologies: How Do Worms Form Vesicles?, *Journal of the American Chemical Society* 133(41) (2011) 16581-16587.
- [112] R.W. Baker, *Overview of Membrane Science and Technology in, Membrane Technology and Applications*, 2nd ed., John Wiley & Sons, Ltd England 2004.
- [113] M. Mulder, *Basic Principles of Membrane Technology*, Springer Netherlands, Dordrecht, 1996.
- [114] P.M. Bungay, Lonsdale, H.K., De Pinho, M.N, *synthetic membranes: Science, Engineering and Applications*, D.reidel publishing Company, Dordrecht/Boston/Lancaster/Tokyo, 1983.
- [115] R.W. Baker, *Membranes and Modules in, Membrane Technology and Application*, 2nd ed., John Wiley & Sons, Ltd England 2004.
- [116] R.W. Baker, *Membrane Transport Theory in, Membrane Technology and Applications*, 2nd edition ed., John Wiley & Sons Ltd England 2004.

- [117] H.J. Kim, M.-Y. Lim, K.H. Jung, D.-G. Kim, J.-C. Lee, High-performance reverse osmosis nanocomposite membranes containing the mixture of carbon nanotubes and graphene oxides, *Journal of Materials Chemistry A* 3(13) (2015) 6798-6809.
- [118] D.-M. Wang, J.-Y. Lai, Recent advances in preparation and morphology control of polymeric membranes formed by nonsolvent induced phase separation, *Current Opinion in Chemical Engineering* 2(2) (2013) 229-237.
- [119] Q. Fu, A. Halim, J. Kim, J.M.P. Scofield, P.A. Gurr, S.E. Kentish, G.G. Qiao, Highly permeable membrane materials for CO<sub>2</sub> capture, *Journal of Materials Chemistry A* 1(44) (2013) 13769-13778.
- [120] S.Y. Yang, I. Ryu, H.Y. Kim, J.K. Kim, S.K. Jang, T.P. Russell, Nanoporous Membranes with Ultrahigh Selectivity and Flux for the Filtration of Viruses, *Advanced Materials* 18(6) (2006) 709-712.
- [121] K.-V. Peinemann, V. Abetz, P.F.W. Simon, Asymmetric superstructure formed in a block copolymer via phase separation, *Nature Materials* 6(12) (2007) 992-996.
- [122] V. Abetz, Isoporous Block Copolymer Membranes, *Macromolecular Rapid Communications* 36(1) (2015) 10-22.
- [123] S. Rangou, K. Buhr, V. Filiz, J.I. Clodt, B. Lademann, J. Hahn, A. Jung, V. Abetz, Self-organized isoporous membranes with tailored pore sizes, *Journal of Membrane Science* 451 (2014) 266-275.
- [124] L. Oss-Ronen, J. Schmidt, V. Abetz, A. Radulescu, Y. Cohen, Y. Talmon, Characterization of Block Copolymer Self-Assembly: From Solution to Nanoporous Membranes, *Macromolecules* 45(24) (2012) 9631-9642.
- [125] S.P. Nunes, R. Sougrat, B. Hooghan, D.H. Anjum, A.R. Behzad, L. Zhao, N. Pradeep, I. Pinnau, U. Vainio, K.-V. Peinemann, Ultraporous Films with Uniform Nanochannels by Block Copolymer Micelles Assembly, *Macromolecules* 43(19) (2010) 8079-8085.
- [126] J.I. Clodt, B. Bajer, K. Buhr, J. Hahn, V. Filiz, V. Abetz, Performance study of isoporous membranes with tailored pore sizes, *Journal of Membrane Science* 495 (2015) 334-340.
- [127] D.S. Marques, U. Vainio, N.M. Chaparro, V.M. Calo, A.R. Bezahd, J.W. Pitera, K.-V. Peinemann, S.P. Nunes, Self-assembly in casting solutions of block copolymer membranes, *Soft Matter* 9(23) (2013) 5557-5564.
- [128] S.P. Nunes, A.R. Behzad, B. Hooghan, R. Sougrat, M. Karunakaran, N. Pradeep, U. Vainio, K.-V. Peinemann, Switchable pH-Responsive Polymeric Membranes Prepared via Block Copolymer Micelle Assembly, *ACS Nano* 5(5) (2011) 3516-3522.
- [129] J.I. Clodt, V. Filiz, S. Rangou, K. Buhr, C. Abetz, D. Höche, J. Hahn, A. Jung, V. Abetz, Double Stimuli-Responsive Isoporous Membranes via Post-Modification of pH-Sensitive Self-Assembled Diblock Copolymer Membranes, *Advanced Functional Materials* 23(6) (2013) 731-738.

- [130] W.A. Phillip, R.M. Dorin, J. Werner, E.M.V. Hoek, U. Wiesner, M. Elimelech, Tuning Structure and Properties of Graded Triblock Terpolymer-Based Mesoporous and Hybrid Films, *Nano Letters* 11(7) (2011) 2892-2900.
- [131] A. Jung, S. Rangou, C. Abetz, V. Filiz, V. Abetz, Structure Formation of Integral Asymmetric Composite Membranes of Polystyrene-block-Poly(2-vinylpyridine) on a Nonwoven, *Macromolecular Materials and Engineering* 297(8) (2012) 790-798.
- [132] Y.M. Li, D. Srinivasan, P. Vaidya, Y. Gu, U. Wiesner, Asymmetric Membranes from Two Chemically Distinct Triblock Terpolymers Blended during Standard Membrane Fabrication, *Macromolecular Rapid Communications* 37(20) (2016) 1689-1693.
- [133] W.A. Phillip, M.A. Hillmyer, E.L. Cussler, Cylinder Orientation Mechanism in Block Copolymer Thin Films Upon Solvent Evaporation, *Macromolecules* 43(18) (2010) 7763-7770.
- [134] J. Hahn, V. Filiz, S. Rangou, B. Lademann, K. Buhr, J.I. Clodt, A. Jung, C. Abetz, V. Abetz, PtBS-b-P4VP and PTMSS-b-P4VP Isoporous Integral-Asymmetric Membranes with High Thermal and Chemical Stability, *Macromolecular Materials and Engineering* 298(12) (2013) 1315-1321.
- [135] R.M. Dorin, D.S. Marques, H. Sai, U. Vainio, W.A. Phillip, K.-V. Peinemann, S.P. Nunes, U. Wiesner, Solution Small-Angle X-ray Scattering as a Screening and Predictive Tool in the Fabrication of Asymmetric Block Copolymer Membranes, *ACS Macro Letters* 1(5) (2012) 614-617.
- [136] R.M. Dorin, W.A. Phillip, H. Sai, J. Werner, M. Elimelech, U. Wiesner, Designing block copolymer architectures for targeted membrane performance, *Polymer* 55(1) (2014) 347-353.
- [137] R.M. Dorin, H. Sai, U. Wiesner, Hierarchically Porous Materials from Block Copolymers, *Chemistry of Materials* 26(1) (2014) 339-347.
- [138] P. Madhavan, K.-V. Peinemann, S.P. Nunes, Complexation-Tailored Morphology of Asymmetric Block Copolymer Membranes, *ACS Applied Materials & Interfaces* 5(15) (2013) 7152-7159.
- [139] J.I. Clodt, S. Rangou, A. Schröder, K. Buhr, J. Hahn, A. Jung, V. Filiz, V. Abetz, Carbohydrates as Additives for the Formation of Isoporous PS-b-P4VP Diblock Copolymer Membranes, *Macromolecular Rapid Communications* 34(2) (2013) 190-194.
- [140] R. Shevate, M. Kumar, H. Cheng, P.-Y. Hong, A.R. Behzad, D. Anjum, K.-V. Peinemann, Rapid Size-Based Protein Discrimination inside Hybrid Isoporous Membranes, *ACS Applied Materials & Interfaces* 11(8) (2019) 8507-8516.
- [141] H. Lee, S.M. Dellatore, W.M. Miller, P.B. Messersmith, Mussel-Inspired Surface Chemistry for Multifunctional Coatings, *Science* 318(5849) (2007) 426.
- [142] Cutler, P., *Size-Exclusion Chromatography in, Protein Purification Protocol*, 2nd ed., Humana press 2004.
- [143] K. Nagy, K. VÉKey, Chapter 5 - Separation methods, in: K. VÉkey, A. Telekes, A. Vertes (Eds.), *Medical Applications of Mass Spectrometry*, Elsevier, Amsterdam, 2008, pp. 61-92.

- [144] S. Mori, Barth, G.H, Size Exclusion Chromatography, Springer-Verlag Berlin Heidelberg New York 1999.
- [145] <<https://chembam.com/definitions/size-exclusion-chromatography/>>, (accessed 15 May, 2020.).
- [146] C.R. Brundle, Evans, C. A. J., Wilson, S, Encyclopedia of Materials Characterization- Surfaces, Interfaces, Thin Film, Elsevier, 2003.
- [147] C. Ni, Scanning Electron Microscopy (SEM), in: Q.J. Wang, Y.-W. Chung (Eds.), Encyclopedia of Tribology, Springer US, Boston, MA, 2013, pp. 2977-2982.
- [148] <[https://en.wikipedia.org/wiki/Scanning\\_electron\\_microscope](https://en.wikipedia.org/wiki/Scanning_electron_microscope)>, (accessed 6 May, 2020.).
- [149] <<https://www.gla.ac.uk/schools/ges/research/researchfacilities/isaac/services/scanningelectronmicroscopy/>>).
- [150] <<http://www.nanoscience.gatech.edu/zlwang/research/tem.html>>, (accessed 12.06.2020.).
- [151] C.Y. Tang, Z. Yang, Chapter 8 - Transmission Electron Microscopy (TEM), in: N. Hilal, A.F. Ismail, T. Matsuura, D. Oatley-Radcliffe (Eds.), Membrane Characterization, Elsevier 2017, pp. 145-159.
- [152] Contact Angle. <<https://www.kruss-scientific.com/services/education-theory/glossary/contact-angle/>>, (accessed 27 April, 2020.).
- [153] S. Förster, M. Zisenis, E. Wenz, M. Antonietti, Micellization of strongly segregated block copolymers, *The Journal of Chemical Physics* 104(24) (1996) 9956-9970.
- [154] M. Antonietti, S. Heinz, M. Schmidt, C. Rosenauer, Determination of the Micelle Architecture of Polystyrene/Poly(4-vinylpyridine) Block Copolymers in Dilute Solution, *Macromolecules* 27(12) (1994) 3276-3281.
- [155] D.W.N. Van Krevelen, K. T., Cohesive Properties and Solubility. In *properties of Polymers*, 4th ed., Elsevier, Amsterdam, The Netherlands, 2009.
- [156] R.F. Blanks, J.M. Prausnitz, Thermodynamics of Polymer Solubility in Polar and Nonpolar Systems, *Industrial & Engineering Chemistry Fundamentals* 3(1) (1964) 1-8.
- [157] E.H.I. J. Brandrup, E. A. Grulke, A. Abe, D. R. Bloch, In *Polymer Handbook*, Wiley, New York, 1999.
- [158] S.H. Kim, M.J. Misner, T.P. Russell, Solvent-Induced Ordering in Thin Film Diblock Copolymer/Homopolymer Mixtures, *Advanced Materials* 16(23-24) (2004) 2119-2123.
- [159] Y. Xuan, J. Peng, L. Cui, H. Wang, B. Li, Y. Han, Morphology Development of Ultrathin Symmetric Diblock Copolymer Film via Solvent Vapor Treatment, *Macromolecules* 37(19) (2004) 7301-7307.
- [160] Q. Zhang, Y.M. Li, Y. Gu, R.M. Dorin, U. Wiesner, Tuning substructure and properties of supported asymmetric triblock terpolymer membranes, *Polymer* 107 (2016) 398-405.

- [161] F.K. Wolf, A.M. Hofmann, H. Frey, Poly(isoglycerol methacrylate)-b-poly(D or L-lactide) Copolymers: A Novel Hydrophilic Methacrylate as Building Block for Supramolecular Aggregates, *Macromolecules* 43(7) (2010) 3314-3324.
- [162] T. Ishizone, A. Mochizuki, A. Hirao, S. Nakahama, Protection and Polymerization of Functional Monomers. 24. Anionic Living Polymerizations of 5-Vinyl- and 4-Vinyl-1,3-benzodioxoles, *Macromolecules* 28(11) (1995) 3787-3793.
- [163] A. Hirao, H. Kato, K. Yamaguchi, S. Nakahama, Polymerization of monomers containing functional groups protected by trialkylsilyl groups. 5. Synthesis of poly(2-hydroxyethyl methacrylate) with a narrow molecular weight distribution by means of anionic living polymerization, *Macromolecules* 19(5) (1986) 1294-1299.
- [164] M. Gallei, S. Rangou, V. Filiz, K. Buhr, S. Bolmer, C. Abetz, V. Abetz, The Influence of Magnesium Acetate on the Structure Formation of Polystyrene-block-poly(4-vinylpyridine)-Based Integral-Asymmetric Membranes, *Macromolecular Chemistry and Physics* 214(9) (2013) 1037-1046.
- [165] G. Goncalves, P.A.A.P. Marques, A. Barros-Timmons, I. Bdkin, M.K. Singh, N. Emami, J. Grácio, Graphene oxide modified with PMMA via ATRP as a reinforcement filler, *Journal of Materials Chemistry* 20(44) (2010) 9927-9934.
- [166] M. El Achaby, F.Z. Arrakhiz, S. Vaudreuil, E.M. Essassi, A. Qaiss, Piezoelectric  $\beta$ -polymorph formation and properties enhancement in graphene oxide – PVDF nanocomposite films, *Applied Surface Science* 258(19) (2012) 7668-7677.
- [167] H. Zarrin, D. Higgins, Y. Jun, Z. Chen, M. Fowler, Functionalized Graphene Oxide Nanocomposite Membrane for Low Humidity and High Temperature Proton Exchange Membrane Fuel Cells, *The Journal of Physical Chemistry C* 115(42) (2011) 20774-20781.
- [168] C. Zhao, X. Xu, J. Chen, F. Yang, Effect of graphene oxide concentration on the morphologies and antifouling properties of PVDF ultrafiltration membranes, *Journal of Environmental Chemical Engineering* 1(3) (2013) 349-354.
- [169] G. He, C. Chang, M. Xu, S. Hu, L. Li, J. Zhao, Z. Li, Z. Li, Y. Yin, M. Gang, H. Wu, X. Yang, M.D. Guiver, Z. Jiang, Tunable Nanochannels along Graphene Oxide/Polymer Core–Shell Nanosheets to Enhance Proton Conductivity, *Advanced Functional Materials* 25(48) (2015) 7502-7511.
- [170] X. Huang, K.L. Marsh, B.T. McVerry, E.M.V. Hoek, R.B. Kaner, Low-Fouling Antibacterial Reverse Osmosis Membranes via Surface Grafting of Graphene Oxide, *ACS Applied Materials & Interfaces* 8(23) (2016) 14334-14338.
- [171] E. Aliyev, V. Filiz, M.M. Khan, Y.J. Lee, C. Abetz, V. Abetz, Structural Characterization of Graphene Oxide: Surface Functional Groups and Fractionated Oxidative Debris, *Nanomaterials* 9(8) (2019) 1180.
- [172] D.C. Marcano, D.V. Kosynkin, J.M. Berlin, A. Sinitskii, Z. Sun, A. Slesarev, L.B. Alemany, W. Lu, J.M. Tour, Improved Synthesis of Graphene Oxide, *ACS Nano* 4(8) (2010) 4806-4814.

- [173] V. Vatanpour, S.S. Madaeni, R. Moradian, S. Zinadini, B. Astinchap, Fabrication and characterization of novel antifouling nanofiltration membrane prepared from oxidized multiwalled carbon nanotube/polyethersulfone nanocomposite, *Journal of Membrane Science* 375(1) (2011) 284-294.
- [174] N.V. Medhekar, A. Ramasubramaniam, R.S. Ruoff, V.B. Shenoy, Hydrogen Bond Networks in Graphene Oxide Composite Paper: Structure and Mechanical Properties, *ACS Nano* 4(4) (2010) 2300-2306.
- [175] C. Cha, S.R. Shin, X. Gao, N. Annabi, M.R. Dokmeci, X. Tang, A. Khademhosseini, Controlling Mechanical Properties of Cell-Laden Hydrogels by Covalent Incorporation of Graphene Oxide, *Small* 10(3) (2014) 514-523.
- [176] S. Niyogi, E. Bekyarova, M.E. Itkis, J.L. McWilliams, M.A. Hamon, R.C. Haddon, Solution Properties of Graphite and Graphene, *Journal of the American Chemical Society* 128(24) (2006) 7720-7721.
- [177] Y. Liang, D. Wu, X. Feng, K. Müllen, Dispersion of Graphene Sheets in Organic Solvent Supported by Ionic Interactions, *Advanced Materials* 21(17) (2009) 1679-1683.
- [178] D. Yu, L. Dai, Self-Assembled Graphene/Carbon Nanotube Hybrid Films for Supercapacitors, *The Journal of Physical Chemistry Letters* 1(2) (2010) 467-470.
- [179] E. Aliyev, S. Shishatskiy, C. Abetz, Y.J. Lee, S. Neumann, T. Emmler, V. Filiz, SI-ATRP Polymer-Functionalized Graphene Oxide for Water Vapor Separation, *Advanced Materials Interfaces* n/a(n/a) 2000443.
- [180] G.J. Dunderdale, J.P.A. Fairclough, Coupling pH-Responsive Polymer Brushes to Electricity: Switching Thickness and Creating Waves of Swelling or Collapse, *Langmuir* 29(11) (2013) 3628-3635.
- [181] L.A. Fielding, S. Edmondson, S.P. Armes, Synthesis of pH-responsive tertiary amine methacrylate polymer brushes and their response to acidic vapour, *Journal of Materials Chemistry* 21(32) (2011) 11773-11780.
- [182] J.-T. Sun, C.-Y. Hong, C.-Y. Pan, Fabrication of PDEAEMA-Coated Mesoporous Silica Nanoparticles and pH-Responsive Controlled Release, *The Journal of Physical Chemistry C* 114(29) (2010) 12481-12486.
- [183] R.N. Wenzel, RESISTANCE OF SOLID SURFACES TO WETTING BY WATER, *Industrial & Engineering Chemistry* 28(8) (1936) 988-994.
- [184] L. Yan, Y.S. Li, C.B. Xiang, S. Xianda, Effect of nano-sized Al<sub>2</sub>O<sub>3</sub>-particle addition on PVDF ultrafiltration membrane performance, *Journal of Membrane Science* 276(1) (2006) 162-167.
- [185] J.H. Hanemaaijer, T. Robbertsen, T. van den Boomgaard, J.W. Gunnink, Fouling of ultrafiltration membranes. The role of protein adsorption and salt precipitation, *Journal of Membrane Science* 40(2) (1989) 199-217.

- [186] C. Höhme, V. Filiz, C. Abetz, P. Georgopoulos, N. Scharnagl, V. Abetz, Postfunctionalization of Nanoporous Block Copolymer Membranes via Click Reaction on Polydopamine for Liquid Phase Separation, *ACS Applied Nano Materials* 1(7) (2018) 3124-3136.
- [187] B. Saini, S. Khuntia, M.K. Sinha, Incorporation of cross-linked poly(AA-co-ACMO) copolymer with pH responsive and hydrophilic properties to polysulfone ultrafiltration membrane for the mitigation of fouling behaviour, *Journal of Membrane Science* 572 (2019) 184-197.
- [188] C. Stegelmeier, V. Filiz, V. Abetz, J. Perlich, A. Fery, P. Ruckdeschel, S. Rosenfeldt, S. Förster, Topological Paths and Transient Morphologies during Formation of Mesoporous Block Copolymer Membranes, *Macromolecules* 47(16) (2014) 5566-5577.
- [189] M. Radjabian, C. Abetz, B. Fischer, A. Meyer, V. Abetz, Influence of Solvent on the Structure of an Amphiphilic Block Copolymer in Solution and in Formation of an Integral Asymmetric Membrane, *ACS Applied Materials & Interfaces* 9(37) (2017) 31224-31234.
- [190] S. Saleem, S. Rangou, C. Abetz, B. Lademann, V. Filiz, V. Abetz, Block Copolymer Membranes from Polystyrene-*b*-poly(solketal methacrylate) (PS-*b*-PSMA) and Amphiphilic Polystyrene-*b*-poly(glyceryl methacrylate) (PS-*b*-PGMA), *Polymers* 9(6) (2017) 216.
- [191] X. Niu, D. Li, Y. Chen, F. Ran, Modification of a polyethersulfone membrane with a block copolymer brush of poly(2-methacryloyloxyethyl phosphorylcholine-co-glycidyl methacrylate) and a branched polypeptide chain of Arg–Glu–Asp–Val, *RSC Advances* 9(44) (2019) 25274-25284.
- [192] F. Yang, Y. Liu, Y. Zhang, B. Ren, J. Xu, J. Zheng, Synthesis and Characterization of Ultralow Fouling Poly(N-acryloyl-glycinamide) Brushes, *Langmuir* 33(49) (2017) 13964-13972.
- [193] Z.-K. Xu, F.-Q. Nie, C. Qu, L.-S. Wan, J. Wu, K. Yao, Tethering poly(ethylene glycol)s to improve the surface biocompatibility of poly(acrylonitrile-co-maleic acid) asymmetric membranes, *Biomaterials* 26(6) (2005) 589-598.
- [194] D. Lazos, S. Franzka, M. Ulbricht, Size-Selective Protein Adsorption to Polystyrene Surfaces by Self-Assembled Grafted Poly(ethylene Glycols) with Varied Chain Lengths, *Langmuir* 21(19) (2005) 8774-8784.
- [195] D.S. Wavhal, E.R. Fisher, Hydrophilic modification of polyethersulfone membranes by low temperature plasma-induced graft polymerization, *Journal of Membrane Science* 209(1) (2002) 255-269.
- [196] B. Jachimska, M. Wasilewska, Z. Adamczyk, Characterization of Globular Protein Solutions by Dynamic Light Scattering, Electrophoretic Mobility, and Viscosity Measurements, *Langmuir* 24(13) (2008) 6866-6872.
- [197] E. Tsuchida, K. Honda, H. Sata, Reversible oxygenation of heme bound to polyvinylpyridine and polyvinylimidazole, *Biopolymers* 13(10) (1974) 2147-2159.

- [198] E. Tsuchida, K. Honda, E. Hasegawa, Complexes between synthetic polymer ligands and ferri- and ferro-protoporphyrin IX, *Biochimica et Biophysica Acta (BBA) - Protein Structure* 393(2) (1975) 483-495.
- [199] Y.-L. Su, W. Cheng, C. Li, Z. Jiang, Preparation of antifouling ultrafiltration membranes with poly(ethylene glycol)-graft-polyacrylonitrile copolymers, *Journal of Membrane Science* 329(1) (2009) 246-252.
- [200] G. Hild, J.P. Lamps, P. Rempp, Synthesis and characterization of anionic 2,3-epoxypropyl methacrylate polymers and of related random and block copolymers with methyl methacrylate, *Polymer* 34(13) (1993) 2875-2882.
- [201] G. Hild, J.-P. Lamps, Diblock copolymers, triblock copolymers and model networks synthesized by sequential anionic polymerization of styrene and 2,3-epoxypropyl methacrylate, *Polymer* 39(12) (1998) 2637-2649.

## Chapter 8: Appendix

### 8.1. Toxicity of chemicals

All used chemicals with H- and P- data are given in the following Table

Substance	GHS Symbol	Hazard Statement	Precautionary statement
Acetic acid	GHS02, GHS05	H226-H314	P280-P305 + P351 + P338-P310
<i>sec</i> -Butyl lithium in cyclohexane	GHS02, GHS05, GHS07, GHS08, GHS09	H225, H250, H260 H304, H314 H336 H410	P210-P261-P273 P280-P301 + P310 P305 + P351 + P338
Calcium hydride	GHS02	H260	P223-P231 + P232 P370 + P378-P422
Chloroform	GHS07, GHS08	H302-H315-H351- H373	P281
Chloroform-d <sub>1</sub>	GHS07, GHS08	H302-H315-H351- H373	P281
Dimethylacetamide	GHS07, GHS08	H312 + H332 +H319-H360D	P201-P280 P305 + P351+P338 P308 + P313
Dimethylformamide	GHS02,GHS07 GHS08	H226-H312 + H332 H319-H360D	P201-P280 P305 + P351 + P338 P308 + P313

1,4-Dioxane	GHS02, GHS07 GHS08	H225-H319-H335 H351	P210-P261-P281 P305 + P351 + P338
1,1-diphenylethylene	GHS 07, GHS09-	H411	P273 + P391 + P501
Dibutylmagnesium	GHS02 GHS05	H260, H225, H304, H314, H336, H410	P280, P301 + P330 + P331, P305 + P351 + P338, P310, P261, P301 + P310, P331, P273, P402 + P404
Ethylaluminium dichloride	GHS02, GHS05, GHS07, GHS08 GHS09	H225-H250-H261 H304-H314-H336 H361-H373-H411	P210-P222 P231 + P232-P261 P273-P422
Ethanol	GHS02, GHS07	H225, H319	P210, P240, P305 + P351 + P338, P403 + P233
<i>n</i> -hexane	GHS02, GHS07 GHS08, GHS09	H225-H304-H315 H336-H361f-H373 H411	P210-P261-P273 P281-P301 + P310 P331
Hydrochloric acid	GHS05, GHS07	H290, H314, H335	P280, P303 + P361+ P353, P304 + P340, P305 + P351+ P338, P310
Lithium chloride	GHS07	H302-H315 H319-H335	P261-P305 + P351 + P338
Methanol	GHS02, GHS06,	H225-H301-H311	P210-P260-P280

	GHS08	H331-H370	P301 + P310-P311
Poly(4-vinylpyridine)	GHS07	H315, H319, H335	P261, P305 + P351 + P338
Sodium hydroxide	GHS05	H314	P280-P305 + P351 + P338-P310
Styrene	GHS02 GHS07 GHS08	H226, H315, H319 H332, H361d, H372	P210, P302 + P352, P305+ P351 + P338 P314
Tetramethylsilane	GHS02	H224	P210

## 8.2. Calculation of the solubility parameters according to HOY method

$$F_t = \sum F_{t,i} N_i$$

$$F_p = \sum F_{p,i} N_i$$

$$V = \sum V_i N_i$$

$$\Delta_T^{(P)} = \sum \Delta_{T,i}^{(P)} N_i$$

$$\alpha(P) = \frac{777 \Delta_T^{(P)}}{V}$$

$$\bar{n} = \frac{0,5}{\Delta_T^{(P)}}$$

$$\delta_t = \frac{F_t + \frac{B}{\bar{n}}}{V}$$

$$\delta_p = \delta_t \left( \frac{1}{\alpha(P)} \frac{F_p}{F_t + \frac{B}{\bar{n}}} \right)^{0,5}$$

$$\delta_h = \delta_t \left( \frac{\alpha(P) - 1}{\alpha(P)} \right)^{0,5}$$

$$\delta_d = (\delta_t^2 - \delta_p^2 - \delta_h^2)^{0,5}$$

PSMA	$F_{t,i}$ ( $(\text{MJ}/\text{m}^3)^{0,5} / \text{mol}$ )	$F_{p,i}$ ( $(\text{MJ}/\text{m}^3)^{0,5} / \text{mol}$ )	$\Delta T_{i,(P)}$	$V_i$ ( $\text{cm}^3 / \text{mol}$ )
3-CH <sub>3</sub>	910.5	-	0.066	64.65
1 >C<	65.5	-	0.040	3.56
2 -O-	470	432	0.036	12.9
3-CH <sub>2</sub>	807		0.060	46.65
1 -COO-	640	528	0.050	23.7
2 >CH-	352	-	0.026	19.12
Sum	3254	960	0.278	170.58
	$\delta_t = 19.98$	$\delta_p = 9.35$	$\delta_d = 16.76$	$\delta_h = 5.54$

PGMA	$F_{t,i}$ ( $(\text{MJ}/\text{m}^3)^{0.5}/\text{mol}$ )	$F_{p,i}$ ( $(\text{MJ}/\text{m}^3)^{0.5}/\text{mol}$ )	$\Delta T_{i}^{(P)}$	$V_i$ ( $\text{cm}^3/\text{mol}$ )
1-CH <sub>3</sub>	303.5	-	0.022	21.55
3-CH <sub>2</sub>	807	-	0.060	46.65
1 -COO-	640	528	0.050	23.7
1-OH sec	591	591	0.049	12.45
1-OH pri	675	675	0.049	12.45
2 >CH-	352	-	0.026	19.12
Sum	3368.5	1794	0.256	135.92
	$\delta_t = 25.8$	$\delta_p = 9.2$	$\delta_d = 19.2$	$\delta_h = 14.5$

### 8.3. Synthesis and characterization of poly(glycidyl methacrylate) (PGM) homopolymer

Glycidyl methacrylate (GM) was fractionally vacuum distilled from finely ground calcium hydride (CaH<sub>2</sub>) under a highly pure argon atmosphere. The first fraction was discarded and just before polymerization the pure monomer was distilled in high yield. The homopolymer was synthesized through sequential living anionic polymerization described in the literature before [200].

The synthesized polymer is summarized in Table (8.1).

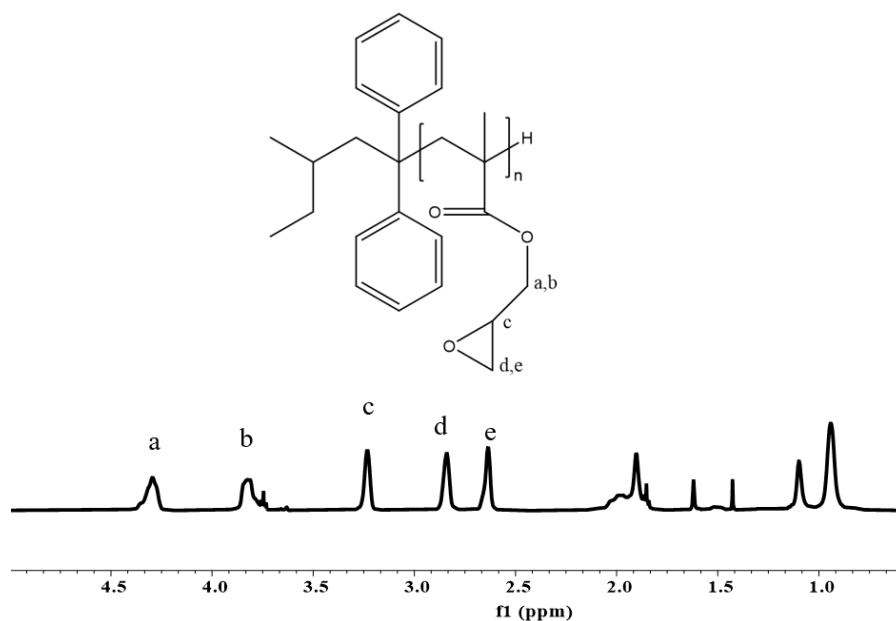


**Figure 8. 1.** <sup>1</sup>H-NMR spectra of PGMA homopolymer in CDCl<sub>3</sub>

**Table 8. 1** Molecular weight and dispersity index of the PGM homopolymer

Polymers	M <sub>n</sub> (kg/mol) <sup>a</sup>	D <sup>a</sup>
PGM	9.4	1.06

a) Molecular weights and dispersity index were determined with SEC

### 8.3.1 Synthesis and characterization of polystyrene-*block*-poly(glycidyl methacrylate) (PS-*b*-PGM) diblock copolymer

PS-*b*-PGM diblock copolymers were synthesized through sequential living anionic polymerization [201] as given in Scheme (3.2.2). The electron affinity of methacrylic esters (GM) is higher than styrene, it was added last in the polymerization procedure to yield PS-*b*-PGM.

As shown in Table 8.2 and Figure 8.3 the molar mass distribution of the diblock copolymer is rather narrow which indicates the absence of any homopolymer contamination. PS-*b*-PGM diblock copolymer was characterized by <sup>1</sup>H-NMR spectroscopy by recording the spectra where

tetramethylsilane (TMS) was used as internal standard and deuterated chloroform ( $\text{CDCl}_3$ ) as a solvent.

Five characteristic peaks at 2.6-4.3 ppm (c, d, e, f, g) responsible for five protons of GM was shown in Figure 8.2 whereas the presence of e, f, g peaks confirms the oxyranyl protons of epoxy rings of poly(GM). The two large peaks (a, b) characterize the aromatic protons of poly(styrene and 1,1-diphenylethylene. The block copolymer composition was determined by direct comparison between five characteristic protons of poly(glycidyl methacrylate) and five aromatic protons of polystyrene by taking in account the aromatic protons of DPE.

**Table 8. 2.** Characterization data of PS-*b*-PGM block copolymers

Batch no	Polymer	$M_n$ (kg/mol)	PGM (wt%)	$\bar{D}$
130516-1	PS- <i>b</i> -PGM	112	20.5	1.08

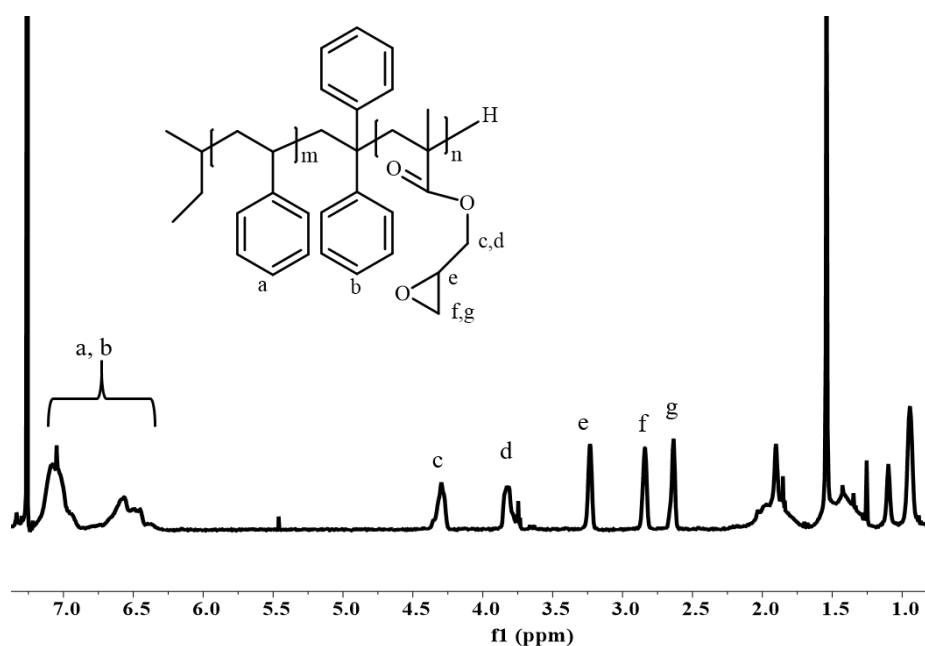


**Figure 8. 2.**  $^1\text{H-NMR}$  spectrum of PS<sub>79.5</sub>-*b*-PGM<sub>20.5</sub><sup>112</sup> in  $\text{CDCl}_3$

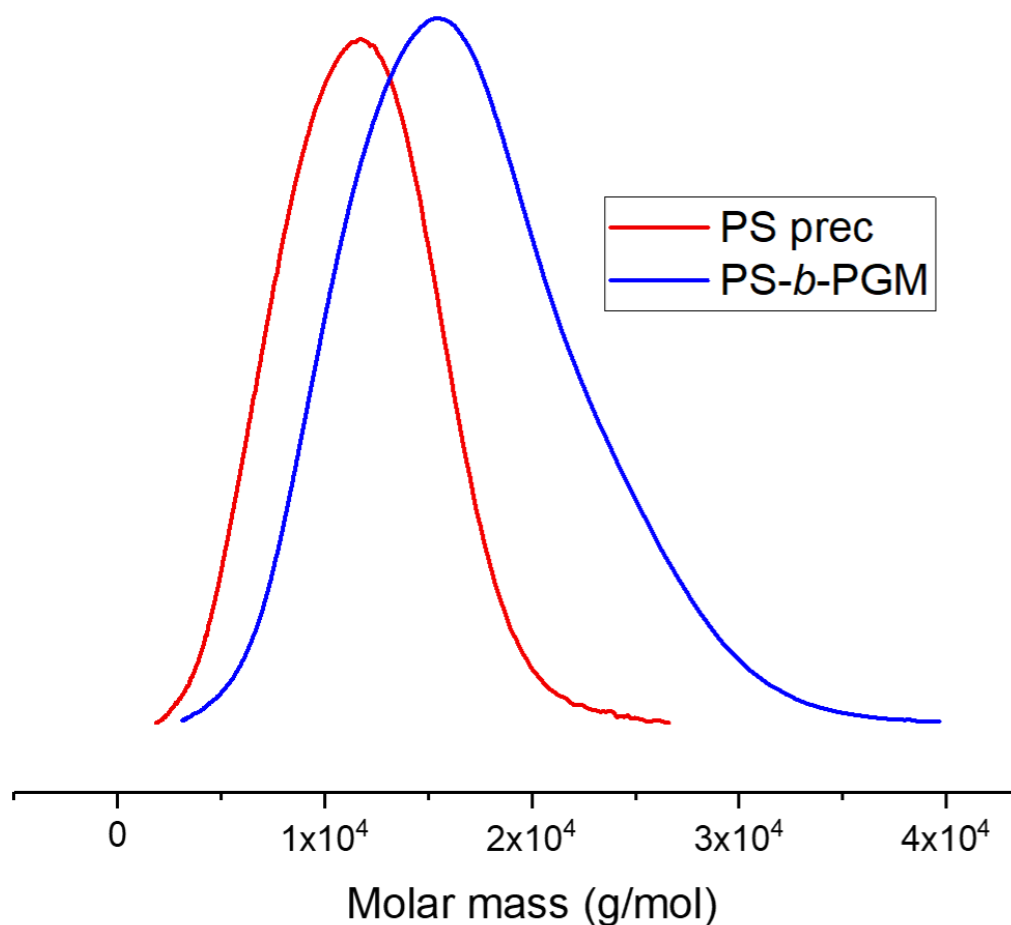


**Figure 8. 3.** SEC chromatogram of PS homopolymer and PS<sub>79.5</sub>-*b*-PGM<sub>20.5</sub><sup>112</sup> diblock copolymer

### 8.3.2 Synthesis and characterization of polystyrene-*block*-poly(4-vinylpyridine)-*block*-poly(glycidyl methacrylate) (PS-*b*-P4VP-*b*-PGM) triblock terpolymer

The polystyrene-*block*-poly(4-vinylpyridine)-*block*-poly(glycidyl methacrylate) linear triblock terpolymers used in this study were synthesized for the first time by sequential anionic polymerization technique. The complete process of polymerization was optimized regarding

the purification of monomers, initiation of monomers, end capping of carbanion and duration to complete polymerization.

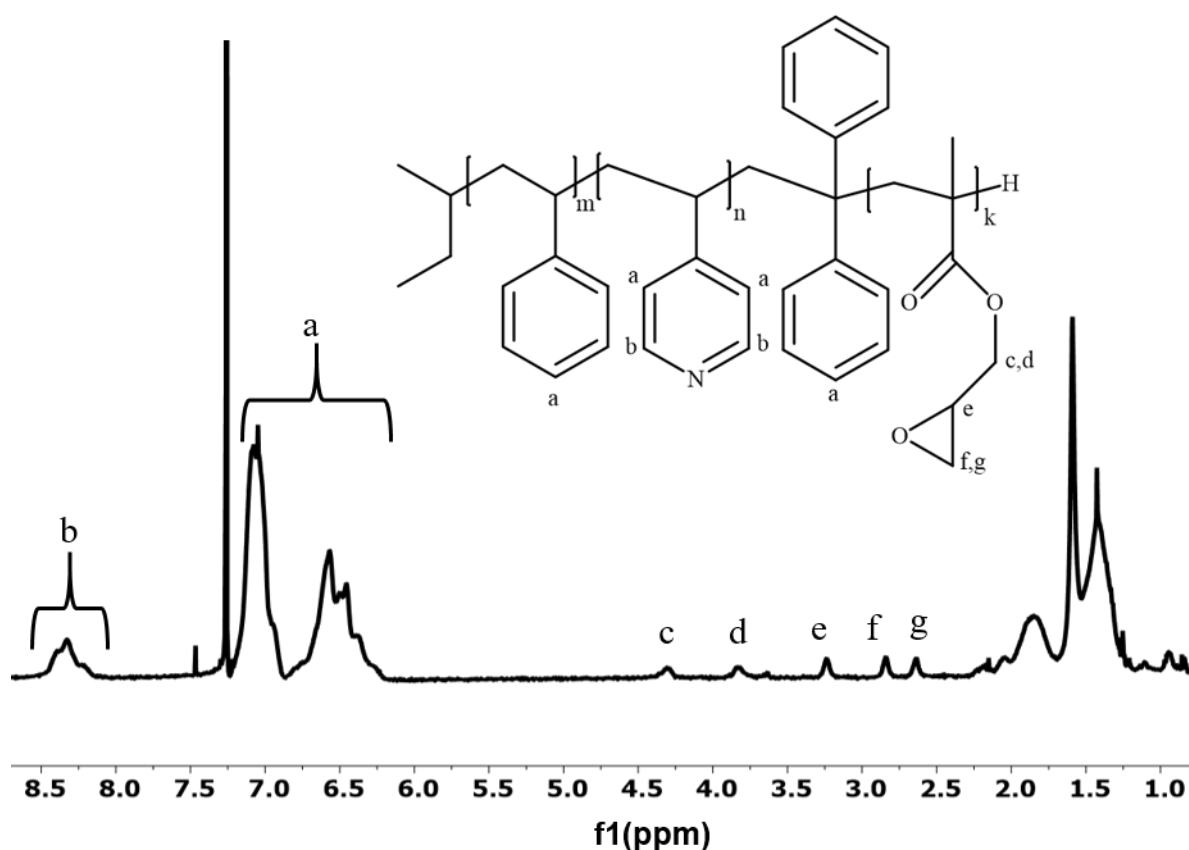


**Figure 8. 4.**  $^1\text{H-NMR}$  spectra of PS-*b*-P4VP-*b*-PGM in  $\text{CDCl}_3$

The first two blocks PS-*b*-P4VP were synthesized by following the method reported before in literature [123]. As described earlier in Section 3.1.4 about the reactivity of (glycidyl methacrylate) (GM) block, the reactivity of PS-*b*-P4VP macro initiator was reduced by the addition of 1,1-diphenylethylene (DPE). After half an hour glycidyl methacrylate was added to the polymer solution and maintained the temperature for 2 h. The polymer solution was terminated and precipitated in methanol/water solution.

The triblock terpolymer characteristics were determined by a combination of size exclusion chromatography (SEC) and <sup>1</sup>H-NMR spectroscopy. Figure 8.4 shows <sup>1</sup>H-NMR spectra of PS-*b*-P4VP-*b*-PGM where peaks (c, d, e, f, g) corresponding to the five protons of glycidyl methacrylate (GM).

The peaks at 8.3 ppm are responsible for the protons of 4-vinylpyridine whereas the rest of the aromatic protons of styrene, 1,1-diphenylethylene (DPE) and 4-vinylpyridine lies under two large peaks denoted as (a) in the NMR spectra. The molecular weight distribution of triblock terpolymer is given in Table 8.3.

**Table 8. 3.** Characterization data of PS-*b*-P4VP-*b*-PGM triblock terpolymer

<b>Batch no.</b>	<b>Polymer</b>	<b>M<sub>n</sub></b> <b>(kg/mol)</b>	<b>P4VP</b> <b>(wt%)</b>	<b>PGM</b> <b>(wt%)</b>	<b>D</b>
130416	PS- <i>b</i> -P4VP- <i>b</i> -PGM	235	21.5	29.5	1.1

## Acknowledgement

I would like to express my gratitude to my supervisor Prof. Volker Abetz for providing me the opportunity to conduct research at the institute of Polymer Research in Helmholtz-Zentrum Geesthacht. I am grateful for all his insightful discussions and assistance about the research throughout this project. I am thankful for allowing me to present my work in international conferences.

I truly appreciate the guidance and support of Dr. Volkan Filiz, my immediate supervisor who familiarized me with this topic. I truly admire his positive approach and providing a lot of space to work freely.

I express my heartfelt gratitude to Dr. Sofia Rangou for her valuable input and continuous interest in my research work.

I would like to thank Clarissa Abetz, Anke Lisa Höhme, Erik Schneider and Evgeni Sperling for doing microscopic investigations and for all the discussions regarding microscopic analysis throughout this period. I am greatly thankful to Brigitte Lademann for her tremendous support in synthesizing the polymers. I am thankful to Silvio Neumann, Thomas Emmeler, Maren Brinkmann and Barbara Bajer for NMR, TGA, DSC, SEC and water flux measurements. I would like to thank Elvin Aliyev for providing nanosheets to prepare hybrid membranes.

I cordially thank to all my fellow colleagues Dr. Muntazim Munir Khan, Dr. Karabi Halder, Dr. Kirti Sankhala, Dr. Christian Höhme, David Meis, Jiali Wang and Zhenzhen Zhang.

I am deeply grateful to my brother Ahmed Faraz and my sisters Munnaza, Faiza, Ammara for their endless love, care, faith and support throughout my life. I would like to thank my uncle Rehan Aman Ullah for his continuous moral support.

Lastly, I cannot thank my husband enough whose eternal love, support and motivation helped me turn this whole Ph.D. into a success.

I would like to thank Helmholtz Association for financial support during this whole period of my Ph.D. research.

I would like to dedicate this thesis to my beloved mother (late) who always encouraged me to dream big.

## Curriculum Vitae

### Contact details

Address: Querstraße 23, 21502 Geesthacht, Germany

E-mail: sarahsaleem@outlook.com

sarahsaleem015@gmail.com

Mobile no.: +4915236295158

### Education

06/2015 – 10/2019

#### **Ph.D Student**

University of Hamburg, Dept. of Physical Chemistry  
Grindelallee 117, 20146 Hamburg, Germany

09/2010 - 07/2012

#### **Master of Science**

COMSATS University, Dept. of Chemistry Abbottabad,  
Pakistan.

09/2008 - 08/2010

#### **Master of Science**

Institute of Chemistry, University of the Punjab, Institute of  
Chemistry Lahore, Pakistan.

09/2006 - 08/2008

#### **Bachelor of Science**

Chemistry with Botany and Zoology, National Science College,  
Gujranwala, Pakistan.

### Personal information

Date of birth: 23.08.1986

Nationality: Pakistani

## **Declaration of Oath**

I hereby declare that this thesis on “Integral asymmetric isoporous membrane formation from novel block copolymers” accommodates the original work of my Ph.D. Several parts of this dissertation had been published in international peer reviewed journal and therefore, the similarities with those published work exist. This dissertation is written by me and has not ever been submitted to any other university or institution to pursue a degree.

Sarah Saleem